INVESTIGATIONS ON A GEOSYNTHETIC REINFORCED BEARING LAYER UNDER STATIC AND DYNAMIC LOADING

A DISSERTATION

Submitted in partial fulfillment of the
requirements for the award of the degree
of
MASTER OF TECHNOLOGY
in
EARTHQUAKE ENGINEERING
(With specialization in Soil Dynamics)

by
JYOTI AGARWAL
Enrollment Number: - 14525008

DEPARTMENT OF EARTHQUAKE ENGINEERING
INDIAN INSTITUTE OF TECHNOLOGY
ROORKEE – 247667 (INDIA)
MAY 2016

CANDIDATE'S DECLARATION

I hereby declare that the work which is being presented in the project report entitled "**Investigations on a geosynthetic reinforced bearing layer under static and dynamic loading**" for the partial fulfillment of the requirements for the award of the Degree of **Master of Technology** with specialization in **Soil Dynamics**, and submitted in the Department of Earthquake Engineering, **Indian Institute of Technology, Roorkee**, India is an authentic record of my own work carried out during the period from July, 2015 to May, 2016 under the supervision of **Dr. Ravi S. Jakka**, Associate Professor, Department of Earthquake Engineering, Indian Institute of Technology Roorkee, India and **Prof. Dr.-Ing. habil. Christian Moormann**, Institut für Geotechnik (IGS), Universität Stuttgart, Germany.

The matter embodied in this current project report has not been submitted to any university or institute for the award of any degree.

Date:

Place: Roorkee **(Jyoti Agarwal)**

CERTIFICATE

This is to certify that the statement made by the candidate in declaration is correct to the best of my knowledge and belief.

(Dr. Ravi S. Jakka)

Associate Professor
Department of Earthquake Engineering
Indian Institute of Technology, Roorkee

ACKNOWLEDGEMENT

I would like to express my deepest gratitude to my supervisor, **Dr. Ravi S. Jakka**, Associate Professor, Department of Earthquake Engineering, IIT Roorkee, for his timely suggestions and constant encouragement throughout the course of preparing this report.

I would like to express a thankful note to **Prof. Dr.-Ing. habil. Christian Moormann**, Institut für Geotechnik (IGS), Universität Stuttgart, Germany for his intuitive and careful guidance, and **Mr. Julian Lehn**, Institut für Geotechnik (IGS), Universität Stuttgart, Germany for providing his timely guidance and motivation throughout my work. I would also like to thank **Dr. Fursan Hamad**, Institut für Geotechnik (IGS), Universität Stuttgart, Germany for his helpful suggestions and support. I am also grateful to the Institut für Geotechnik (IGS) of Universität Stuttgart for providing valuable resources to aid my research.

I am also grateful to German Academic Exchange Service (DAAD) for providing me an opportunity to carry out my research work in Germany.

I would like to thank all the lab colleagues who were good friends, and were always willing to help and give best suggestions. Finally, I would like to thank Debdeep Sarkar for his helpful suggestions, encouraging words and moral support.

Date: 31 May 2016

Place: Roorkee (Jyoti Agarwal)

ABSTRACT

Reinforced layered soil system is generally used under the foundations, to make the weak soil like soft clay safe and stable and to avoid shear failure and excessive settlements due to static and dynamic loads. Reinforced layered soil system is also used for working platforms which are required for installing heavy construction machines and vehicles on weak soils like soft clay which are not suitable for taking so much loads, and show excessive settlements. Provided fill creates a suitable load bearing surface on which concentrated load may be applied, without the shear failure and excessive deformations.

In this work static and dynamic analysis have been carried out using Finite Element Software PLAXIS 2D on the two layer unreinforced and reinforced soil systems to see the effect of providing geogrid as reinforcement in the two layer soil system and other parameters, on the bearing capacity and settlement behavior of two layer system. Two layer soil systems consisted of soft clay soil overlain by compacted granular fill. Loading is applied on a circular plate. Axisymmetric analysis is performed to simulate the circular plate in 2D. For static analysis results obtained from numerical analysis are in good agreement with the existing experimental results. For dynamic analysis, it is required to provide viscous boundaries in PLAXIS to reduce the boundary effects and to prevent the reflection of waves from boundaries. So a study have been carried out to compare the various methods of providing silent boundaries and to see the effectiveness of viscous boundaries used in PLAXIS. Inclusion of geogrid layer as reinforcement in soil caused a significant improvement in the load bearing and settlement behavior of soil. This improvement also depends on the position, number and stiffness of geogrid layers.

Contents

List of Figures

List of Tables

Chapter 1

Introduction

1.1 Motivation

Two layer reinforced soil system is generally used for working platforms and under the shallow foundations. Under the shallow foundation reinforced layered soil system is used to make soft clay soil safe and stable for construction when subjected to static and dynamic loading. Provided fill creates a suitable load bearing surface on which static and dynamic loads may be applied, without the shear failure and excessive deformations. In this thesis, main focus is on the use of geogrid reinforcement in the layer of granular fill, placed on a soft clay subgrade.

The scarcity of suitable land for construction has forced civil engineers to improve sites containing weak soil, to make it fit for safe and stable construction and to avoid high cost involved in deep foundations. In recent decades, soil replacement has gained acceptance among other ground improvement techniques as they are applicable to a broad range of ground conditions and different soil strengths. The replacement of these problematic soils with strong soil like dense sand layer on top is a soil improvement technique, which is widely used. Results of reinforcement inclusion in the top soil bed are improvement in the bearing capacity and reduction in settlement, it also helps in reducing the depth of replaced top soil layer. Now-a-days, geosynthetics are being used extensively as reinforcement in soils.

Many researchers have investigated the behavior of two layer reinforced soil system under static loads and found significant improvement in the bearing capacity and settlement behavior. While there are very few studies which are conducted under dynamic loads. So there is a strong need to do dynamic bearing capacity analysis of two layer soil system, which is additionaly reinforced with geogrid reinforcement, as we know due to cyclic loads bearing capacity of soil may reduce drastically and may result in the collapse of structures.

The finite element method (FEM) is a numerical method which is widely used in research and design of real civil engineering problems. In FEM continuous media is divided in to

finite number of elements with different geometries. With this material behavior of the soil can be idealized, which is non-linear with plastic deformations, in a more rational manner. This method can be used to determine the behavior of footings on soil under static and dynamic loading.

1.2 Objective

Objective of this thesis is to study the response of a foundation resting over two layer unreinforced and reinforced soil systems under static and dynamic loading and to determine the effect of various parameters on the performance of foundations. These objectives have been achieved through the following task:

- Literature review on existing design approaches and guidelines of two layered systems and working platforms.
- Description of the soil behavior under dynamic loading.
- Formulation of the requirements regarding to the numerical simulation of dynamic actions.
- Numerical simulation of two layered systems (with and without geosynthetic reinforcement) under static and dynamic loads.
- Comparison of the calculation results of the different systems with regard to the determination of the influence of various parameters on the load-bearing and deformation behavior.
- Evaluation of the achievements and identification of further research needs.

1.3 Outline of the Thesis

- **Chapter 1** deals with the motivation, objectives of the study and outline of thesis.
- **Chapter 2** includes the various concepts of bearing capacity, different bearing capacity failure critrea and various methods for the determination of bearing capacity of single and two layer systems analytically. This chapter also include the effect of introduction of geotextile reinforcement in the two layer system. A wide laboratory and numerical investigations available in literature are also described here briefly.

- **Chapter 3** includes the numerical basics used in numerical simulations of two layer system, various soil models used in simulation, dynamic simulation and calculations, and numerical modelling of geogrids.

- **Chapter 4** represents the various methods developed by many researchers which are adopted for providing Silent Boundaries. This chapter also include the analysis of existing methods of proving silent boundary with a vertical bar problem.

- **Chapter 5** includes the back analysis of a field test under static load available in the literature for single layer, two layer unreinforced and two layer reinforced soil systems.

- **Chapter 6** includes the dynamic analysis of two layer unreinforced and reinforced soil systems. Parametric studies have been carried out to determine the effect of some parameters on the bearing capacity and settlement behavior of the two layer unreinforced and reinforced soil systems under vertical dynamic loads.

Chapter 2

Literature Review

Bearing capacity of soil is its capacity to bear the loads applied on it without showing shear failure or excessive settlement. Footing and superstructure always impose an additional stresses on foundation soil.

Terminologies related to bearing capacity of soil:

Ultimate Bearing Capacity (q_u): It is the maximum intensity of loading (pressure) that a foundation soil can support before it fails in shear.

Net ultimate Bearing Capacity (q_n): In addition to overburden pressure, the maximum extra pressure that a foundation soil can support before it fails in shear.

$$q_n = q_u - q_o \tag{2.1}$$

where,
q_o = Overburden pressure at foundation level = γD
γ = Unit weight of soil
D = Depth to foundation

Safe Bearing Capacity (q_s): It is the safe additional pressure acting on the foundation soil in addition to initial overburden pressure.

$$q_s = q_n/F + q_o \tag{2.2}$$

Here F represents the factor of safety.

Allowable Bearing Pressure (q_a): It is the maximum loading intensity that a foundation soil can support considering both shear failure and settlement.

Bearing capacity failure mechanism

Modes of shear failure:

1. **General shear failure:** This type of failure is observed in dense soil. In this type of

failure a well defined failure pattern develops and bulging of soil mass adjacent to footing is visible.

2. **Local shear failure:** This type of failure is observed in relatively loose and soft soil. In this type of failure, failure surface remains only beneath the foundation and slight bulging of soil mass adjacent to footing is visible.

3. **Punching shear failure:** This type of failure is observed in loose and soft soil and at deeper elevations. In this no failure pattern is found and no bulging of soil mass is observed adjacent to the footing.

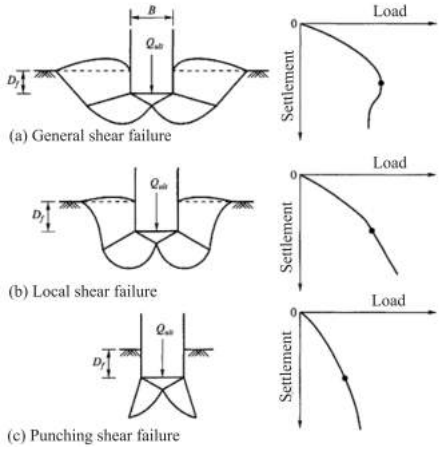

Figure 2.1: Bearing capacity failure mechanism *(Vesic,1963)*

2.1 One layer soil system

There are various theories given by different authors to determine the bearing capacity of a foundation on a single layer soil system. Every theory has their assumption which was made at the time of deriving a formula for the determination of bearing capacity. Some most widely used theories are-

- Terzaghi's bearing capacity theory
- Meyerhof's bearing capacity theory
- Hansen's bearing capacity theory

2.1.1 *Terzaghi's bearing capacity theory*

Terzaghi (1943) proposed a theory for the evaluation of the safe bearing capacity of shallow foundation with rough base.

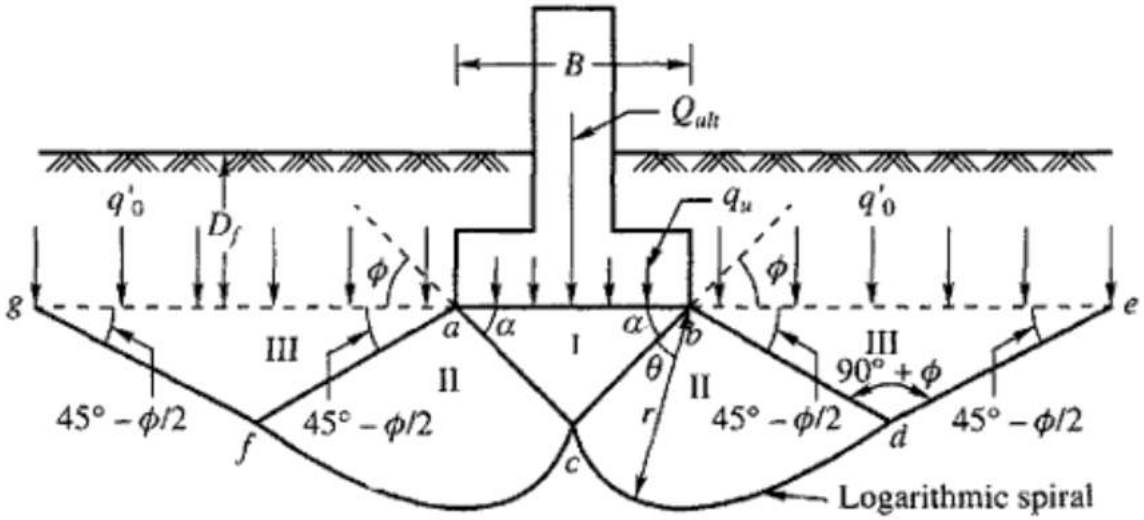

Figure 2.2: Terzaghi's bearing capacity failure surface *(Terzaghi, 1943)*

Figure 2.2 shows a strip footing with width B, due to the weight of superstructure footing compresses the foundation soil gradually. Let q_u be the ultimate load. The failure surface divided in to three zones, Zone I is elastic, Zone II is the zone of radial shear and Zone III is the zone of linear shear.

Ultimate bearing capacity for strip footing,

$$q_u = cN_c + \gamma D_f N_q + 0.5\gamma BN_\gamma \tag{2.3}$$

where,
B = Width of foundation,
c = Cohesion,
D_f = Depth of foundation,
γ = Unit weight of soil,
N_c, N_q, N_γ = Bearing Capacity factors which depends on ϕ.

Ultimate bearing capacity for circular footing,

$$q_u = 1.3cN_c + \gamma D_f N_q + 0.3\gamma BN_\gamma \tag{2.4}$$

Ultimate bearing capacity for square footing,

$$q_u = 1.3cN_c + \gamma D_f N_q + 0.4\gamma BN_\gamma \tag{2.5}$$

Ultimate bearing capacity for rectangular footing,

$$q_u = (1 + 0.3B/L)cN_c + \gamma D_f N_q + (1 - 0.2B/L)0.5\gamma BN_\gamma \tag{2.6}$$

Where, L= length of footing $(L > B)$

2.1.2 *Meyerhof's bearing capacity theory*

Meyerhof (1951, 1963) proposed a similar equation to determine the bearing capacity of soil as proposed by Terzaghi but included a shape factor s_q with the depth term Nq. He also included depth factors and inclination factors. Among all the bearing capacity theories Meyerhof's bearing capacity theory is most widely used because this can be applied on rough shallow and deep foundations.

2.2 Two layer soil system

There are various cases in which foundations rest on a two layer soil system. It may be natural or may be done with the replacement of weak and loose soil with strong and dense soil. For determination of bearing capacity of two layer soil system there are some approaches available in literature. It is assumed that the upper layer serves principally to spread the load thus reducing its intensity on the lower layer. Predicted ultimate bearing capacity obtained by this method depends mainly on the assumed load distribution through the upper layer thus results seems to be on conservative side because the shearing resistance of upper layer is ignored.

Hanna et al. presented a rational approach to solve cases of footings on layered soils. In this approach an assumption was made that is at ultimate load a soil mass in the upper sand layer was assumed as a truncated pyramid in shape, which is pushed in to a lower layer. A vertical punching failure surface was assumed in the upper layer (of thickness H below the footing base). Forces in this surface can be taken as the passive earth pressure (P_p), inclined at an average angle δ, acting upwards, thus for a strip footing of width B and depth D, the ultimate bearing capacity is give by

$$q_u = q_b + 2(P_p sin\delta)/B - \gamma_1 H \leq q_t \tag{2.7}$$

In which q_b and q_t are ultimate bearing capacities of the strip footing on a very thick bed of the lower and upper layers, respectively.

When lower layer is of weak sand

$$q_b = 0.5\gamma_2 BN_{\gamma 2} + \gamma_1(H + D)N_{q2} \tag{2.8}$$

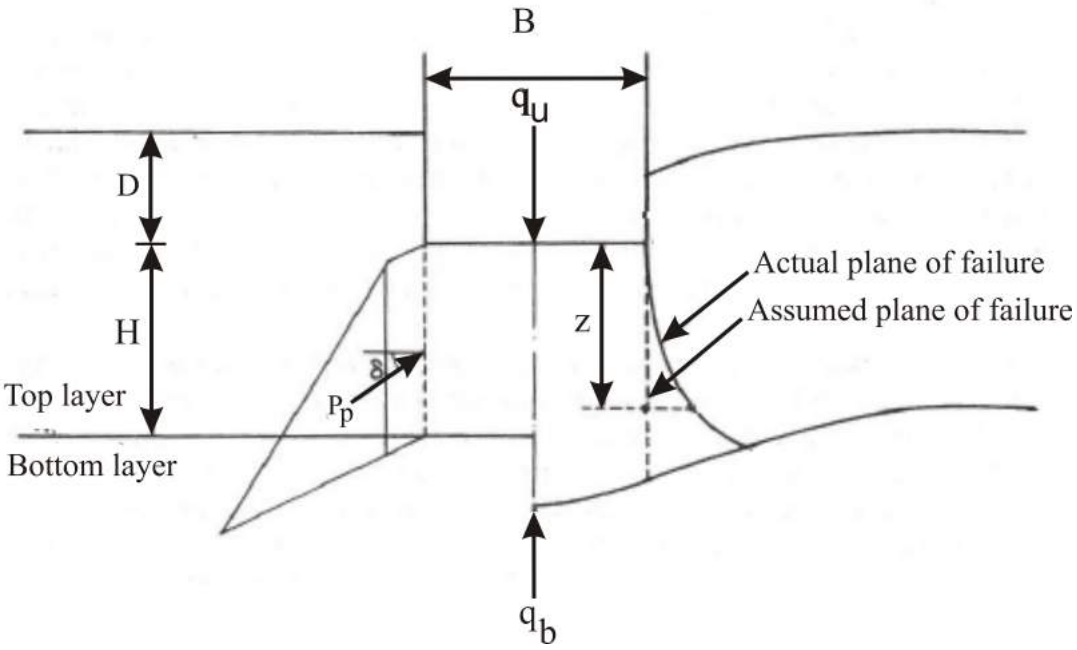

Figure 2.3: Strip footing on two layer soil system (*Hanna et al.,1981*)

When lower layer is of soft clay

$$q_b = cN_c \tag{2.9}$$

$$q_b = 0.5\gamma_1 BN_{\gamma 1} + \gamma_1 DN_{q1} \tag{2.10}$$

$$P_b = 0.5\gamma_1 H^2(1 + 2D/H)(K_p/cos\delta) \tag{2.11}$$

In which
$N_{\gamma 1}$, N_{q1} and $N_{\gamma 2}$, N_{q2} = the bearing capacity factors corresponding to the plane-strain angles of shearing resistance, ϕ_1 and ϕ_2 of the upper and lower sand layers respectively,
c = cohesion of lower clay layer,
N_c= bearing capacity factor of the lower clay layer,
γ_1 and γ_2 = unit weights of upper and lower layer of soil respectively,
K_p = coefficient of passive earth pressure.

Michalowski and Shi (1995) used the kinematic approach of limit analysis to determine the bearing capacity of footings resting on two-layer soil. When collapse mechanisms were considered, the theory provided the failure load which is similar to the true collapse loads of elastic-perfectly plastic bodies. According to upper-bound theorem with the help of material properties and geometry of a collapse mechanism, an upper bound of the true limit load can be found by equating the rate of work of external forces to the rate of internal energy dissipation. From this method limit pressures are obtained as results in place of bearing capacity factors. These results are dependent on the internal friction angle and thickness of the sand, cohesion and strength of the clay and the surcharge

pressure.
Above method can be used for any combination two different soil layers, but the results are limited to the case when top layer is of granular soil is placed on clay.

Okamurai and Kimura (1998) proposed a new limit equilibrium method to determine the bearing capacity of two layer system in which soft clay in overlain by sandy soil. In this limit equilibrium of forces acting on an imaginary sand block between the base of the footing and the sand/clay interface was considered. Failure mechanism adopted in this method was same as was given in previous methods. In this method vertical effective

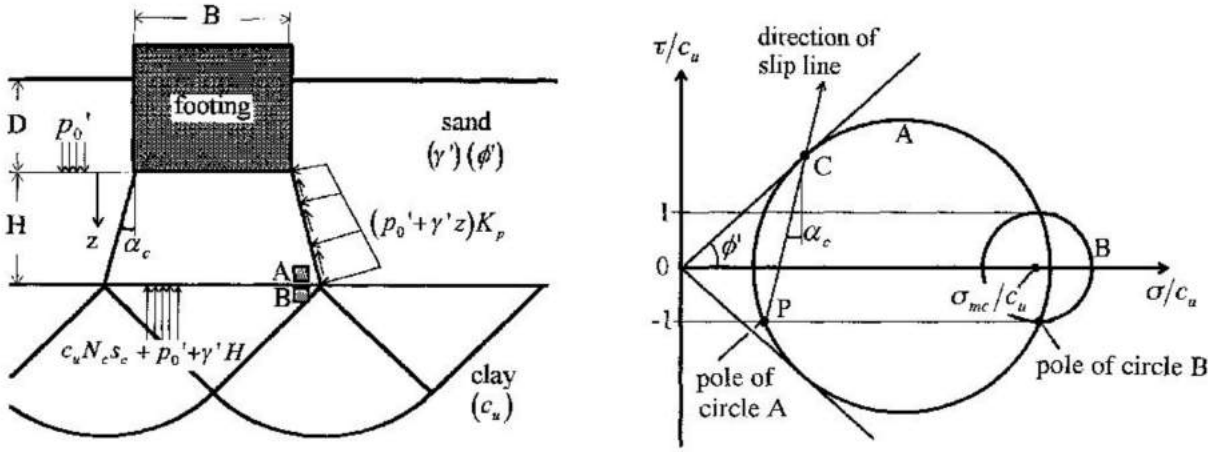

(a) Failure mechanism assumed

(b) Mohr's circle of stress for soil element A and B

Figure 2.4: Failure pattern and Mohr's circle (*Okamurai and Kimura, 1998*)

stresses acting on the base of the sand block, q'_{c1ay}, are assumed to be the ultimate bearing stresses of a rigid footing with rough base on clay subject to the effective surcharge pressure, which is given by following equation.

$$q'_{clay} = p'_0 + \gamma' H + c_u N_c s_c \tag{2.12}$$

In this method, Rankine's passive coefficient K_p, was adopted. The normal stress of K_p times the vertical stress is assumed to act on the side of the sand block. Consideration of equilibrium of the forces acting on the block, including self weight of the block, yields bearing capacity formulae as follows:

for a strip footing;

$$q_f = \left(1+2\frac{H}{B}\tan\alpha\right)(c_u N_c + p'_0 + \gamma' H) + \left(\frac{K_p \sin(\phi' - \alpha_c)}{\cos\phi' \cos\alpha'}\right)\frac{H}{B}(p'_0 + \gamma H) - \gamma' H\left(1+\frac{H}{B}\tan\alpha_c\right) \tag{2.13}$$

for a circular footing;

$$q_f = \left(1 + 2\frac{H}{B}\tan\alpha\right)^2 (c_u N_c s_c + p_0' + \gamma' H) + \left(\frac{4K_p \sin(\phi' - \alpha_c)}{\cos\phi' \cos\alpha_c}\right)\left\{\left(p_0' + \frac{\gamma' H}{2}\right)\frac{H}{B} + p_0' \tan\alpha_c \left(\frac{H}{B}\right)^2 + \frac{2}{3}\gamma' H \tan\alpha_c \left(\frac{H}{B}\right)^2\right\} - \frac{\gamma' H}{3}\left\{4(\frac{H}{B})^2 \tan^2\alpha_c + 6\frac{H}{B}\tan\alpha_c + 3\right\} \tag{2.14}$$

It should be noted that the Mohr's circle for the clay element B in the figure is represented in terms of total stress excluding static water pressure, whereas for the circle for sand element A in terms of effective stress. The direction of the slip surface in sand represented by a straight line P-C in Figure 2.4 is assumed to be that of the side of sand block. α_c can be obtained as:

$$\alpha_c = \tan^- 1\left(\frac{\sigma_{mc}/c_u - \sigma_{ms}/c_u(1 + \sin^2\phi')}{\cos\phi' \sin\phi' \sigma_{ms}/c_u + 1}\right) \tag{2.15}$$

$$\sigma_{mc}/c_u = N_c s_c \left(1 + \frac{1}{\lambda_c}\frac{H}{B} + \frac{\lambda_p}{\lambda_c}\right) \tag{2.16}$$

$$\sigma_{ms}/c_u = \frac{\sigma_{mc}/c_u - \sqrt{(\sigma_{mc}/c_u)^2 - \cos^2\phi'((\sigma_{mc}/c_u)^2 + 1)}}{\cos^2\phi'} \tag{2.17}$$

where,
λ_c = Normalized bearing capacity of underlying clay = $c_u N_c/\gamma' B$,
λ_p = Normalized overburden pressure = $p_0'/\gamma' B$.

In this proposed limit equilibrium method in which the variation of the side angle of the sand block with the parameters including H/B, λ_c and λ_p was taken into account. Bearing capacities calculated from the proposed method compared well with the observations, irrespective of shape, depth of footing and strength of underlying clay.

Shenawy and Karni (2005) derived the ultimate bearing capacity equation for a weak clay layer overlaid by a top dense sand layer, as a function of the properties of soils, the footing width, and the topsoil thickness, assuming that the failure surface is a punching shear failure through the upper sand layer, as shown in Figure 2.5.

Equation of ultimate bearing capacity in dimensionless form:

$$\frac{q_u}{\gamma_s B} = 5.14\frac{c_u}{\gamma_s B} + \frac{D}{B} + K_p \tan\delta\left(\frac{H}{B}\right)^2 + 2K_p \tan\delta\left(\frac{D}{B}\right)\left(\frac{H}{B}\right) \tag{2.18}$$

The new design charts were obtained, was found to be useful in overcoming the problern of the design charts that were developed by *Michalowski and Shi (1995)*, which provide large value of bearing capacity because of the use of the upper bound theorem.

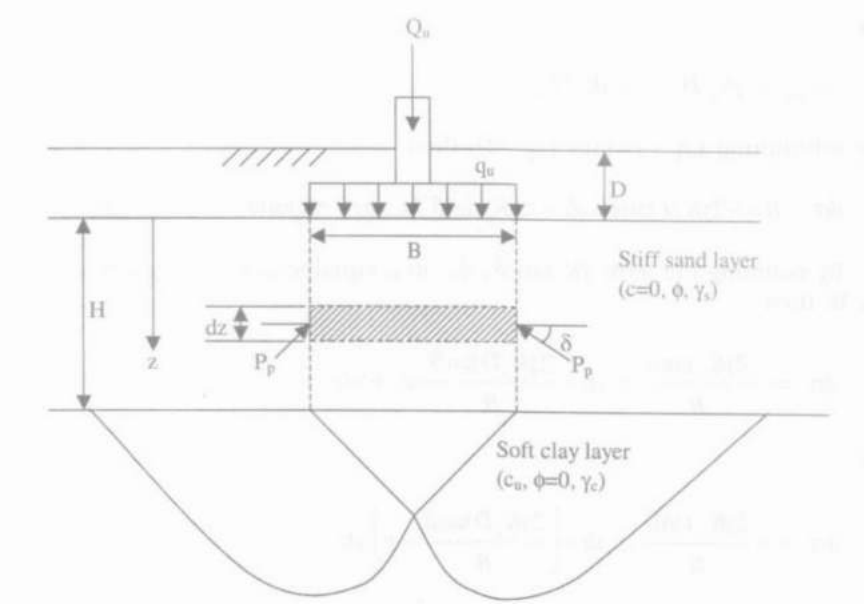

Figure 2.5: Punching shear model of strip footing over a two-layer soil (*Shenawy and Karni, 2005*)

Joshi and Shrivastava (2015) presented a theoretical equation for the bearing capacity of a circular footing placed on layered soil using punching shear failure mechanism following projected area approach. For the analysis frustum was considered to be a linearize curve for the actual shape of failure and a bearing capacity equation is deduced adopting certain assumptions. The equation of bearing capacity was obtained as a function of upper and lower layer properties.

The footing was assumed to be of radius r'embedded at depth D in a dense layer of sand resting on top of soft and saturated clay. The distance below the base of the footing up to the interface of dense sand and saturated soft clay is taken as H. The various soil properties for the dense sand and saturated soft clay are taken as γ_1, ϕ_1 and γ_2, c_2 respectively. The external load is assumed to spread linearly at an angle α with respect to the vertical from the base area of circular footing and hence the load intensity decreases with depth. From the above procedure following equation for determining the ultimate bearing capacity of circular footing resting on two layer soil is determined:

$$q_{ult} = q_b + K_p \gamma_1 \sec\alpha \ \sin\delta \left(\frac{2H(H+2D)}{D' + 2H\tan\alpha} \right) - \gamma_1 H \tag{2.19}$$

Where, K_p is the coefficient of passive earth pressure whose value is taken from Rankine passive earth pressure theory. K_p also varies with the angle of shearing resistance ϕ_1 on the assumed failure surface. K_p value can be determined from the following equation.

$$K_p = \frac{1}{\cos\delta} \left(\frac{1+\sin\phi}{1-\sin\phi} \right) \tag{2.20}$$

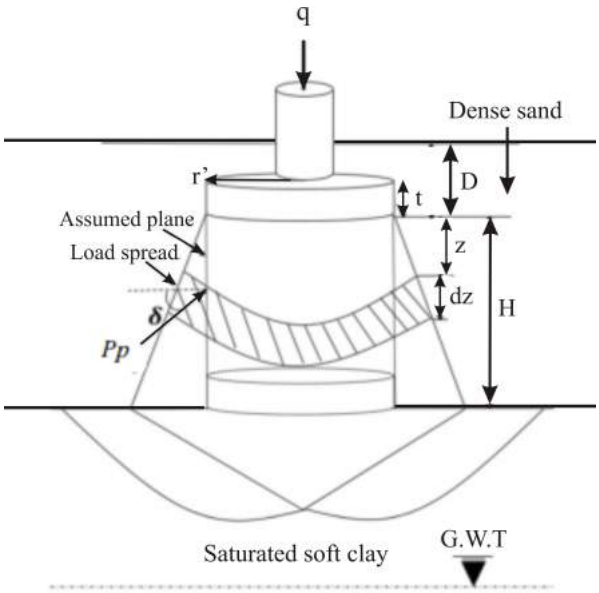

Figure 2.6: Assumed failure pattern for circular footing resting on layered soil (*Joshi and Shrivastava, 2015*)

q_b is the ultimate bearing capacity of circular footing on a very thick bed of lower soft saturated clay layer, which can be determine by following equation

$$q_b = cN_c s_c + \gamma_2 D \tag{2.21}$$

where s_c = 1.3 for fircular footing.
Parametric study was carried out and the results were compared and validated with other theoretical equation/experimental results available in the literature. The proposed equation appears to be effective as the results obtained are in good agreement with the plate load tests conducted by *Ibrahim (2014)* whereas the equation proposed by *Meyerhof (1974)* overestimate the ultimate bearing capacity for high values of load spread angle .

2.3 Two layer reinforced soil system

Poor soil can be reinforced by inclusion of reinforcing elements in soil to improve its engineering characteristics. Combination of soil and its reinforcing element causes an increase in the shear strength of the soil mass and reduction in settlement under the load. It also improves its resistance to liquefaction. The reinforcing element can be either inserted in the situ soil or placed in the soil mass as it constructed.

One of the methods of reinforcement is using a group of materials known as geosynthetics. Geosynthetics are manmade flexible and planar. They are manufactured from

synthetic polymeric materials and sometimes from natural materials. These geosynthetics are usually classified into:

- **Geotextiles:** They are porous geosynthetics that resemble a strong cloth or blanket with its strands and fibers visible. They can be woven, non-woven or knitted. These are usually made from polypropylene and sometimes from polyester, polyethylene or natural fibers such as jute.

- **Geomembranes:** They are impervious geosynthetics that resemble thick, flexible plastic sheets and are usually smooth surfaced. They are manufactured using high density polyethylene (HDPE), very flexible polyethylene (VFPE) and sometimes polyvinyl chloride (PVC) and other materials.

- **Geogrids:** They are mesh-like or grid-like geosynthetics with square or rectangular apertures that resemble plastic meshes. They are usually made from HDPE or polypropylene and sometimes from polyester. These have mass per unit area of 200 to 1500 gsm.

- **Geonets:** These are similar to geogrids but have thinner members and angular apertures, not square or rectangular, but resembling parallelograms.

- **Geocomposites:** They are multi-layered geosynthetics attached or bonded to each other, comprising of geotextiles, geomembranes, geogrids and geonets with themselves or along with other materials.

Functions geosynthetics are separation, filtration, reinforcement, drainage, hydraulic barriers, erosion control and slope protection.

2.3.1 *Reinforcement-soil interaction*

Following factors governed the effectiveness of a reinforcing element inserted in soil:

- Tensile strength of the element.

- The amount of elongation gained by the reinforcing element under tensile stress.

- The shearing resistance between the reinforcement and surrounding soil.

The mechanism by which grids and geogrids develop their shear resistance is different from that of strips, bars and sheets. The transverse element of grid develop passive resistance or bearing resistance offered by the soil which fills the aperture . The pullout

resistance is thus be a sum of the friction adhesion resistance along the longitudinal elements that are parallel to the direction of pull and the bearing capacity type of resistance along the transverse elements that are perpendicular to the direction of pull.

In case of low tensile strength, breakage or yielding of reinforcing element occur which make it ineffective. When the tensile strength is sufficient but its elongation due to tensile stress is high, then the inadequate stiffness of the soil-reinforcement system causes a large movement of soil (lateral movement or settlement). Lastly if the reinforcement is adequately rigid and strong but bond strength between the soil and the reinforcement is inadequate, this causes a relative movement, which make the reinforcement ineffective.

2.3.2 *Reinforcement of soil beneath the foundation*

Soils having low bearing capacity can be reinforced beneath shallow footings with the replacement of top weak soil with strong and dense soil, to increase the bearing capacity. These reinforcements have to be designed to withstand rupture and slippage.

Placement of reinforcement beneath footings requires excavation of the soil and backfilling in layers with careful placement of reinforcement and proper compaction of the soil. Placement of reinforcement at the interface of the footing and soil beneath can be an alternative in which excavation can be avoided. However such reinforcements are required to possess high strength, high stiffness and high shear resistance to soil, a combination of which is not feasible at present.
Placement of reinforcement in top soil below the footing produce the following effect due to which its bearing capacity and settlement behavior improve :

1. **Shear stress reduction effect:** Because of inclusion of geosynthetic layer the transmitted shear stresses, from the top soil to the the bottom soil reduces. This effect of geosynthetics inclusion called shear stress reduction effect. This effect causes

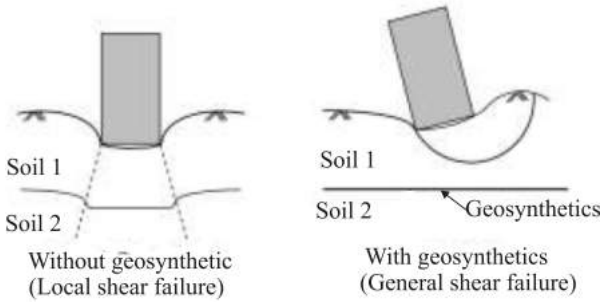

Figure 2.7: Shear stress reduction effect due to reinforcement (*Shukla and Yin, 2006*)

general-shear failure in place of local-shear failure, thus resulting in an increase in

the load-bearing capacity of the foundation.

2. **Confinement effect:** Inclusion of geosynthetic layer causes redistribution of the surface load acted on it, due to this applied normal stress on the bottom foundation soil reduced. This is called slab effect or confinement effect of geosynthetics. The friction mobilized between the soil and the geosynthetic layer plays an important role in confining the soil.

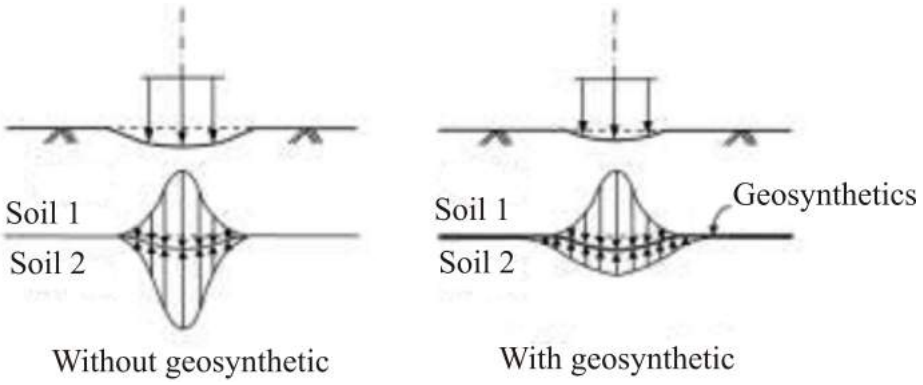

Figure 2.8: Confinement effect due to reinforcement (*Shukla and Yin, 2006*)

3. **Membrane effect:** The deformed geosynthetic, has a membrane force which has a vertical component that resists applied loads, thus the membrane effect of geosynthetics is that in which a vertical support is provided by deformed geosynthetic, to the top soil mass subjected to loading. The membrane effect of geosynthetics

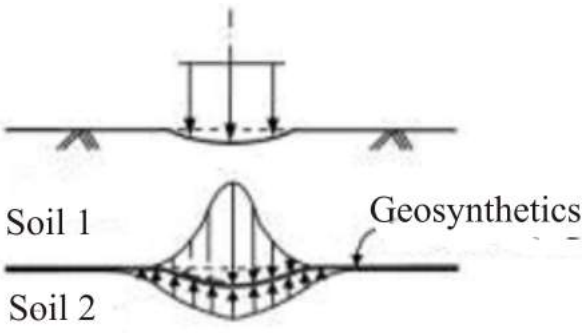

Figure 2.9: Membrane effect due to reinforcement (*Shukla and Yin, 2006*)

results in the reduction in heave potential of foundation soil.

4. **Interlocking effect** Interlocking of the soil mass through the apertures of geogrids is known as interlocking effect. In this effect stress transfer from soil to the geogrid is occured by end bearing (passive resistance). However interlocking effect is negligible, when soil particles are too small.

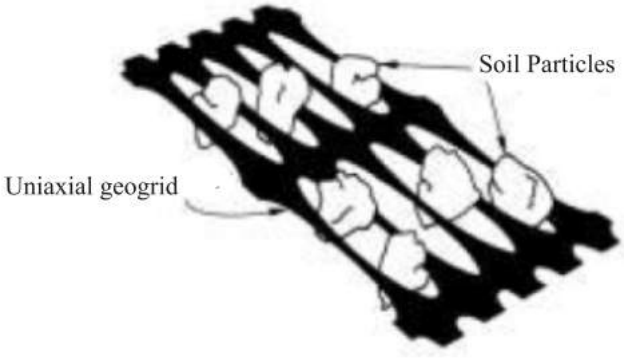

Figure 2.10: Interlocking effect of geogrid

2.4 Model and field tests in literature

Hanna (1981) conducted tests on model strip and circular footing resting on dense sand layer overlying loose as well as compacted sand in order to verify his theory. It was found that observed bearing capacity increased rapidly with increasing thickness of the dense sand below the footing base from a minimum value equal to the ultimate bearing capacity of the footing on homogenous lower weak sand layer to a maximum value equal to the ultimate bearing capacity of footing on homogenous upper strong sand layer.

Kumar and Walia (2006) proposed a method to determine the ultimate bearing capacity of a square footing placed on reinforced soil. The validation of results was done by comparing them with the model tests. These tests were conducted on two layered soil, where both layers were compacted at different densities and overlying layer was reinforced with geogrid reinforcement. Obtained values of ultimate bearing capacity were found in very good agreement with experimental results.

Mustafa Laman and Demir (2012) investigated the bearing capacity of a circular shallow rigid footing on unreinforced and geogrid-reinforced granular fill layer constructed above natural clay deposits using physical field modeling. A significant improvement in the bearing capacity of footing was found when fill layer of limited thickness was placed on soft clay subsoil and bearing capacity was further increased by the inclusion of geogrid layer within compacted fill. Geogrid reinforcement in the granular fill increases the stability of footing by mobilized tensile force in the reinforcement and providing a confining effect against lateral shear stress.

Tafreshi and Dawson (2010) performed a large number of laboratory model tests on strip footings resting on sand which is reinforced with the 3D and planar geotextiles, subjected to a combination of static and repeated loads. It was found that for the same mass of geotextile material used in the tests, behavior of 3D geotextiles reinforcement system

was much better than planar reinforcement under dynamic loading.

Sawwaf and Nazir (2012) performed an experimental study on eccentrically loaded ring footing resting on layered sandy soils. It was found that by placing a layer of compacted sand on the top of loose deposits the bearing capacity and settlement behavior of model ring footing was improved. It was also found that reinforcement of soil causes a significant reduction in the replaced sand layer depth for the same footing settlement and more improvement was achieved with more relative density of replaced sand.

Khing et al.(1994) performed laboratory model tests for determination of ultimate bearing capacity of a strip footing resting on a two layer soil system. Top layer system contained strong sand layer of limited thickness overlying weak clay. A layer of geogrid was placed at the interface of sand and clay as reinforcement. Two types of geogrids were used in these tests and it was found that optimum height of the strong sand layer should be about two-third of foundation width in order to determine maximum benefit of reinforcement.

Palmeira et al.(2010) performed a study to determine the effect of geosynthetic reinforcement in the unpaved roads on poor subgrade under cyclic loading. Nonwoven geotextile and geogrid were used as reinforcing layers placed at the interface of fill and subgrade. It was found that inclusion of reinforcement caused an significant increase in the number of load cycles for a given rut depth to be reached and reduction of stresses and strains in the subgrade. It was also found that geogrid reinforcement was more effective than geotextile.

Dutta and Mandal (2016) conducted plate load tests on unreinforced and geocell-reinforced fly ash beds placed at the top of soft Marine clay. As a separator, jute geotextile was kept on the top of clay. Geocell mattress was prepared by plastic bottles. Height and width of geocell was varied and and effects of these parameters were analyzed with the help of model test results. It was found that reinforcing the fly ash bed caused an enhancement in the bearing capacity of footing around seven times when compared with the bearing capacity of unreinforced fly ash bed. It was also found that increment in the height of fly ash caused improvement in the bearing capacity of footing.

Zhou and Wen (2008) studied the soft soil foundation problem of the Qin-Shen railway in China. The large scale laboratory model tests were carried out to analyze the effects of using geogrid and geocell-reinforced sand cushion placed at the top of soft soil on the bearing capacity of soil. In this model test a flexible lateral boundary conditions were used. Air bag were used for applying pressure. It was found that geocell-reinforced sand caused a reduction in settlement of the bottom soft soil and surface earth pressure. The deformation was reduced up to 44%.

Floss and Braeu (1990) carried out laboratory model test to simulate the behavior of geosynthetics used in roads under dynamic loading. Two layer soil system with soft

cohesive bottom soil and coarse grain top soil was tested with and without different types of geotextiles as reinforcement.It was found that intensity of loading determines the behavior of geotextile.

Dash and Sitharam (2003) performed small scale model tests to determine the effectiveness of geocell and geogrid reinforcement placed in the granular fill overlying soft clay beds. It was found that with inclusion of geocell reinforcement in the top sand layer, an improvement was observed in the load carrying capacity. It was also found that surface heaving of the foundation bed also reduced due to reinforcement. This load bearing capacity behavior further improved when an additional layer of geogrid was placed at the base of the geocell mattress.

Yadu and Tripathi (2013) conducted small scale laboratory model tests to determine effectiveness of geogrid-reinforced granular fill placed on soft subgrade soil. Substantial improvement in the bearing capacity and settlement behavior was found because of placement of geogrid in the granular fill. A significant increase in the BCR was observed upto width of geogrid to width of footing ratio of 4, but there was no significant improvement in bearing capacity ratio observed beyond this value and not significant chagnes in the settlement reduction factor (SRR) was observed beyond this ratio of 2.

Subaida and Sankar (2009) performed a experimental study to determine the effect of woven coir geotextiles placement in a two-layer pavement. It was found that ultimate bearing capacity and bearing capacity at any settlement was increased when coir geotextile was placed at mid depth of the base course. It was also found that due to reinforcement permanent vertical deformations due to repeated loading was also decreased.

Oda and Win (1990) performed model tests to determine the effect of interstratified clay layer between two sand layers on the ultimate bearing capacity of strip footing lies on the top soil. It was found that inclusion of a clay layer between two sand layers reduces the ultimate bearing capacity even at a depth five times grater than the width of the footing. This reduction depends on the thickness and depth of clay layer. It was also found that the appreciable amount of plastic strain occurs in a clay layer which causes a decrease in the stability of the upper sand bed.

Batali and Klompmaker (2014) performed an insitu experimental test to verify the real behavior of geosynthetic reinforcement. Authors monitored a geosynthetic reinforced working platform in terms of stresses and starins, to prepare a finite element model to varify the experimental results. It was observed that the real level of stress and strain in geosynthetic, compared to overall stress-strain curve of the material was very low and outcome of numerical analysis, which used a non-linear Mohr-Coulomb model matched the results obtained by insitu experiments.

Table 2.1: Model and field tests

Author	Test	Shape of footing	Type of Load	Top soil	Bottom soil	Reinforcement
Hanna et al. (1981)	Model	Strip, circular	Static	Dense sand	Loose and compacted sand	None
Ibrahim et al. (2014)	Field	Circular	Static	Granular sandy	Saturated soft clay	None
Kumar and Walia (2006)	Model	Square	Static	Well graded sand	Poorly graded sand	Geogrid
Tafreshi and Dawson (2010)	Model	Strip	Cyclic	Silica sand	Silica sand	Planer and 3D geotextiles
Sawwaf and Nazir (2012)	Model	Ring	Eccentric	Compacted sand	Loose sand	Geogrid
Ornek and Laman (2012)	Field	Circular	Static	Compacted granular fill	Natural clay	Geogrid
Khing et al. (1994)	Model	Strip	Static	strong sand	Weak clay	Geogrid
Dutta and Mandal (2016)	Model	Square	Static	Fly ash	Soft clay	Geocell mattress with Jute geotextile
Palmeira et al. (2010)	Model	Circular	Static and Cyclic	Well graded gravel	Highly plastic clay	Geogrid and woven Geotextile
Zhou and Wen (2008)	Model	Air bags	Static	Sand cushion	Soft soil	Geogrid and Geocell
Floss and Braeu (1990)	Model	Circular	Dynamic	Coarse grain	Soft cohesive	Geotextiles
Dash and Sitharam (2003)	Model	Circular	Static	Dry sand	Silty clay	Geocell mattress and geogrid
Yadu and Tripathi (2013)	Model	Strip	Static	Granulated blast furnace slag	Soft clay	Geogrid
Subaida and Sankar (2009)	Model	Circular	Monotonic and repeated	Well graded crushed stone	Highly plastic clay	Woven coir geotextiles

2.5 Numerical investigations in literature

Cicek and Guler (2015) proposed a limit equilibrium method to determine the bearing capacity of strip footings on geosynthetic reinforced sand soils and compared with the bearing capacities obtained from Finite Element. A two-layered granular soil was consisting of the loose in situ soil and the compacted fill above the reinforcement. The bearing capacities were also calculated for different reinforcement geometries and soil properties. The bearing capacities obtained from Finite Element and Limit Equilibrium analyses were seen in a good agreement. The ultimate bearing capacities of reinforced

soils for two extreme geosynthetic lengths were considered. One extreme is the case where the reinforcement length is equal to the footing width (L = B). The second extreme is that a very long reinforcement is used. When results are evaluated it was determined that for L $\geq$ 4B, the case of long reinforcement is valid. It was also found that the bearing capacities determined for the long reinforcement is 1.23 times higher than the bearing capacity obtained for the short reinforcement length (L = B). However, an improvement is also obtained for a reinforcement that is only as wide as the footing itself.

Ibrahim et al. (2014) performed numerical analysis using Mohr Column model and results was ensured by the field plate loading observations. It was found that ultimate bearing capacity is directly proportional to the angle of internal friction of granular soil, the granular layer thickness, extension of granular soil and the foundation depth while at the same time it is inversely proportional to the footing diameter. The ultimate bearing capacity of surface footing was increased about 67% when granular soil changes from medium to very dense sand.

Demir and Ornek (2014) investigated the bearing capacity of a circular rigid footing on geogrid-reinforced granular fill layer constructed above natural clay deposits using 3D finite element program Plaxis and compared its results with results of physical field modeling. It was found that results from the numerical analysis were closely matched with those from physical model tests for short term stability. Reduction in the horizontal and vertical displacements for reinforced case was also found from numerical analysis.

Mosadegh and Nikraz (2015) investigated two cases to determine bearing capacity of foundation and to determine the influence of various parameters on ultimate bearing capacity, using finite element software ABAQUS. In first case foundation was placed on one layer soil and in second case foundation was resting on two layer soil systems. In two layer system it was found that bearing capacity decreases by adding the clay layer on the top of sand layer.

Burd and Frydman (1997) carried out a study of bearing capacity of sand layers overlying clay soils. A parametric study was also carried out using both finite element and finite difference methods. It was found that load spread angle increased with increasing sand friction angle.

Zhu and Michalowski (2005) performed a finite element analysis of square and rectangular footings over two layer clay foundation soil. Variation of bearing capacity was determined with different variables. It was found that bearing capacity of clay was reduced if a weaker layer of clay is present below a stronger one and bearing capacity was affected by by both the depth of the weaker layer and the ratio of the strengths of the two layers. Shape factors were found to vary distinctly with the change in the strength ratio of two layer and depend weakly on the depth.

Ghazavi and Eghbali (2008) developed a analytical limit equilibrium method for calcu-

lating bearing capacity factors of shallow footing placed on a two layered granular soil system. Then the ultimate bearing capacity computed from the equivalent bearing capacity factors N_q and N_γ was compared with ultimate bearing capacity obtained from finite element method. It was found that results obtained from the proposed method were acceptably comparable with those obtained by FEM.

Table 2.2: Numerical investigations

Author	**Program**	**Shape of Footing**	**Soil Model**	**Top Soil**	**Bottom Soil**	**Reinforcement**
Ibrahim et al. (2014)	PLAXIS	Circular	Mohr-Coulomb	Granular	Saturated soft clay	None
Guler and Cicek (2015)	PLAXIS	Strip	Mohr-Coulomb	Strong sand	Weak sand	Geosynthetics
Mosadegh and Nikraz (2015)	ABAQUS	Strip	Drucker-Prager	Soft clay	Dense sand	None
Burd and Frydman (1997)	OXFEM FLAC	Strip	Mohr-Coulomb	Sand	Clay	None
Demir and Ornek (2014)	PLAXIS	Circular	Mohr-Coulomb	Compacted granular fill	Natural clay	Geogrid
Zhu and Michalowski (2005)	ABAQUS	Rectangular square and strip	Drucker-Prager	Compacted Strong clay	Weak clay	None
Merifield and Nguyen (2006)	ABAQUS	Circular square and strip	Mohr-Coulomb	Strong and weak clay	Weak and strong clay	None
Zhu (2006)	ABAQUS	strip	Mohr-Coulomb	Weak and strong clay	Strong and weak clay	None

Merifield and Nguyen (2006) performed a finite element analysis to determine the undrain bearing capacity of footings placed on layered clays. The soil profile was assumed to consist two clay layers. The results were compared with previous solutions. It was found that when soft clay is placed on strong clay layer with ratio of depth of top soil to width of footing is more than 0.375, the contribution of stronger bottom layer was very less in the ultimate bearing capacity, irrespective of the ratio of undrain shear strengths of soils but for this ratio less than 0.375 bearing capacity factor increases with the decrease in ratio of undrain shear strength of clays. It was also found that bearing capacity reduces when strong clay placed on soft clay, up to a depth of top layer to width of footing ratio less than 1, for this ratio more than 1 failure was likely to be occur within top layer only.

Zhu (2004) carried out a parametric study to determine the ultimate bearing capacity of a rough strip footing resting on two-layer clay soil. It was found that when soft clay is placed on strong clay, the bearing capacity factor decreases as thickness of the top layer increases. Where as, when strong clay is placed on soft clay, a critical depth was found where the shear strength of the bottom layer does not affect the bearing capacity and failure mechanism was contained in the top layer only.

Chapter 3

Numerical Modelling

There are four major approaches to determine the bearing capacity of footing: limit equilibrium, limit analysis approach, semi empirical approach and finite element method. Finite Element Method (FEM) is widely used in geotechnical studies to investigate soil behavior. Finite element method based computer programs are develop, which are used as the powerful tool for solving complex problems.

3.1 Finite element method

The finite element method (FEM) is a numerical technique for finding approximate solutions to boundary value problems for partial differential equations. The basic concept in the FEM is that in this method numerical model is devided into non-overlapping elements of simple geometry called finite elements. Elements are connected to each other at nodes. Each node contains a finite number of degrees of freedom.

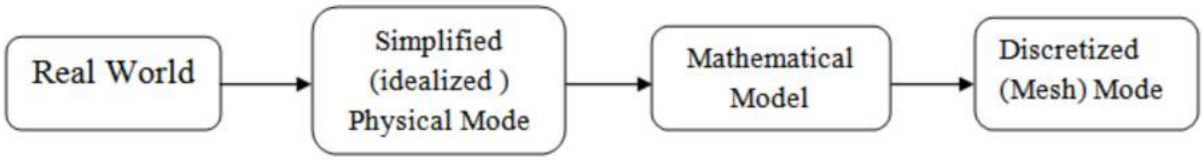

Figure 3.1: Finite element method

3.1.1 *Element nodes*

In one-dimension, elements are usually straight lines or curved segments. In two dimensions they are of triangular or quadrilateral shape. In three dimensions the most

common shapes are tetrahedra, pentahedra (also called wedges or prisms), and hexahedra. Each element possesses a set of distinguishing points called nodal points or nodes. Nodes are usually located at the corners or end points of elements. In refined or higher-order elements nodes are also placed on sides or faces, as well as possibly at the interior of the element.

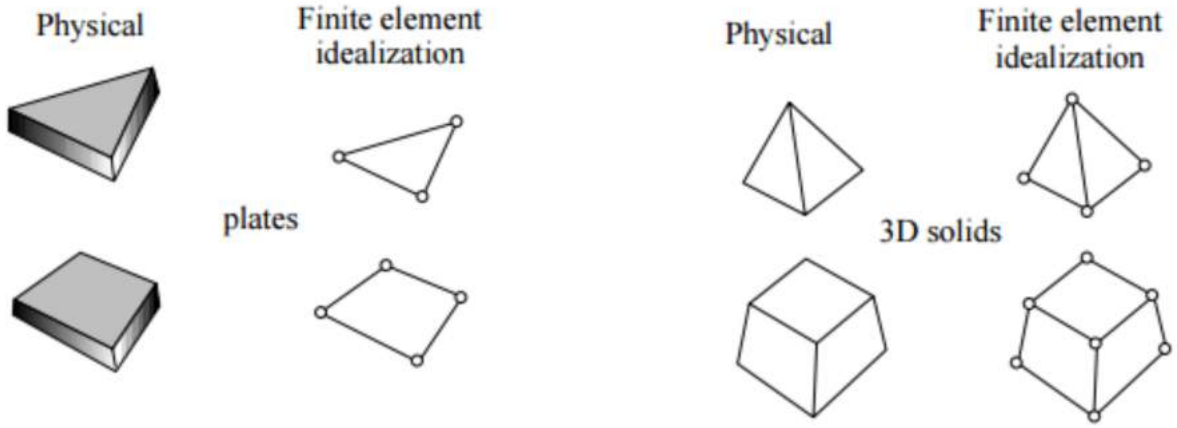

Figure 3.2: Finite element idealization examples

3.1.2 *Shape Functions*

The shape of the any finite element model between nodes of model, is approximated by functions. These functions called shape functions which allow to relate the coordinates of every point of a finite element with the positions of its nodes. Thus The shape function is the function which interpolates the solution between the discrete values obtained at the mesh nodes.
With in an element the displacement field {u} is obtained from the discrete nodal displacement values {v} using interpolation function or shape function assembled in matrix form [N]:

$$\{u\} = [N]\{v\} \tag{3.1}$$

3.1.3 *Stiffness matrix*

For a structural finite element, the stiffness matrix contains the geometric and material behavior information. Nodal displacement function can be detrmined from the following equation. Where {F} is the applied force vector for each degree of freedom on nodes and [k] is the stiffness matrix. The stiffness matrix for whole system can be obtained by

simply superposition of the individual element stiffness matrices.

$$\{v\} = [k]^{-1}\{F\} \tag{3.2}$$

3.2 Soil models used in the simulation

A material model gives a relationship between stress and strain in the form of mathematical equations. Behavior of soil is complicated, it behaves non-linearly and often shows anisotropic and time dependent behavior when subjected to stresses. Under working loading condition Hooke's law of linear elasticity is used to describe soil behavior and under collapse state Coulomb's law of perfect plasticity is used to describe soil behavior. The combination of Hooke and Coulomb's law is formulated in a plasticity framework and is known as Mohr-Coulomb model. Soil behavior is not linearly elastic and perfectly plastic for the entire range of loading, but it is different in primary loading, unloading and reloading. Several researchers have proposed various constitutive models to describe complicated soil behavior in details and to apply such models in finite element modelling for geotechnical engineering applications. However no soil constitutive model is available that can completely describe the complex behavior of real soils under all conditions.

3.2.1 *Linear elastic model*

The linear elastic model will well represent the engineering materials up to their elastic limit. This model is based on Hook's law of isotropic elasticity. It involves two basic elastic parameters, i.e. Young's modulus E and Poisson's ratio ν. It will also represent the complete stress-strain response up to the point of fracture of many very brittle materials.The response of a linear elastic material, where the stress is proportional to the strain, is shown in Fig. 3.3

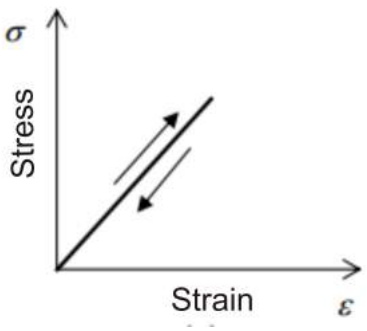

Figure 3.3: Linear elastic model

$$\{\sigma\} = [D]\{\varepsilon\} \tag{3.3}$$

where
$\{\sigma\}$ = stress vector,
$[D]$ = stiffness matrix,
$\{\epsilon\}$ = Strain vector.

$$\{\sigma\} = \begin{bmatrix} t_x \\ t_y \\ t_z \end{bmatrix} = \begin{bmatrix} \sigma_{xx} & \sigma_{xy} & \sigma_{xz} \\ \sigma_{yx} & \sigma_{yy} & \sigma_{yz} \\ \sigma_{zx} & \sigma_{zy} & \sigma_{zz} \end{bmatrix} \tag{3.4}$$

For moment equilibrium of the element, the following shear stress relationships are required:

$$\sigma_{xy} = \sigma_{yx} \qquad \sigma_{yz} = \sigma_{zy} \qquad \sigma_{zx} = \sigma_{xz} \tag{3.5}$$

Which implies that only six components are required to define the whole stress state of an element or elastic soils.
Where, σ_{xx} indicates the normal stress component in direction of x-axis and acting on plane which is perpendicular to x-axis. σ_{xy} and σ_{xz} denote the shear stress components acting on plane which is perpendicular to x-axis, in direction of y-axis and z-axis respectively, similarly for others. This implies that subscripts describe the working direction of stress components. The strain components can be expressed as strain tensor as given below:

$$\{\varepsilon\} = \begin{bmatrix} \varepsilon_{xx} & \varepsilon_{xy} & \varepsilon_{xz} \\ \varepsilon_{yx} & \varepsilon_{yy} & \varepsilon_{yz} \\ \varepsilon_{zx} & \varepsilon_{zy} & \varepsilon_{zz} \end{bmatrix} \tag{3.6}$$

$$\varepsilon_{xy} = \varepsilon_{yx} \qquad \varepsilon_{yz} = \varepsilon_{zy} \qquad \varepsilon_{zx} = \varepsilon_{xz} \tag{3.7}$$

Where, ε_{xx} indicates the normal strain component in direction of x-axis and acting on plane which is perpendicular to x-axis. ε_{xy} and ε_{xz} denote the shear strain components acting on plane which is perpendicular to x-axis, in direction of y-axis and z-axis respectively, similarly for others.

$$[D] = \frac{E}{(1+\nu)(1+2\nu)} \begin{bmatrix} 1-\nu & \nu & \nu & 0 & 0 & 0 \\ \nu & 1-\nu & \nu & 0 & 0 & 0 \\ \nu & \nu & 1-\nu & 0 & 0 & 0 \\ 0 & 0 & 0 & \frac{(1-2\nu)}{2} & 0 & 0 \\ 0 & 0 & 0 & 0 & \frac{(1-2\nu)}{2} & 0 \\ 0 & 0 & 0 & 0 & 0 & \frac{(1-2\nu)}{2} \end{bmatrix} \tag{3.8}$$

For geotechnical purposes, it is more convenient to characterize soil behavior in terms of shear modulus G and bulk modulus K.
Since,

$$G = \frac{E}{2(1+\nu)} \qquad K = \frac{E}{3(1-2\nu)} \tag{3.9}$$

So,

$$[D] = \begin{bmatrix} K + \frac{4G}{3} & K - \frac{2G}{3} & K - \frac{2G}{3} & 0 & 0 & 0 \\ K - \frac{2G}{3} & K + \frac{4G}{3} & K - \frac{2G}{3} & 0 & 0 & 0 \\ K - \frac{2G}{3} & K - \frac{2G}{3} & K + \frac{4G}{3} & 0 & 0 & 0 \\ 0 & 0 & 0 & G & 0 & 0 \\ 0 & 0 & 0 & 0 & G & 0 \\ 0 & 0 & 0 & 0 & 0 & G \end{bmatrix} \tag{3.10}$$

As we know that soil behavior is highly nonlinear and irreversible thus linear elastic model is not suitable to model soil.

3.2.2 *Mohr-Coulomb model*

Mohr-Coulomb model is an elastic-perfectly plastic model which is often used to model soil behaviour in general. Stress-strain curve behaves linearly in the elastic range, this behavior can be defined by two parameters, from Hooke's law these parameters are Young's modulus (E) and Poisson's ratio (ν). Parameters which defines the failure criteria are the friction angle (ϕ), cohesion (c) and dilatancy angle (ψ).

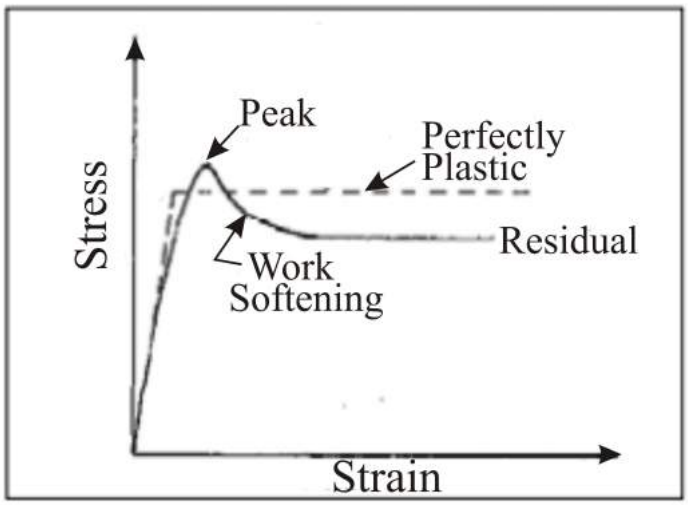

Figure 3.4: Elastic-perfectly plastic assumption for Mohr-Coulomb model (*Kok Sien Ti and Sew, 2009*)

Stress-strain relationship for linear elastic perfectly plastic behavior :

Figure shows linear elastic perfectly plastic stress-strain response. The stress-strain relation can be expressed as following:

$$d\underline{\sigma}' = \underline{\underline{D}}^{ep} \times d\underline{\varepsilon} \tag{3.11}$$

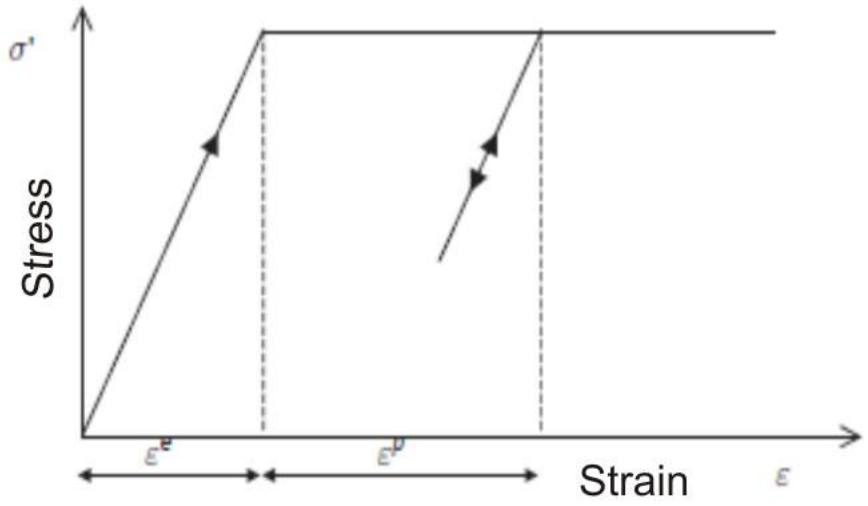

Figure 3.5: Elastic-perfectly plastic model (*Brinkgreve and Vermeer, 2013*)

where,

$d\underline{\sigma}'$ = Total incremental effective stress vector

$\underline{\underline{D}}^{ep}$ = Elasto-plastic stiffness matrix

$\underline{\varepsilon}$ = Total incremental strain vector

The total incremental strain can be decomposed into elastic part and plastic part:

$$d\underline{\varepsilon} = d\underline{\varepsilon}^e + d\underline{\varepsilon}^p \tag{3.12}$$

Since, the total incremental effective stress is related to the incremental elastic strain by Hooke's law. Then,

$$d\underline{\sigma}' = \underline{\underline{D}}^e \times d\underline{\varepsilon}^e = \underline{\underline{D}}^e \times (d\underline{\varepsilon} - d\underline{\varepsilon}^p) \tag{3.13}$$

Now, incremental plastic strain can be expressed as following:

$$d\underline{\varepsilon}^p = \lambda \frac{\partial q}{\partial \underline{\sigma}'} \tag{3.14}$$

where λ is plastic scalar multiplier and q is a plastic potential function.

$$\text{For} \quad f < 0, \quad \lambda = 0 \quad \text{(Elasticity)} \tag{3.15a}$$

$$\text{For} \quad f = 0, \quad \lambda > 0 \quad \text{(Plasticity)} \tag{3.15b}$$

From above written equations, the following relation can be expressed:

$$d\underline{\sigma}' = \underbrace{\left(\underline{\underline{D}}^e - \frac{\alpha}{d}\underline{\underline{D}}^e \frac{\partial q}{\partial \underline{\sigma}'} \frac{\partial f^T}{\partial \underline{\sigma}'} \underline{\underline{D}}^e\right)}_{\underline{\underline{D}}^{ep}} \times d\underline{\varepsilon} \tag{3.16a}$$

where,

$$d = \frac{\partial f^T}{\partial \underline{\sigma}'} \underline{\underline{D}}^e \frac{\partial q}{\partial \underline{\sigma}'} \tag{3.16b}$$

Where α is used as switch parameter: for elastic and plastic behavior $\alpha = 0$ and 1 respectively.

Formulation of Mohr-Coulomb model:

From equations 3.16a and 3.16b, it can be seen that in stress-strain relationship, elasto-plastic stiffness matrix is a function of elastic stiffness matrix which is already defined in equation 3.8 and derivatives of yield function and plastic potential function with respect to effective stresses. For evaluation of elasto-plastic stiffness matrix, yield function and plastic potential function are required to express. Therefore, different models have different expression of stiffness matrix. Mohr-Coulomb failure criterion is illustrated in Figure 3.6 and expressed in equation 3.17.

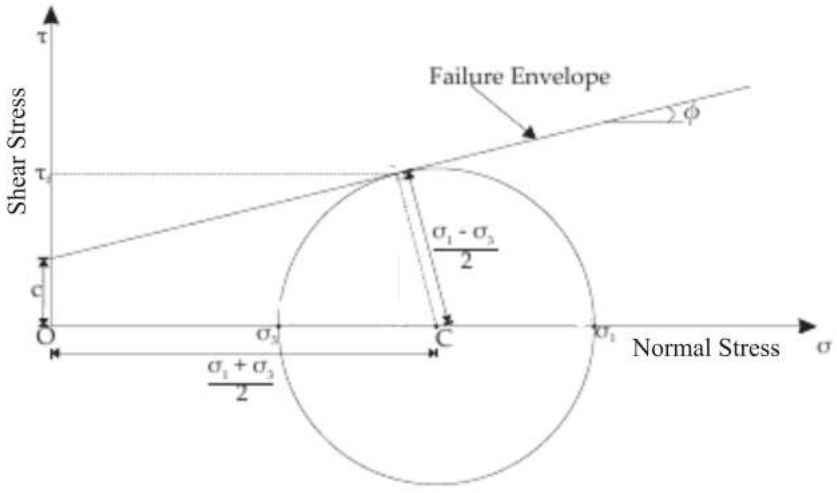

Figure 3.6: Graphical representation of Mohr-Coulomb failue surface

$$\tau_f = c + \sigma'_n \tan\phi \tag{3.17}$$

From figure 3.6, equation 3.17 can be exprssed in terms of principle stresses.

$$\frac{\sigma'_1 - \sigma'_3}{2} = \frac{\sigma'_1 + \sigma'_3}{2} \sin\phi + c\cos\phi \tag{3.18}$$

Since six yield functions exist in this model. Therefore one of the yield function can be expressed like this:

$$f = \frac{\sigma'_1 - \sigma'_3}{2} - \frac{\sigma'_1 + \sigma'_3}{2} \sin\phi - c\cos\phi \leq 0 \tag{3.19}$$

where,
τ_f = Failure Shear stress,
c = Cohesion of soil,
ϕ = Friction angle,
σ'_n = Effective normal stress,
σ'_1 = Effective major principal stress,
σ'_3 = Effective minor principal stress.

When plastic behavior occurs, all yield functions have zero value. And these functions create a fixed hexagonal cone in principal stress space as illustrated in Figure 3.7.

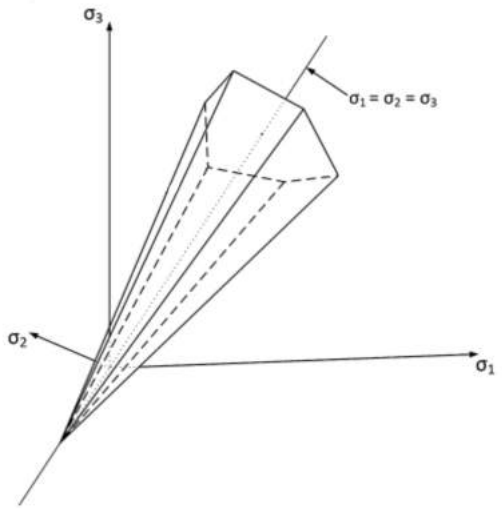

Figure 3.7: Mohr-Coulomb yield surface in principal stress space

3.2.3 *Hardening soil model*

The hardening soil model does not have a fixed yield surface, but can expand due to plastic straining. There are shear and compression two type of hardening. Shear hardening is used to model irreversible strains due to primary deviatoric loading whereas compression hardening is used to model irreversible plastic strains due to primary compression in oedometer loading and isotropic loading. Some features of the model are:

- Stress dependent stiffness according to power law through a parameter- m

- Plastic straining due to primary deviatoric loading- E_{50}^{ref}
- Plastic straining due to primary compression- E_{oed}^{ref}
- Elastic unloading/reloading- E_{ur}^{ref}, ν_{ur}
- Failure according to Mohr-Coulomb criterion- c, φ and ν

For stress dependency on stiffness and oedometer conditions of stress and strain, the value of m is considered 1 for soft soils. In such cases, a relationship between the modified compression index λ^* as:

$$E_{oed}^{ref} = p_{ref}/\lambda^* \tag{3.20}$$

$$\lambda^* = \lambda/(1 + e_0) \tag{3.21}$$

where p_{ref} is the reference pressure. In a similar way, the unloading-reloading modulus relates to the modified swelling index κ^* or to standard swelling index κ as:

$$E_{ur}^{ref} \simeq 2p_{ref}/\kappa \qquad\qquad \kappa* = \kappa/(1 + e_0) \tag{3.22}$$

The various other parameters used in the hardening soil model are related to each other in various forms. The parameter E_{50} is the confining stress dependent stiffness modulus for primary loading given by:

$$E_{50} = E_{50}^{ref}(\frac{c\cos\varphi - \sigma_3^{'}\sin\varphi}{c\cos\varphi + p_{ref}\sin\varphi})^m \tag{3.23}$$

where E_{50}^{ref} is the reference stiffness modulus corresponding to the reference confining pressure p^{ref}= 100 stress units. The value of m is within 0.5-1 as per different reports. The ultimate deviatoric stress, q_f and the quantity q_a are given as:

$$q_f = (c\cot\varphi - \sigma_3^{'})\frac{2\sin\varphi}{1-\sin\varphi} \qquad\qquad q_a = \frac{q_f}{R_f} \tag{3.24}$$

where R_f refers to the failure ratio, obviously less than 1.

$$E_{ur} = E_{ur}^{ref}(\frac{c\cos\varphi - \sigma_3^{'}\sin\varphi}{c\cos\varphi + p_{ref}\sin\varphi})^m \tag{3.25}$$

where E_{ur} is the reference Young's modulus for unloading and reloading, corresponding to the reference pressure p^{ref}.
The hardening soil models is specially useful in dynamic calculations. There is a strong need to correctly specify elastic stiffness parameter E_{ur}^{ref} to calculate the wave velocities correctly. Plastic strains will be generated when subjected to cyclic or dynamic loading. Rayleigh damping may be defined to account for the damping characteristics in the soil. Figure 3.9 shows the failure contour for the Hardening soil model in the principal stress plane.

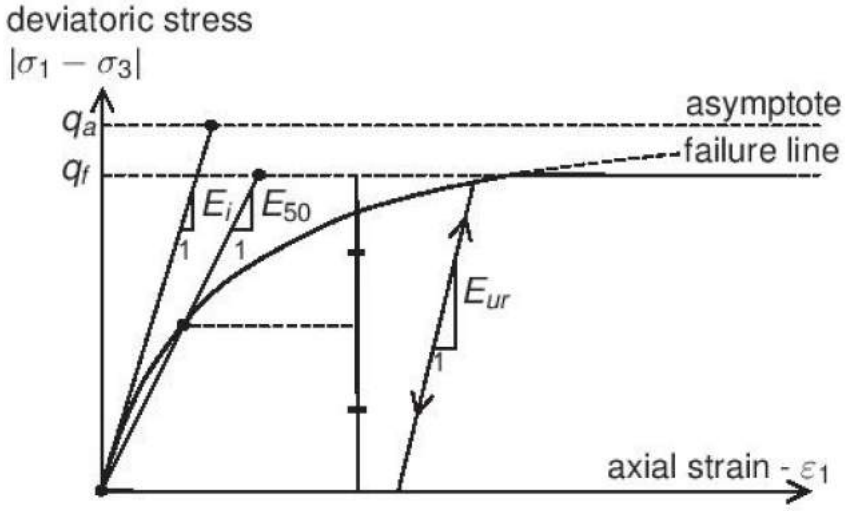

Figure 3.8: Hyperbolic stress-strain relation in primary loading for a standard drained triaxial test *(Plaxis 3D 2013.01 material models manual)*

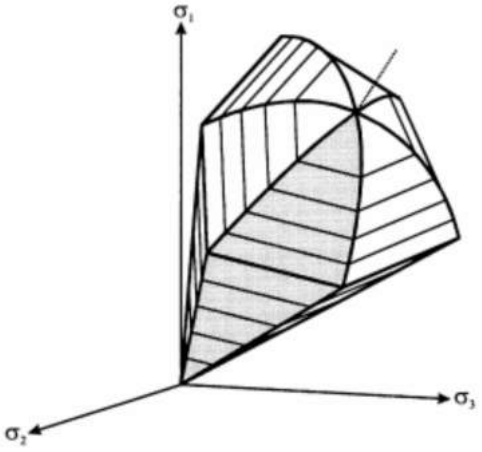

Figure 3.9: Representation of the total yield contour of the Hardening soil model in principal stress space for cohesionless soil *(Schanz and Bonnier, 1999)*

3.2.4 *Hardening soil model with small strain stiffness (HSS)*

The Hardening soil model assumes elastic behavior of material during unloading and loading. However the starin range in which soils can be considered truly elastic, is very small. With increasing starin amplitude, soil stiffness decays nonlinearly. Curve plotted between soil stiffness and log of strain is a S shape curve and called stiffness reduction curve shown in figure 3.10. According to figure 3.10. the soil stiffness related to the strain at the end of any construction should not be used in the analysis of geotechnical structures. But non-linear dependency of very small soil stiffness on strain amplitude should be properly taken into account.

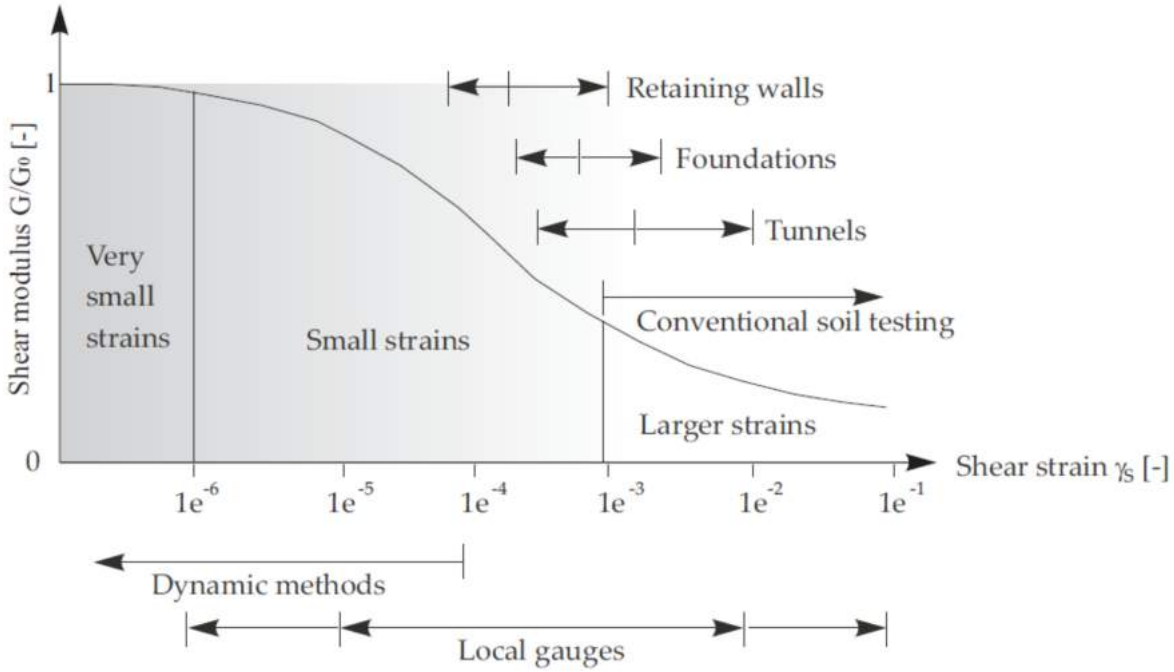

Figure 3.10: Characterstic stiffness-strain behavior of soil with typical strain ranges *(Atkinson and Sallfors, 1991)*

The HS Small model used in PLAXIS is based on the Hardening soil model and uses two addtional parameters required to describe the variation of stiffness with strain:

- The initial or very small-strain shear modulus G_0.
- The shear strain level $\gamma_{0.7}$ at which the secant shear modulus G_s is reduced to about 70% of G_0.

3.3 Dynamic calculations and simulations

3.3.1 *Equation for dynamic behavior*

The basic equation of time dependent movement of a volume under the influence of dynamic load is

$$[M]\{\ddot{u}\} + [C]\{\dot{u}\} + [K]\{u\} = [F] \tag{3.26}$$

where,

$[M]$ = mass matrix,
{u} = displacement vector,

$[C]$ = damping matrix,
$[F]$ = load vector.

The displacement u, velocity $\dot{u}$ and acceleration $\ddot{u}$ can vary with time. $[K]\{u\} = [F]$ term denotes the static deformation.

Damping matrix

The matrix [C] represents the material damping of the materials. With more viscosity and plasticity more energy can be dissipated. In finite element calculations [C] is formulated as a function of mass and stiffness matrices.

$$[C] = \alpha_R[M] + \beta_R[K] \tag{3.27}$$

where α_R and β_R Rayleigh coefficients.

3.3.2 *Model boundaries*

Precribed boundary displacements are used at the boundaries of finite element model to make them completely free or fix, when static analysis is performed. For dynamic analysis the boundaries should be placed further away than those of static analysis, otherwise reflection of stress waves from the boundaries will takes place and causing the distortions in computed results. But it is not possible to place the boundaries too far because it requires a lot of extra memory and large calculation time. Thus to prevent these reflections, special measures are adopted, which are called 'viscous or silent boundaries'.

Viscous boundaries

In viscous boundaries a damper is used instead of applying prescribed displacements at the boundaries in a certain direction. The damper absorbs the increase in stress on the boundary and prevent reflection.

In PLAXIS viscous boundary are used according to the method described by *Lysmer and Kuhlemeyer (1969)*. The normal and shear stress components absorbed by a damper in x direction are:

$$\sigma_n = -C_1 \rho V_p \dot{u}_x \tag{3.28a}$$

$$\tau = -C_2 \rho V_s \dot{u}_y \tag{3.28b}$$

where,
ρ = density of material,
V_p = pressure wave velocity,
V_s = shear wave velocity,

C_1 and C_2 are relaxation coefficients. It was found till now that use of $C_1 = 1$ and $C_2 = 0.25$ results in a reasonable absorption of waves at boundary.

3.4 Numerical modelling of geogrids and geosynthetics

When a foundation soil is reinforced using geosynthetic reinforcement, the reinforcement is always covered with a soil layer. Therefore, in general there are two soil layers below the foundation. It is also knowm from literature that the effect of reinforcement changes with increasing the distance of reinforcement from the base of the footing. Geogrid can only sustain tensile forces and no compression. These objects are generally used to model soil reinforcement.

3.4.1 *2D Geogrids*

In 2D geogrids are composed of line elements with two translational degrees of freedom in each node (u_x,u_y). Figure 3.11 represent the positions of nodes and stress points in geogrid element.

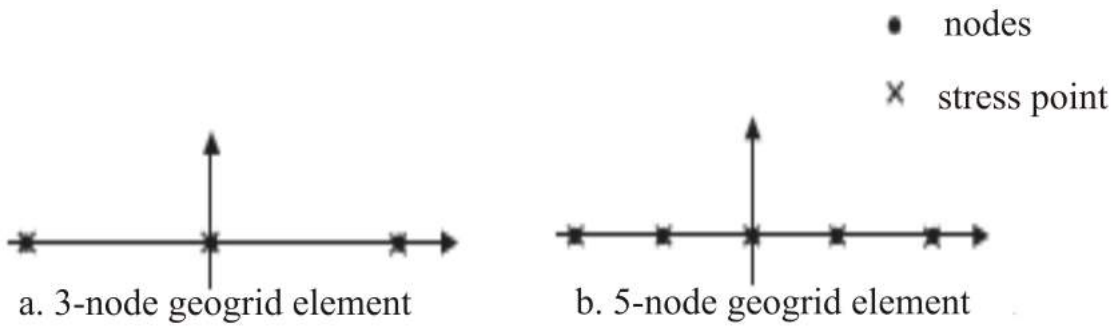

Figure 3.11: Position of nodes and stress points in geogrid elements(*Brinkgreve and Vermeer, 2013*)

The relationship between the force and the strain in axysymmetric model is defined as:

$$\begin{bmatrix} N \\ H \end{bmatrix} = \begin{bmatrix} EA_1 & 0 \\ 0 & EA_2 \end{bmatrix} \begin{bmatrix} \varepsilon \\ \varepsilon_H \end{bmatrix} \tag{3.29}$$

where H is the hoop force, N is the tension force and ε_H is the hoop strain.
For plane strain model $H = 0$.

Chapter 4

Silent Boundary Scheme

In many problems of engineering and physics semi-infinite domains exist, for example modeling of the soil underneath a footing. However, every numerical model must be terminated at some finite boundary. In numerical simulations of problems involving wave propagation, the use of finite boundaries leads to reflection of waves upon reaching the boundaries of the mesh. These reflected waves get superimposed with progressing waves and distort the computed results. This problem can be slove by placing boundary at a larger distance. But this requires introduction of a large number of elements to model regions and take more memory and time for computation. In addition for computational efficiency it is desirable to place the boundary as close as possible to the finite structure. Thus there is a need to create a boundary which is perfectly radiating to outgoing waves and transparent to incoming waves, this boundary is called Silent Boundary. Silent boundaries are also called absorbing boundaries or transmitting boundaries or non-reflecting boundaries.

There are various method developed by many researchers which are adopted for providing Silent Boundaries:

- Where the infinite boundary condition is specified at a finite boundary placed at a large distance from object.
- Using infinite element.
- Use of standard viscous boundaries.
- Use of Unified viscous boundaries.
- Use of Viscous-spring transmitting boundary.
- Use of Paraxial boundary conditions.
- Use of Perfectly Matched Layer method.
- Use of Extended boundary.

Above methods of providing silent boundaries are investigated by many researchers, and introduction and application of each of above method of proving silent boundary is given in the wide literature review.

4.1 Investigations on silent boundary scheme in literature

Lysmer and Kuhlemeyer (1969) proposed a general method through which an infinite system is approximated by a finite system with a special viscous boundary condition by absorbing the striking waves towards the boundary. Different possibilities of expressing this boundary condition were investigated by the writers and they have found that the most promising way is to express it by the conditions given below:

$$\sigma = -a\rho V_p \dot{w} \tag{4.1a}$$

$$\tau = -b\rho V_s \dot{u} \tag{4.1b}$$

where,
σ and τ are the normal and shear stresses. respectively. $\dot{w}$ and $\dot{u}$ are the normal and tangential velocities of boundary points respectively.

V_p = velocities of P-waves = $\sqrt{\frac{E}{\rho}}$

V_s = velocities of S-waves = $\sqrt{\frac{G}{\rho}}$

where, E and G are young's modulus of elasticity and shear modulus of material respectively in which wave propagates and a and b are dimensionless parameters.

It was found that the viscous boundary corresponding to a = b = 1 gives maximum absorption and is 98.5% effective in absorbing P-waves and 95% effective in absorbing S-waves and nearly perfect absorption is obtained when angle of incident from horizontal is greater than 30°. Viscous boundary corresponding to a = b = 1 is called standard viscous boundary.

According to Miller and Pursey 67% of the energy radiating from a vertically vibrating footing is transmitted in the form of a Rayleigh wave and this type of wave cannot be completely absorbed by standard viscous boundary. Therefore a viscous boundary was also designed to absorb Rayleigh waves. It is similar to the standard viscous boundary except that the parameters a and b vary with the distance from free surface.

The above method was applied to the foundation vibration problem. Then displacement functions were found by using both standard viscous boundary and Rayleigh wave boundary and results were compared with the existing solution for infinite system. A

significant gain in accuracy was found by using Rayleigh wave boundary over standard viscous boundary. Then the effect of embedment of a vibrating and rough footing in to soil was also analyzed here which was unsolvable before.

Kim (2014) investigated the validity of the silent boundary conditions proposed by two researchers. Lysmer-Kuhlemeyer proposed a=b=1 and White et al. suggested the different values of a and b for different poison's ratio. In analytical study it was found that the Lysmer-Kuhlemeyer absorbing boundary is perfectly satisfied, when wave attacks the boundary perpendicularly and performance of boundaries of White et al. was not perfect for absorbing S waves.
In numerical study boundaries were modeled as semicircles and as rectangles, to examine the absorbing boundaries for waves attacking perpendicularly and having inclined angles of incidence. Dashpots were installed on the boundaries to simulate infinite domains. It was found that absorption ratio was smaller when wave attacking the boundary with an inclination than for the wave perpendicular to the boundary.

Kim (2012) performed a study to improve the capacity of viscous boundary conditions using dashpots. It was found that using the concept of energy ratio between the transmitted energy of reflected and incident wave the efficiency of viscous boundary condition can be improved for an arbitrary angle of incidence and materials.

Shen and Chen (2005) developed a simple silent boundary method for dynamic analysis. By using this method dynamic deformation could be simulated in a small computational domain without discretizing the whole problem domain. It was found that this method could effectively reduce the reflection of incident longitudinal, shear and lateral stress waves with good convergence in terms of mesh size and number of material points per cell in MPM. A better understanding on the failure mechanisms of film delamination was obtained with the use of proposed silent boundary method as compared with the fixed boundary and it was found that convergence is more closely tied to the number of particles in each cell then cell size.

Ross (2004) presented four typical methods for applying a silent boundary for an infinite domain. These are plane wave approximation (PWA), viscous damping boundary method, perfectly matched layers (PML) and infinite elements. The PWA is a boundary element method for creating a silent boundary and ideally suited for fluid media. Viscous damping boundary method is similar to PWA and is used for elastic media. In PML the boundary layer is made of the same elements as computational domain however boundary layer has slightly different properties. In this method a new wave equation is constructed which creates plane waves that decay exponentially in the PML and will have the same form at the interface of the computational domain and the PML, thus any propagating waves get pass through the interface without generating any reflected wave. In the infinite elements the basic idea is to place element with special shape function to represent the infinite boundary.

Kellezi (2000) proposed a cone boundary for transient analysis. This boundary condition includes both a dashpot and a spring to simulate infinite boundary condition. In this paper, method of analyzing problems in dynamic soil-structure-interaction (SSI) was investigated. To analyze only a finite region of the foundation medium transmitting or silent boundaries were provided to prevent the reflection of outgoing waves at boundary region. Plane strain analysis and axisymmetric analysis were performed using finite element models and transmitted boundaries. It was found that performance of proposed silent boundaries were better than viscous boundaries. Thus an improvement was reported when unified dashpot is combined with the stiffness of the cones.

Liu and Jerry (2003) proposed a gradually damped artificial boundary to simulate a non-reflecting boundary condition. The damping was applied by an exponentially increasing function. This boundary was employed to analyze a plate subjected to harmonic load and it was found that the results obtained were in good agreement with strip element method. While method proposed by Lysmer-Khulemeyer, which is applicable in Abaqus as 'infinite elements' was employed for the same problem and it was found that results were not satisfactory.

Li and xiang Song (2015) proposed a general viscous-spring transmitting boundary for numerical analysis of wave propagation in unbounded saturated porous media. Proposed boundary and traditional boundaries were implemented in a finite element code and their performance was compared. It was found that proposed boundary is more efficient and this boundary is capable of solving dynamic problems in saturated porous media due to its wide suitability and high accuracy.

Zienkiewicz (1967) introduced use of infinite elements. Infinite elements are defined as radiating strips in the exterior regions. The shape functions of such elements include, for instance, an exponential decay term so that they mimic the asymptotic behavior at infinity. However infinite elements involve more computations than the finite elements as they use more parameters. Furthermore, the choice of the decay length is somewhat arbitrary.
From above investigations it is known that infinite elements and viscous boundaries are most efficient methods to prevent the reflection of waves. A viscous boundary is the most adopted method for providing silent boundary as it is effective and simple in application.

4.2 Analysis of existing methods of providing silent boundary

In this report three methods of providing silent boundaries will be analyzed using a 2D finite element program.

4.2.1 *Viscous Boundaries*

While adopting viscous boundaries, a dashpot is used in place of applying fixities on the boundaries. The dashpot absorbs the increase in stress on the boundary without rebounded. In this thesis the use of viscous boundaries will be based on the method proposed by *Lysmer and Khulmeyer (1969)*. The normal and shear stress components absorbed by a damper are represented in Eq. 4.1. Negative sign shows that these stresses act in the direction opposite to the normal and tangential velocities.

4.2.2 *Local damping*

In local damping a damping factor is introduced to damp out the energy of incident wave and damping force is proportional to the out of balance force. For any degree-of-freedom in the considered system, the local damping can be described as follows by *AL-Kafaji (2013)*:

$$f^{damp} = -\alpha \mid f \mid sign(v) \tag{4.2}$$

where,

$$f = f^{ext} - f^{int} \tag{4.3}$$

and

$$sign(v) = \frac{v}{\mid v \mid} \tag{4.4}$$

In the above equation f^{damp} acts opposite to the direction of the velocity at the considered degree-of-freedom. The parameter α is a dimensionless damping factor and $sign(v)$ is defined for nonzero values of v.

4.2.3 *Extended boundary*

The concept behind this boundary is to introduce a section of elements before the finite element boundary of the finite element model to prevent the reflections of waves. Damping force will be calculated and applied as given in Eq. 4.2. In this report, this type of extended region is provided by two ways:

- Provide a constant damping factor throughout the extended region.
- Provide a linearly varying damping factor which is zero at the junction of extended region and finite element model and maximum on the other side of extended region.

4.3 Analysis with vertical bar problem

The above three methods of providing silent boundary are analyzed using a 2D finite element program in Fortran. To analyze these methods a simple problem of a two dimensional vertical bar is considered. The vertical bar of 1m length consisting 50 elements of square size and 102 nodes is taken in to account. Bar is restricted against horizontal movement. Hence velocities and displacements at nodes in horizontal direction are zero.

Stresses and displacements at the bottom and top of the bar are determined in vertical direction, for different boundary conditions (fixed, free, viscous boundary, extended region using local damping) and different types of loads. Results are compared using graphs. Properties of bar are given in table 4.1.

Table 4.1: Properties of bar

Parameter	Value
Young's modulus, E (kPa)	1000
Density of material, ρ (1 t/m^3)	1
Cross sectional area, A (m^2)	0.02

4.3.1 *Under the influence of gravitational acceleration only*

In this case bar is subjected to only a gravitational acceleration (g_y = -10 m/s^2) in vertically downward direction and bottom of the bar is fixed (Figure 4.1). Firstly normal stress at the fixed bottom, vertical displacement at the top, potential energy, kinetic energy, strain energy and total energy of bar are determined without any damping. Then a local damping as described above is applied and again normal stress at the fixed bottom, vertical displacement at the top and all the energies are determined. Results are compared using graphs.

It can be seen from the Figure 4.2, that with local damping stress wave amplitude at the fixed bottom reduces and damped out and reached to a constant value. Figure 4.3 shows that with local damping displacement at the top of the bar reduces and damped out and reached to a constant static value. Figure 4.4 shows that total energy of the system is zero because no external force is applied here. Variation of different types of energies can also be seen from above curve. It can be seen from Figure 4.5, that due the application of local damping variations in the energies damped out and total energy of the system become

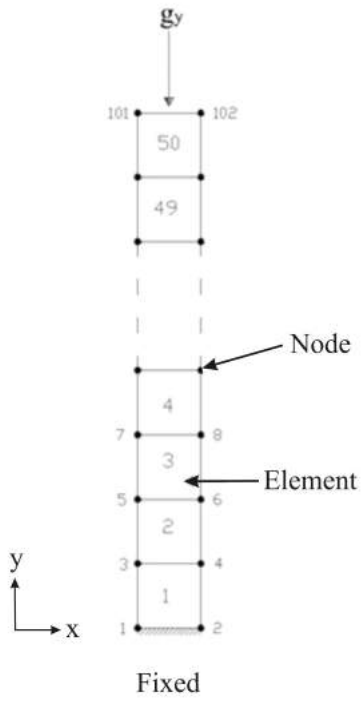

Figure 4.1: Vertical bar subjected to gravitational acceleration

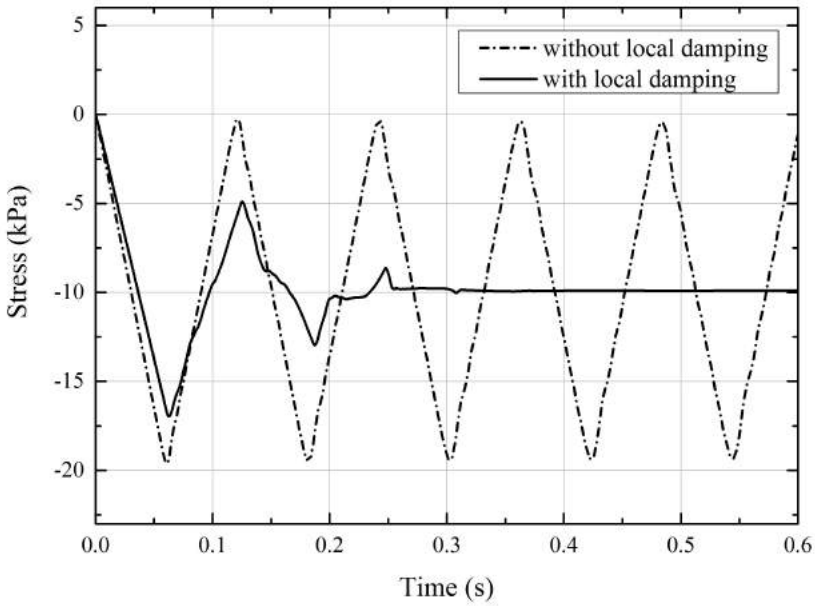

Figure 4.2: Stress at fixed bottom of bar with gravitational acceleration only

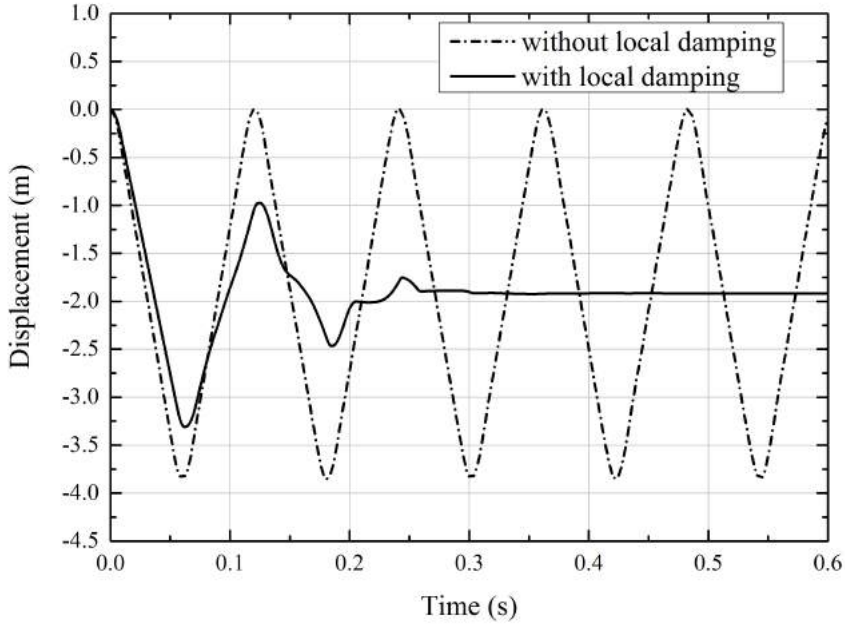

Figure 4.3: Displacement at top of bar with gravitational acceleration only

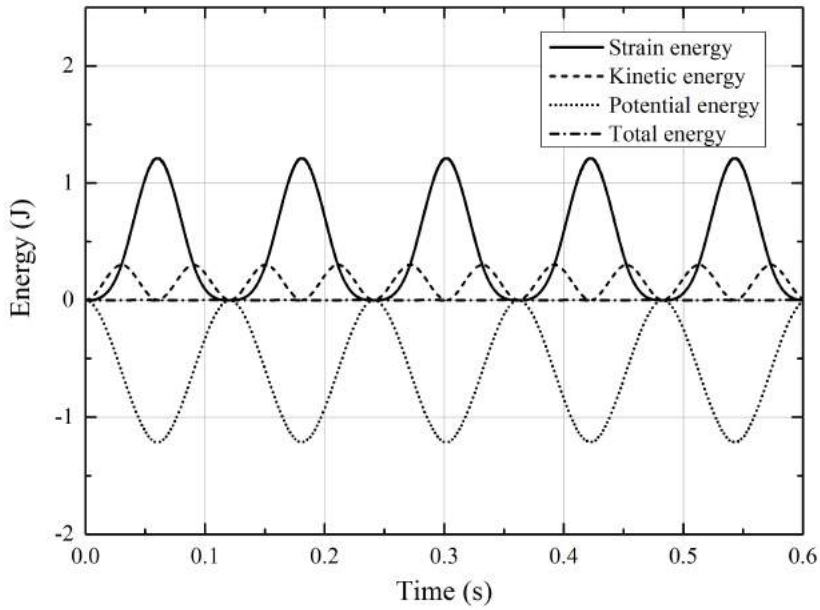

Figure 4.4: Energy of the bar with gravitational acceleration only, without damping

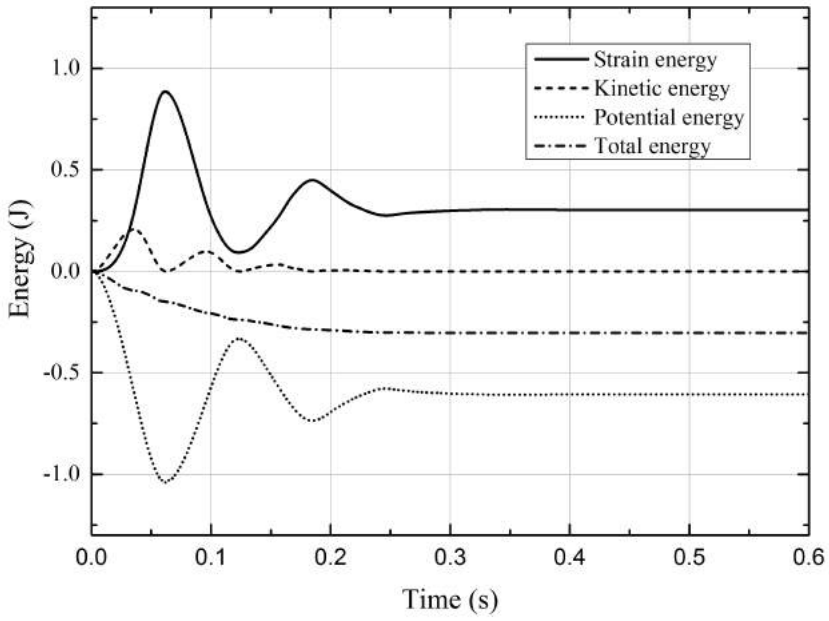

Figure 4.5: Energy of the bar with gravitational acceleration only, with local damping

less than zero. Thus due to the application of local damping total energy of the system decreases.

4.3.2 *Under the influence of half sinusoidal stress wave only*

In this case bar is subjected to only a half sinusoidal stress wave (σ) in vertically downward direction (Figure 4.6). Firstly with fixed boundary (Figure 4.6(a)) normal stress at the fixed bottom, potential energy, kinetic energy, strain energy and total energy of bar are determined without any damping. Then Viscous boundary condition is applied at the bottom (Figure 4.6(b)), as described above and again normal stress at the fixed bottom and all the energies are determined. Then local damping (α=0.3) with fixed bottom is applied and all the parameters are determined. Results are compared using graphs.

$$\sigma = -100\sin(125t)kPa \tag{4.5}$$

From the equation 4.5 it can be seen that frequency of this stress wave is 50 Hz. This force is applied as a pulse for 0.025sec in this case.

Figure 4.8 shows that due to fixed boundary reflection of stress wave occur with double amplitude, which can be effectively reduced with the application of viscous boundary in

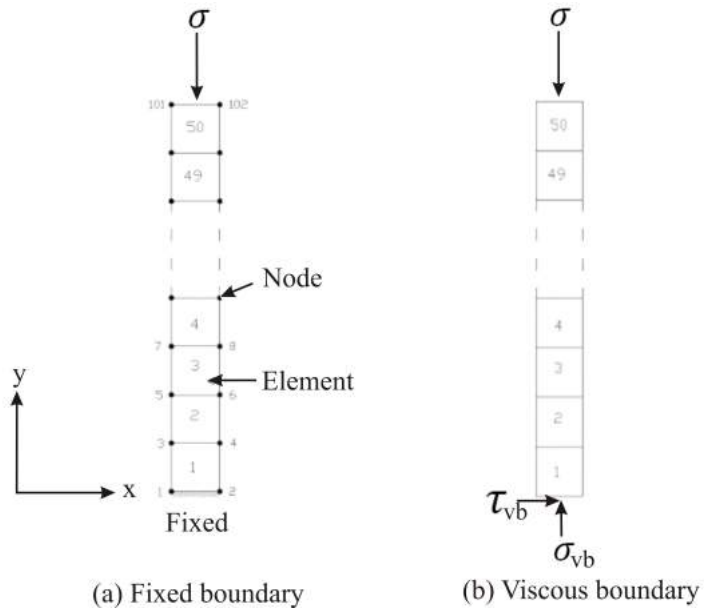

Figure 4.6: Vertical bar with application of normal vertical stress

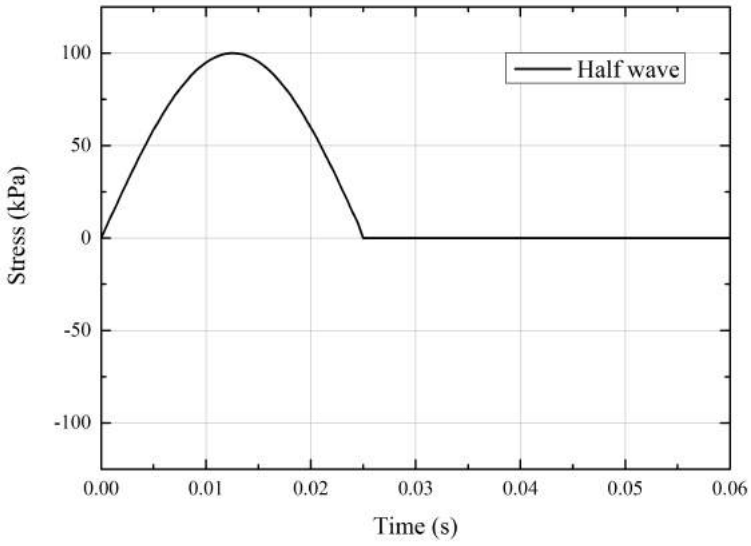

Figure 4.7: Half sinusoidal stress pulse

place of fixed boundary. It can also be noticed that application of local damping also reduced the reflection of wave but some reflection may occur which depends on the value of damping factor. Figure 4.9 shows that with fixed boundary total energy of system increase during the application of load and become constant but with viscous boundary and local damping the total energy of system reduces and becomes zero. Viscous boundary absorbs the total energy without reflection, while some reflection occur in

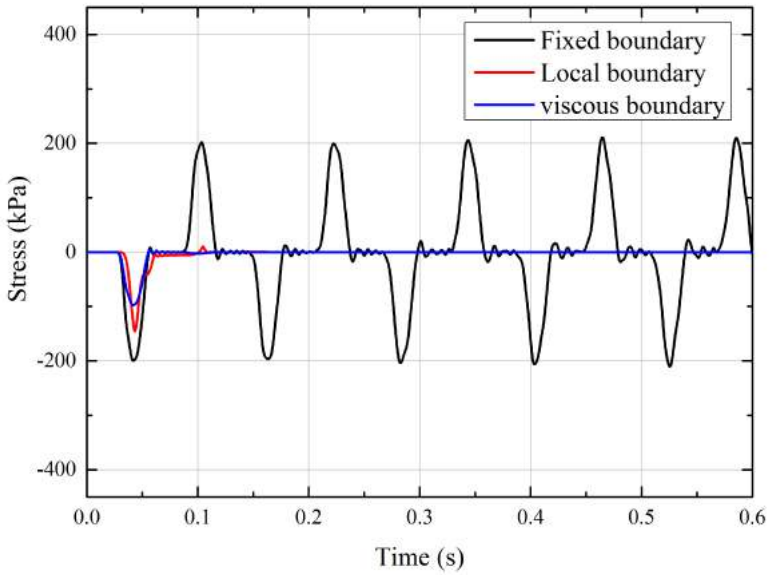

Figure 4.8: Stress at the bottom of bar with half sinusoidal stress wave pulse

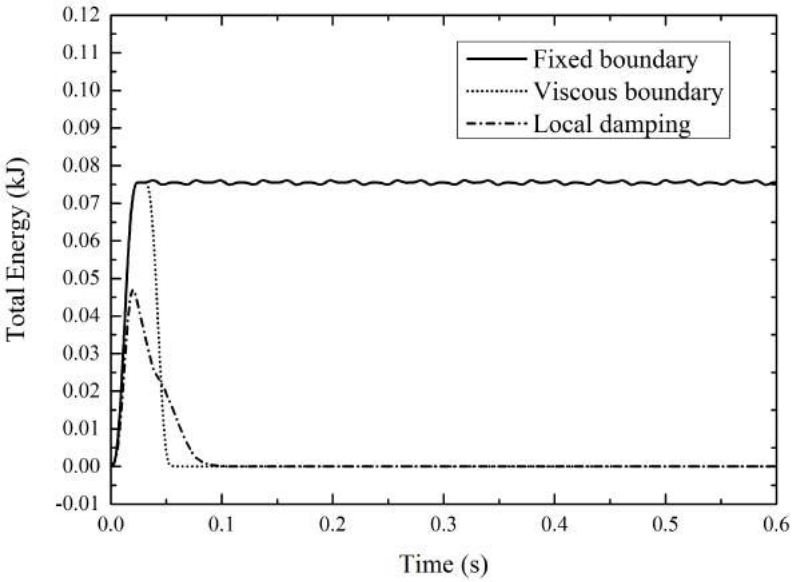

Figure 4.9: Total energy of the vertical bar with half sinusoidal stress wave pulse case of local damping.

4.3.3 *Under the influence of full sinusoidal stress wave only*

In this case bar is subjected to only a full sinusoidal stress wave (σ) in vertically downward direction. Firstly with fixed boundary normal stress at the fixed bottom, potential energy, kinetic energy, strain energy and total energy of bar are determined without any damping. Then viscous boundary condition is applied at the bottom, as described above and again normal stress at the fixed bottom and all the energies are determined. Then local damping with fixed bottom is applied and all the parameters are determined. Results are compared using graphs.

From the equation 4.5, it can be seen that frequency of this stress wave is 50 Hz. This force is applied as a pulse for 0.05sec in this case.

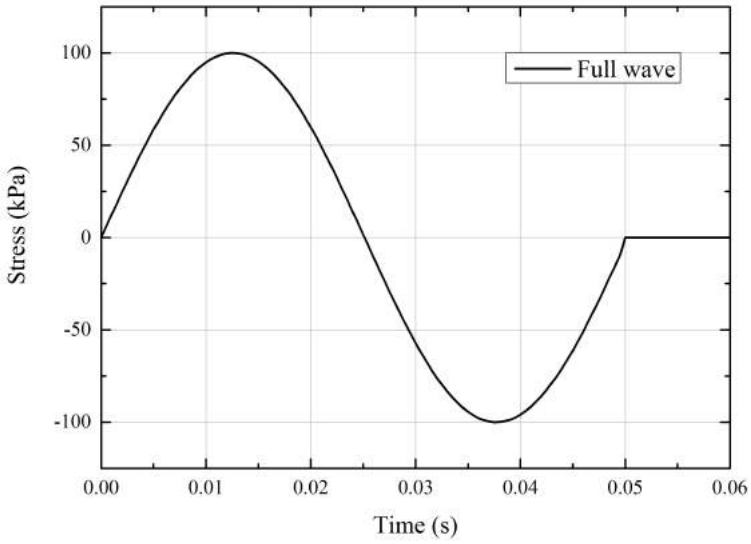

Figure 4.10: Full sinusoidal stress pulse

Figure 4.11. shows similar result as was with half sine wave. Due to fixed boundary reflection of stress wave occur with double amplitude, which can be effectively reduced with the application of viscous boundary in place of fixed boundary. It can also be noticed that application of local damping also reduced the reflection of wave but some reflection may occur which depends on the value of damping factor. Figure 4.12. of total energy also show similar results as was in case of half wave. With fixed boundary total energy of system increases during the application of load and become constant. It can also be noticed that viscous boundary and local damping both reduces the total energy of system and make it zero but viscous boundary absorbs the total energy without reflection, while some reflection occur in case of local damping.

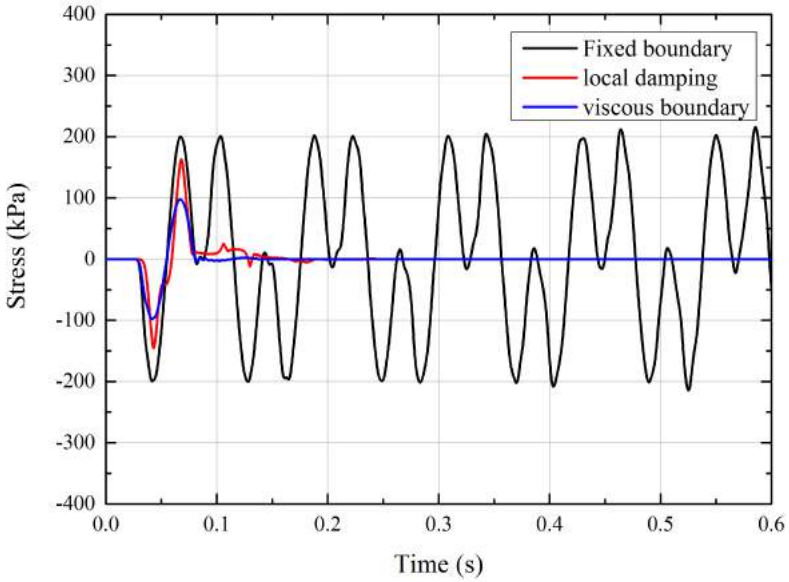

Figure 4.11: Stress at the bottom of bar with full sinusoidal stress wave pulse

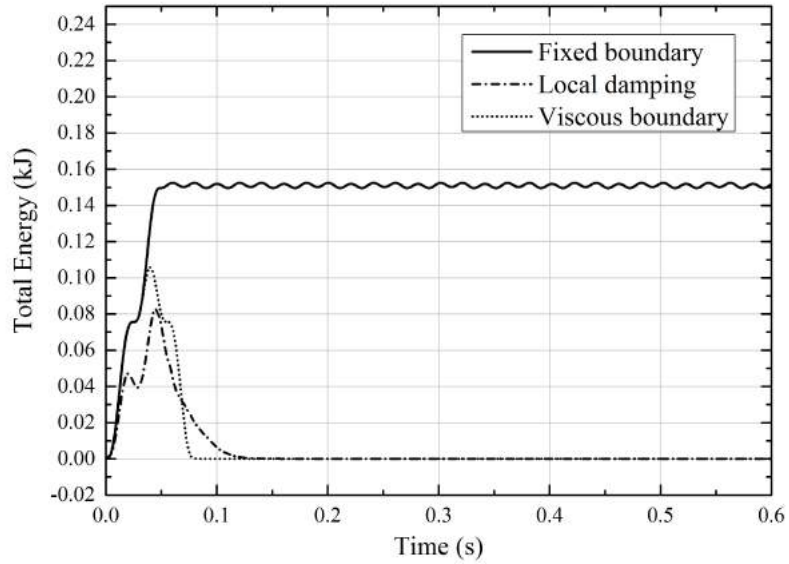

Figure 4.12: Total energy of the vertical bar with full sinusoidal stress wave pulse

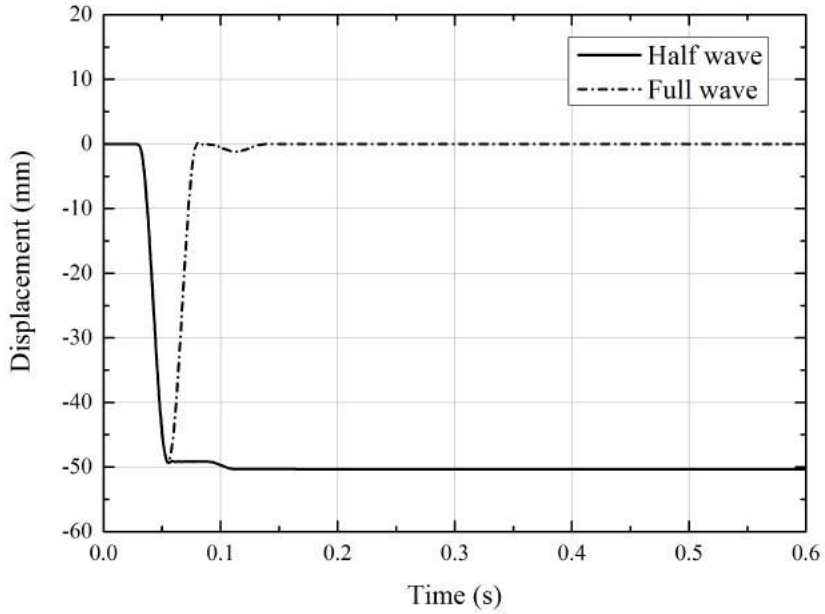

Figure 4.13: Displacement at the bottom of bar with viscous boundary

4.3.4 *Comparison of bottom displacement between half wave pulse and full wave pulse with viscous boundary*

It can be noticed from figure 4.13 that in case of half wave displacement at the bottom increases and become constant after some time, but with the application of full wave, displacement at bottom first increases during 1st half cycle and then decreases during 2nd half cycle and finally becomes zero.

4.3.5 *Use of extended region as boundary*

In this an extended region of 1 m consisting 50 square elements is added at the bottom of bar. In this region a damping factor is provided. This damping factor is provided by two ways. Firstly damping factor is provided as constant value through the whole extended region. Secondly a linearly varying damping factor is provided. Then a full stress wave as given in equation 4.5 is applied on the bar and normal stress at junction of extended region and vertical bar is determined.

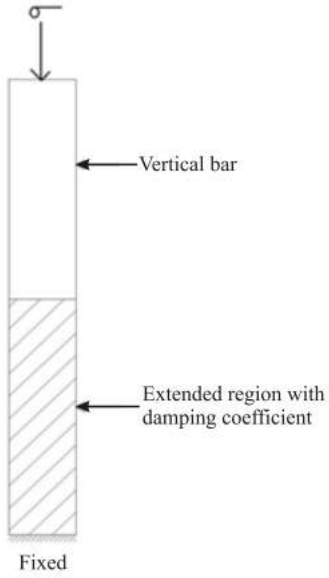

Figure 4.14: Vertical bar with extended region

4.3.5.1 When a constant damping factor is provided through the whole extended region

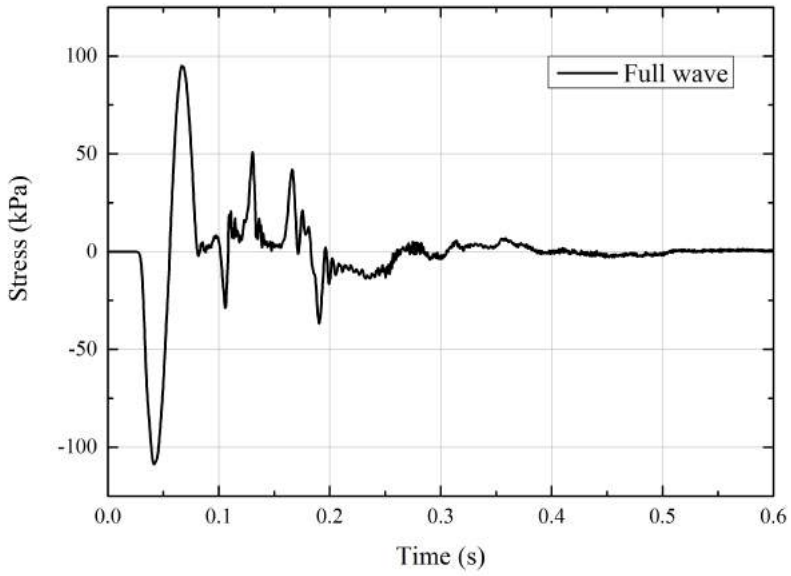

Figure 4.15: Stress at the junction of extended region and bar with application of full stress wave

In this a constant damping factor of 0.3 is provided in the extended region and damping forced is applied as given in the equation 4.2. Figure 4.15. shows that extended region is effective in the prevention of reflection of stress wave but some reflection occurs at the junction because of change in the properties of material from bar to extended region.

4.3.5.2 When a linearly varying damping factor is provided

In this case a linearly varying damping factor is provided in the extended region. This factor is zero at the junction of extended region and bar, and maximum at the end of extended region.

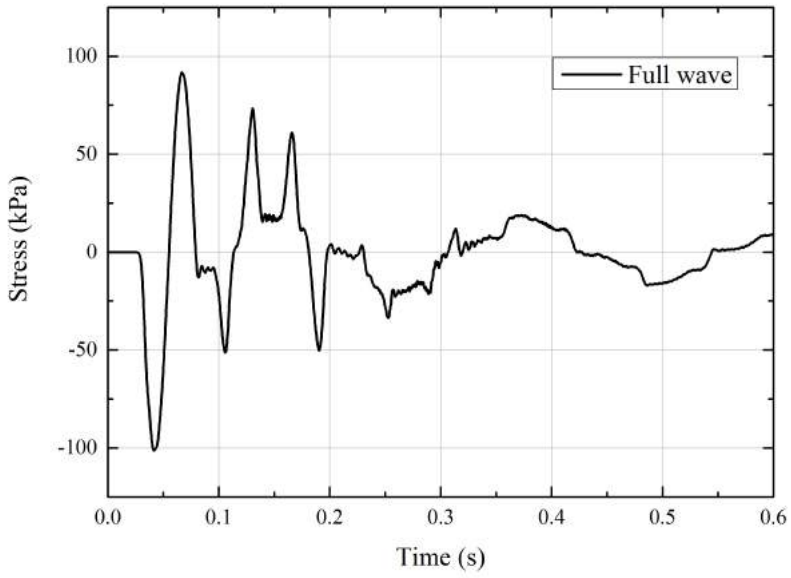

Figure 4.16: Stress at the junction with maximum value of damping coefficient 0.5

In this two cases are taken into account. In first case maximum value of damping coefficient is taken 0.5 and in second case maximum value of damping coefficient is taken 0.9. Figure 4.16 shows that assumed value of damping factor (0.5) is not sufficient in preventing the reflection so now maximum value of damping factor increased up to 0.9 and stress at the junction of extended region and bar is determined.Figure 4.17. shows increase in the maximum value of damping coefficient reduced reflections but some reflection is still present. Thus effective absorption of reflected waves may be occur with selection of correct value of damping factor.

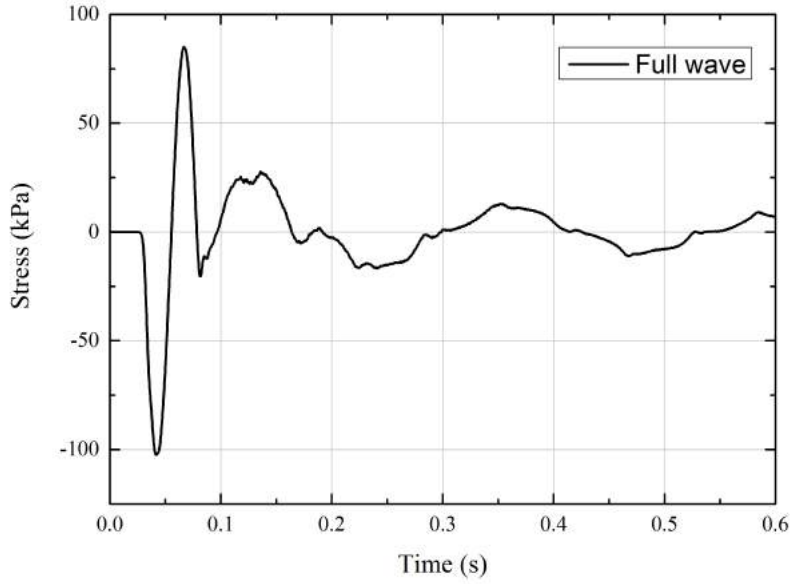

Figure 4.17: Stress at the junction with maximum value of damping coefficient 0.9

4.4 Discussions and concluding remarks

- From the graphs represented above it can be concluded that when only gravitational acceleration is considered stress varies like a wave with same maximum and minimum amplitude, but when local damping is considered stress waves magnitude decreases with time and damped gradually then reaches to a constant value and this decrease in magnitude increases as local damping coefficient increases. Displacement magnitude at the top of the bar is also decreased with time when and gradually attain a constant value when local damping is provided.

- It was also found that when a stress wave strike the fixed boundary it get reversed with double magnitude but when standard viscous boundary is considered stress wave does not reversed and damped out gradually.

- In case when half wave is applied, means when only compressive stress is applied displacement of bottom point of bar get increased with time and never return to its original position. But when full sine wave is applied, means a dynamic force is applied then bottom point of bar moved to a certain distance in first half cycle and then back to its original position in next half cycle. Thus it can be noticed that standard viscous boundaries are not effective for static analysis.

- Application of extended boundary reduced the amplitude of stress wave. This prevention of reflection depends on the provided value of damping factor. It was

noticed that in spite of high damping factor some reflections are present thus it can be concluded that performance of extended boundary is not satisfactory.

Chapter 5

Back Analysis of a Model Test and Validation

Ornek et al. (2012) conducted a series of field tests to determine the effect of granular fill layers on the behavior of large-scale footings on natural clay deposits. Two test-pit (TP1 and TP2) and four boreholes (BH1, BH2, BH3 and BH4) were formed in the test area. Soil contains three layers as shown in figure 5.1, top layer was of depth 0.80m was removed before tests. A standard penetration test (SPT) was performed and the soil profile with SPT values are shown in figure 5.1.

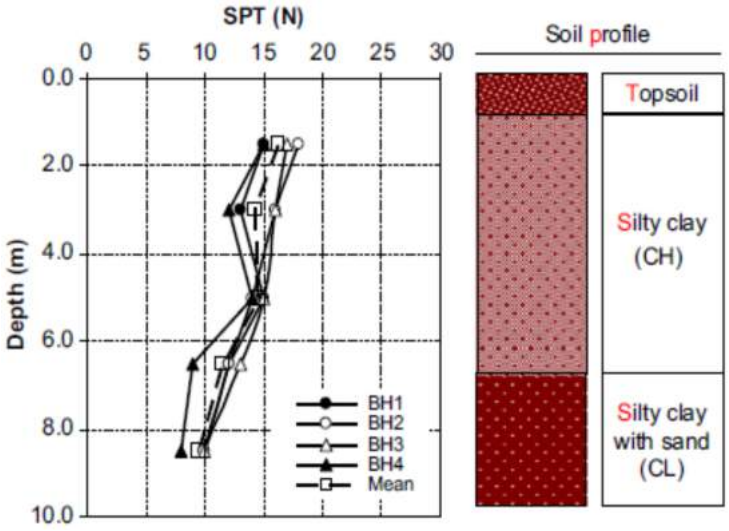

Figure 5.1: SPT values from the boreholes and soil profile (*Ornek et al., 2012*)

Footings used in the analysis were rigid, steel-made and have a thickness of 2cm for footing diameter less than 12cm and 3cm for footing diameter more than 12cm.

Ornek et al. (2014) conducted experimental and numerical investigations to determine the bearing capacity of circular footing on geogrid-reinforced compacted granular fill layer overlying on natural clay deposits. Experimental set up and soil parameters were nearly same as in the Ornek et al.(2012).

5.1 Soil parameters

The upper homogeneous layer on which all the tests were performed was classified as a highly plasticity clay (CH) according to the USCS. The values of the undrained shear strengths of clay (c_u) were in the range of 60 to 80 kN/m^2 obtained by unconfined compression tests and in the range of 70 to 80 kN/m^2 obtained from the unconsolidated undrained, triaxial test. The granular soil was classified as well-graded, gravel-silty gravel, GW-GM according to USCS.

5.2 Experimental set up

Reaction piles were constructed on the test field and then connected to each other with a steel beam. The granular fill was placed and compacted in layers. The load and the corresponding footing settlement were measured with a calibrated pressure guage and two LVDTs, connected to a data logger unit which is connected to computer. The general layout of the test setup is given in Figure 5.2.

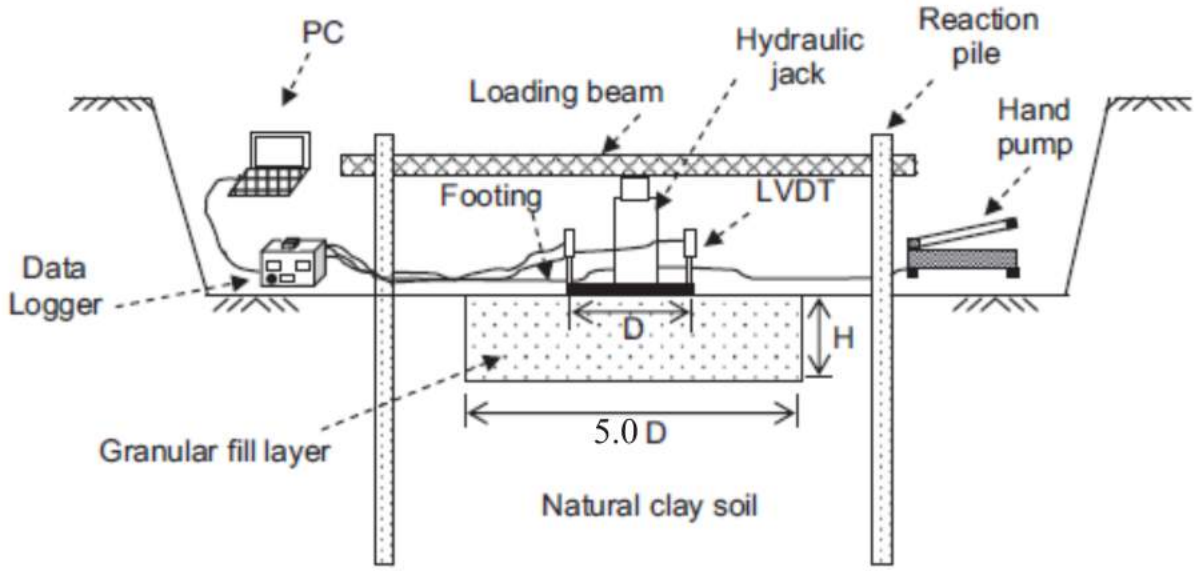

Figure 5.2: Experimental setup and layout of instrumentation (*Ornek et al., 2012*)

5.3 Numerical model and simulation process

Numerical analysis is conducted using PLAXIS 2D AE.02. Axisymmetric analysis is done to simulate the circular footing in 2D. The model boundary conditions are assumed such that the vertical boundaries are free vertically and fixed horizontally, while the bottom horizontal boundary is fixed in both the horizontal and vertical directions. Soil medium is modeled using 15-node triangular elements.

5.3.1 *Numerical model for one-layer, two-layer unreinforced and reinforced system*

In the numerical analysis of one layer, two-layer unreinforced and reinforced system the dimensions of the model are created in the 2D area. To eleminate boundary effects, the horizontal and vertical dimensions are taken as ten times to the diameter of footing. In two layer unreinforced system depth of granular layer is taken equal to the diameter of footing (H=D). In two layer reinforced system depth of granular layer is taken 0.67 times of the diameter of footing (H=0.67D). Depth of geogrid layer (u) were varied from 0.17D to 0.67D. A typical finite-element mesh configuration along with the boundary conditions and the geometry of the soil system used is shown in Figure 5.3.

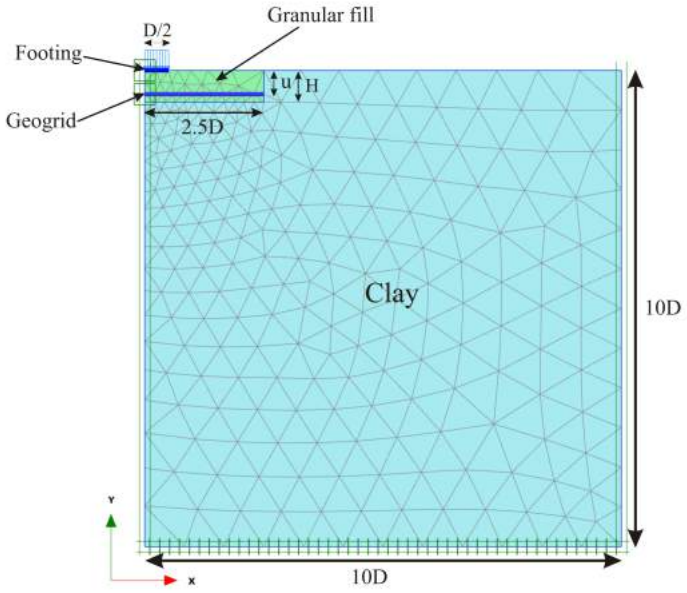

Figure 5.3: Typical mesh configurations in the numerical analyses for one layer two-layer unreinforced and reinforced soil system

An elastic-plastic Mohr Coulomb (MC) model was used for the clay and granular fill material behavior. A circular footing was modeled as a weightless steel plate of 0.3m in diameter (D) and 3cm in thickness. Properties of footing are given below in table. 5.2

Geogrid layers are represented by the use of horizontal plate elements in the program. The stress-strain behavior of geogrid layer was modeled as a linear elastic material. It was assumed as to be isotropic and of thickness 0.015m. Other properties of geogrid are given Table. 5.3.

Table 5.1: Mohr-Coulomb model parameters used in numerical analysis

Parameter	**Clay**	**Granular-fill material**
Unit weight, γ_n (kN/m^3)	18	21
Young's modulus, E_u (kN/m^2)	8500	42500
Cohesion,c (kN/m^2)	80	0.5
Poisson's ratio, ν	0.35	0.2
Friction angle, ϕ (degrees)	0	43
Dilatancy angle, ψ (degrees)	0	13
Permeability, $k_x = k_y$ (m/day)	8.64*10$^-5$	432
Drainage condition	Undrained(B)	Drained

Table 5.2: Properties of footing used in numerical analyses

Young's modulus, E_s (kN/m^2)	200*10^6
Poisson's ratio, ν	0.3

Table 5.3: Properties of geogrid used in numerical analyses

Young's modulus, E (kN/m^2)	7.33*10^5
Poisson's ratio, ν	0.10
Unit weight, γ	0.02 kN/m^3

5.4 Results and comparison with experimental results

Numerical analysis on one layer (only clay), two layer (clay overlain by granular fill) and two layer reinforced (clay overlain by geogrid reinforced layer) are performed and

results are presented in the form of bearing capacity curves. Horizontal axis are representing the load (kPa) and vertical axis are representing the corresponding settlements (mm).

Results obtained by numerical analysis are compared with the experimental results presented by Ornek et al. Numerical analysis with time interval equal to zero (in which load is applied immediately) and time interval equal to half day (in which load is applied in 0.5 days) were performed and results are compared.

5.4.1 *One-layer and two-layer unreinforced system*

Figure 5.4 and Figure 5.5 represents the load settlement curves for one layer system in which only clay soil exists and two layer system in which clay soil is overlain by granular fill and footing load is applied on it. It can be seen from these figures that bearing capacity curves obtain from numerical analysis are comparable with the experimental results presented bs Ornek et al. (2012). Figure 5.6 shows that inclusion of granular layer over clay soil caused a significant increase in the bearing capacity as compared to the one layer system.

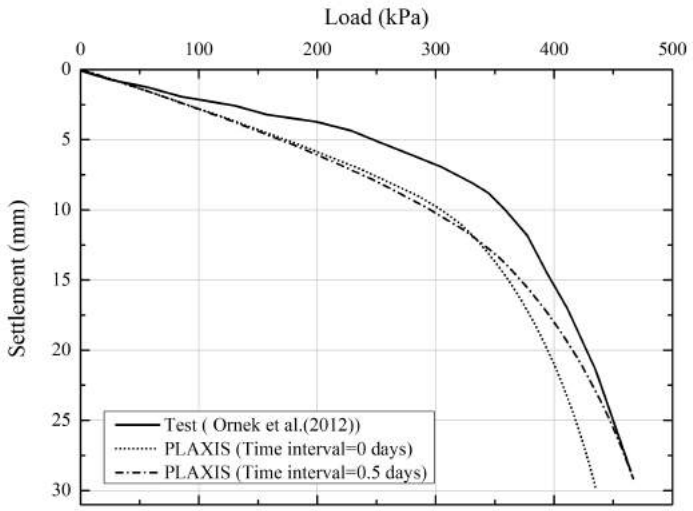

Figure 5.4: Load vs settlement curves for one layer system

It was obtained from numerical analysis that in case of one layer system for time interval zero days maximum value of pore water pressure was 630 kPa, which is unrealistic and for time interval 0.5 days maximum value of pore water pressure was 153.9 kPa. In case

of two layer system for time interval zero days maximum value of pore water pressure was 410.6 kPa, which is unrealistic and for time interval 0.5 days maximum value of pore water pressure was 144.6 kPa. Figure 5.7 and Figure 5.8 show these reduction in the values of pore water pressure.

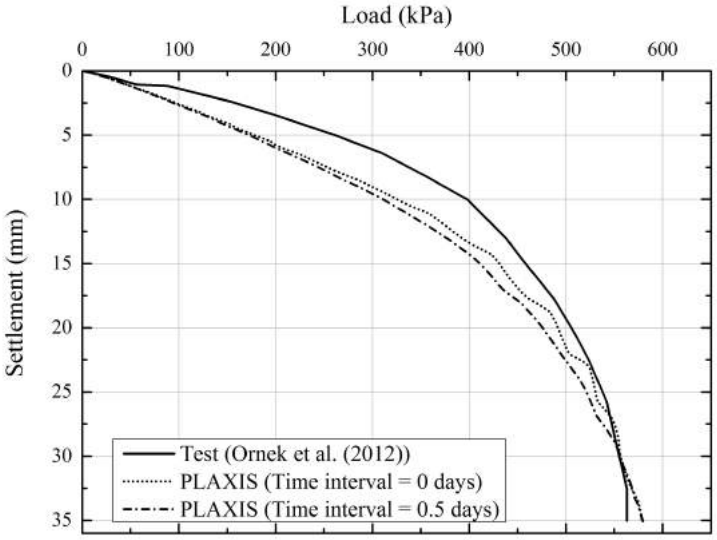

Figure 5.5: Load vs settlement curves for two layer system

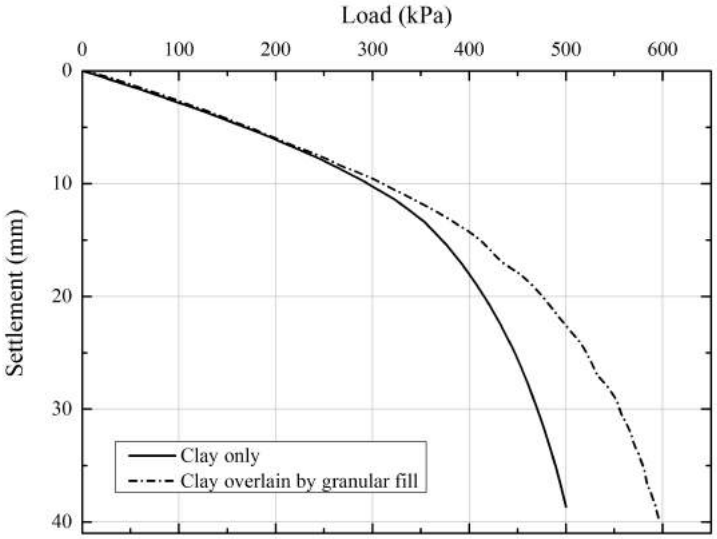

Figure 5.6: Comparison of bearing capacity curves for one and two layer system

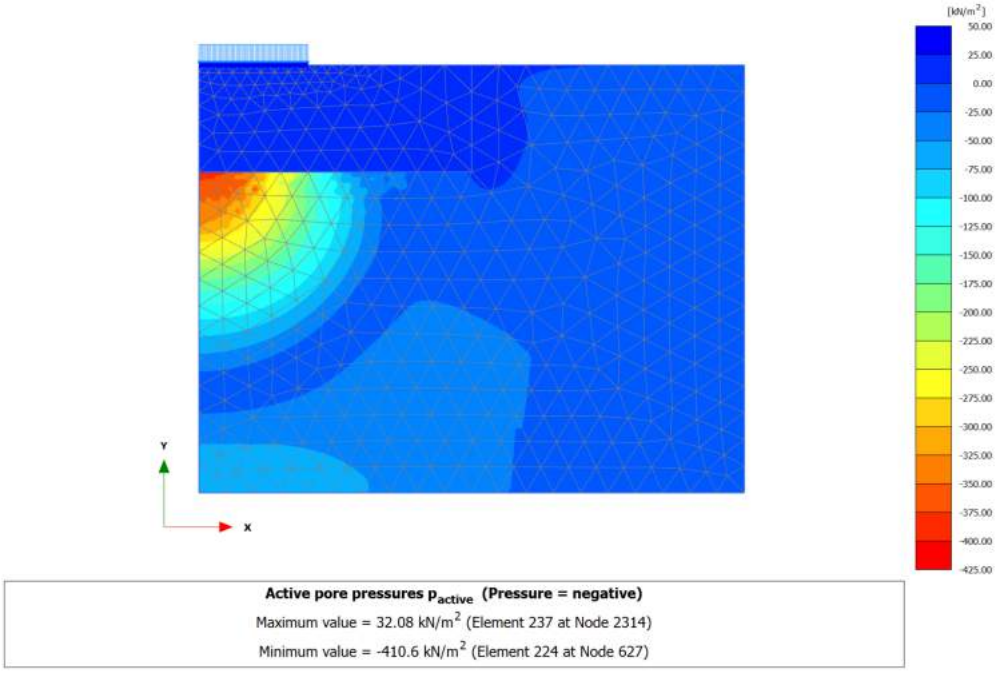

Figure 5.7: Pore water pressure distribution below the footing for two layer system (time = 0 days)

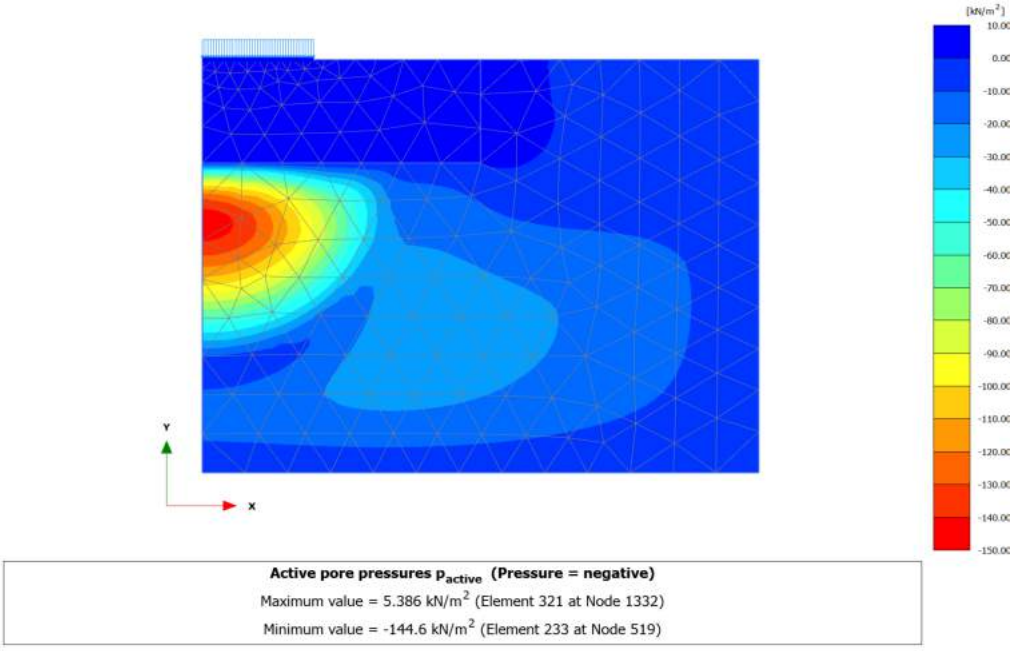

Figure 5.8: Pore water pressure distribution below the footing for two layer system (time = 0.5 days)

5.4.2 *Two-layer reinforced system*

Figure 5.9 and Figure 5.10 represents the load settlement curves for two layer geogrid reinforced system in which clay soil is overlain by granular fill and footing load is applied on it and for position of geogrid at 0.5D and 0.17D from the base of the footing respectively . It can be seen from these figures that bearing capacity curves obtain from numerical analysis are in good agreement with the experimental results presented bs Ornek et al. (2014).

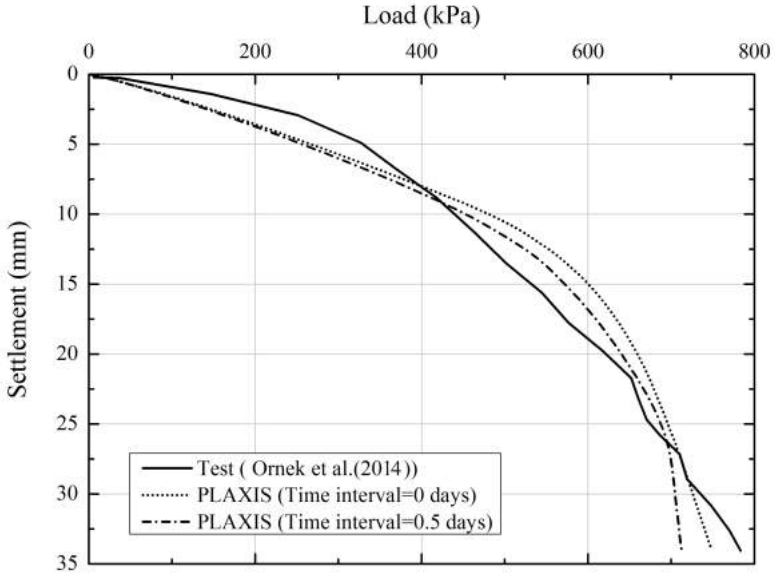

Figure 5.9: Load vs settlement curves for two layer geogrid reinforced system (u=0.5D)

Figure 5.11 reprents the deform mesh for two layer geogrid reinforced system in which geogrid is provided at a distance of 0.5D from the base of footing. Figure 5.12 represents the vertical displacement field below the footing for two layer geogrid reinforced system in which geogrid is provided at a distance of 0.5D from the base of footing.

It was obtained from numerical analysis that in case of two layer reinforced system (u=0.5D) for time interval zero days maximum value of pore water pressure was 348.2 kPa and for time interval 0.5 days maximum value of pore water pressure was 86.66 kPa. In case of two layer reinforced system (u=0.17D) for time interval zero days maximum value of pore water pressure was 296.4 kPa and for time interval 0.5 days maximum value of pore water pressure was 44.7 kPa.

Figure 5.13 shows that inclusion of geogrid layer in granular layer over clay soil caused a further increase in the bearing capacity as compared to the one layer system and two layer unreinforced system. It can also be observed from Figure 5.13 that bearing capacity

increases as the distance of geogrid layer from the base of footing decreases.

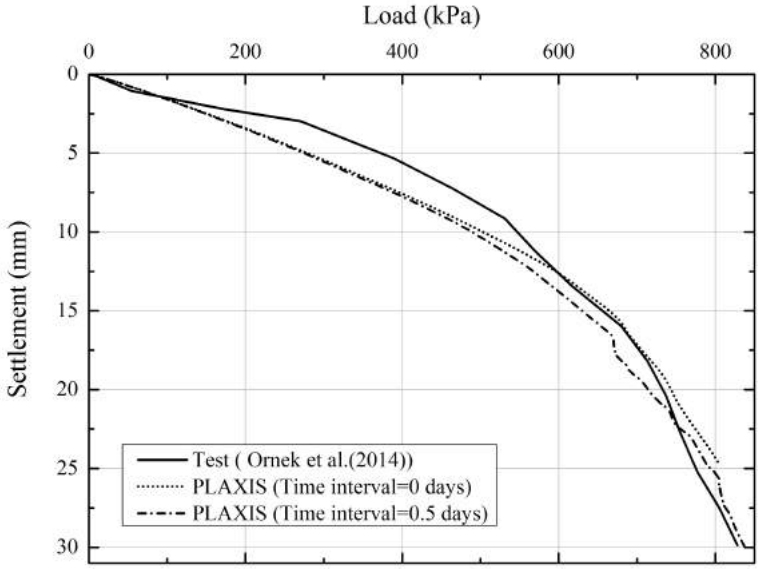

Figure 5.10: Load vs settlement curves for two layer geogrid reinforced system (u=0.17D)

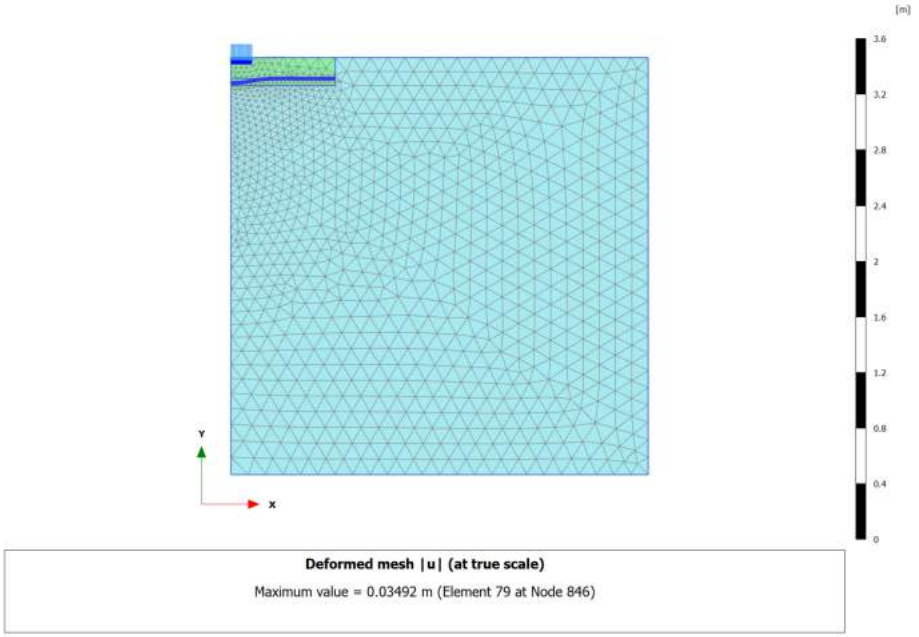

Figure 5.11: Deformed mesh for two layer geogrid reinforced system (u=0.5D)

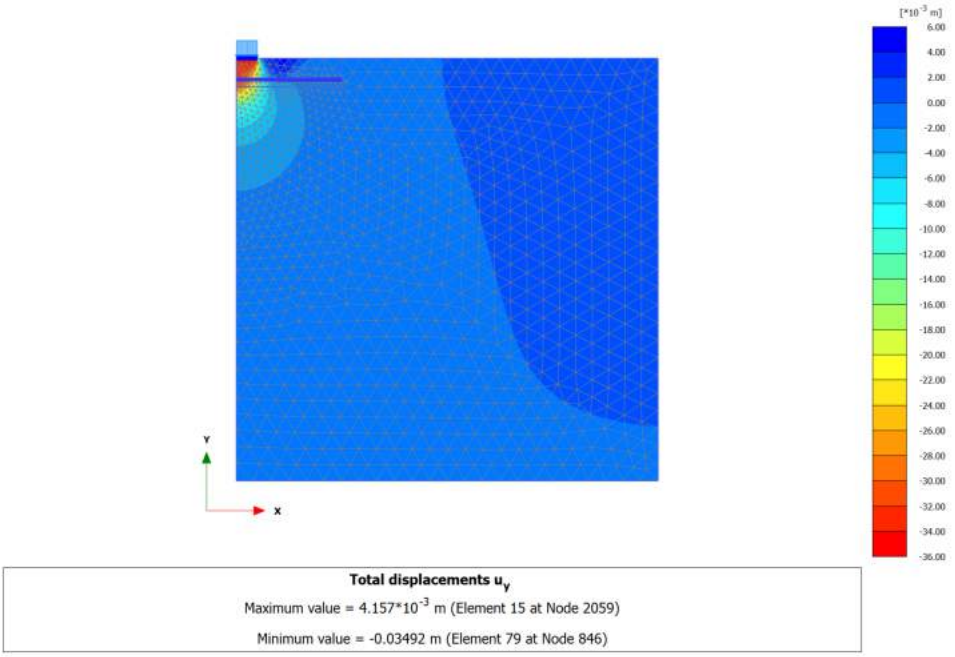

Figure 5.12: Vertical displacement below the footing for two layer geogrid reinforced system (u=0.5D)

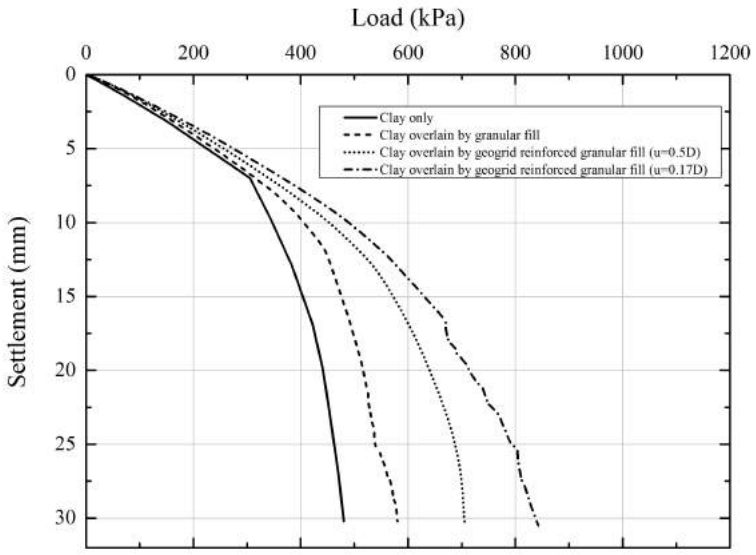

Figure 5.13: Comparison of bearing capacity curves for one and two layer unreinforced and geogrid reinforced system

5.5 Conclusions of the back analysis

- It can be concluded from back analysis that results of numerical analysis using PLAXIS 2D program and Mohr Coulomb model are in very good agreement with the experimental results.

- It is observed that if load is applied immediately (time interval = 0), it gives very high value of pore pressure which is unrealistic but if load is applied with a certain time interval pore pressure values decreases this is because of availability of time for dissipation of pore water pressure.

- It can be observed that bearing capacity of two layer system is more as compare to single layer system depending upon the strength of top and bottom layer.

- It can be observed that inclusion of reinforcement causes an increase in bearing capacity as compare to two layer unreinforced soil system, and with decrease in the depth of this geogrid layer from the base of footing also causes a further increase in bearing capacity.

Chapter 6

Dynamic Analysis of Two Layer Reinforced Soil Systems

Numerical model of two layer reinforced and unreinforced soil system validated in the previous chapter is used for dynamic analysis. A vertical dynamic load of magnitude 100 kPa and frequency 10 Hz is applied for 1.5 sec with a static load of 100 kPa on these models. For dynamic analysis viscous boundaries are used for vertical (X_{max}) and horizontal (Y_{min}) boundaries to prevent the boundary effects as reflection of waves. Parametric study is performed and results are compared.

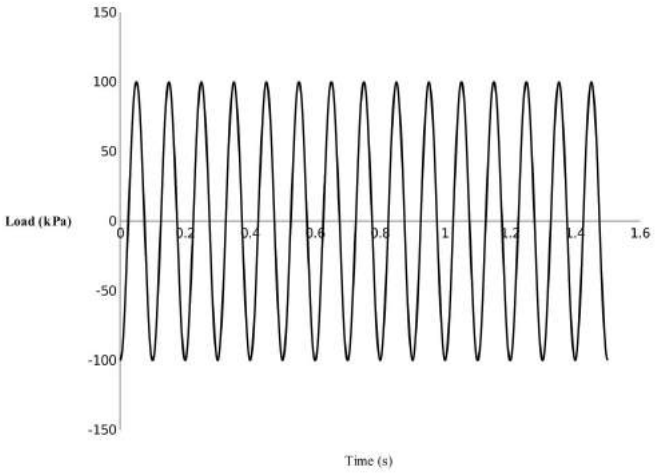

Figure 6.1: Vertical dynamic load applied on the footing

6.1 Parametric study

Different parameters which affects the load bearing and deformation behavior of two layer soil system :

- Depth of reinforcement layer below the base of footing.
- Distance between layers of geogrids in case of two layers of reinforcement.
- Number of layers of reinforcement.
- Stiffness of geogrid.

6.1.1 *Depth of reinforcement layer below the base of footing*

Two layer reinforced soil system shown in figure 5.3 is analysed for 0.67D depth of granular soil (H=0.67D) and different depth of layer of reinforcement (u=0.67D, u=0.5D, u=0.33D, u=0.17D). Three different soil models are used in the dynamic analysis which are Mohr Coulomb model (MC), Hardening soil model (HS) and Hardening soil model with small strain stiffness (HS small).

6.1.2 *Distance between layers of geogrids in case of two layers of reinforcement*

In case of two layer soil system reinforced with two layers of reinforcement, first geogrid layer is always kept at the interface of clay and granular soil, and second layer of geogrid is placed above the first one as shown in figure 6.2. Distance between two layers of geogrid is d. Effect of variation of distance of second layer of geogrid from the first one (d=0.17D, d=0.34D, d=0.5D) is studied. Three different soil models are used in the dynamic analysis which are Mohr Coulomb model (MC), Hardening soil model (HS) and Hardening soil model with small strain stiffness (HS small).

6.1.3 *Number of layers of reinforcement*

Two layer soil system with different number of layers of reinforcement is analysed (number of reinforcement layers(N)=1,2,3). Three different soil models are used in the dynamic analysis which are Mohr Coulomb model (MC), Hardening soil model (HS) and Hardening soil model with small strain stiffness (HS small). In all cases first layer of reinforcement is always kept at the interface of clay and granular fill and other layers are placed above the first layer as shown in figure 6.3. In case of three layer system distance between the layers of reinforcement (d) is 0.17D.

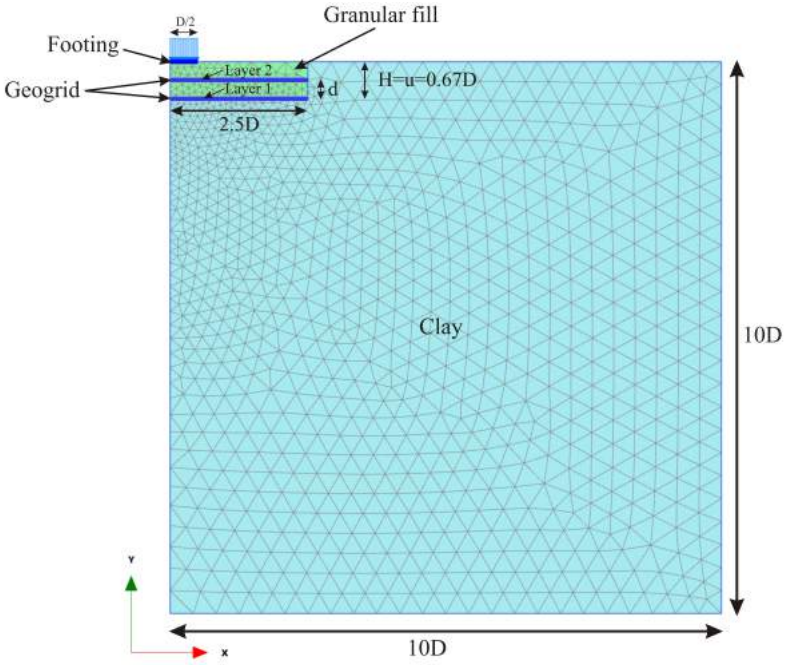

Figure 6.2: Two layer soil system reinforced with two layers of geogrid

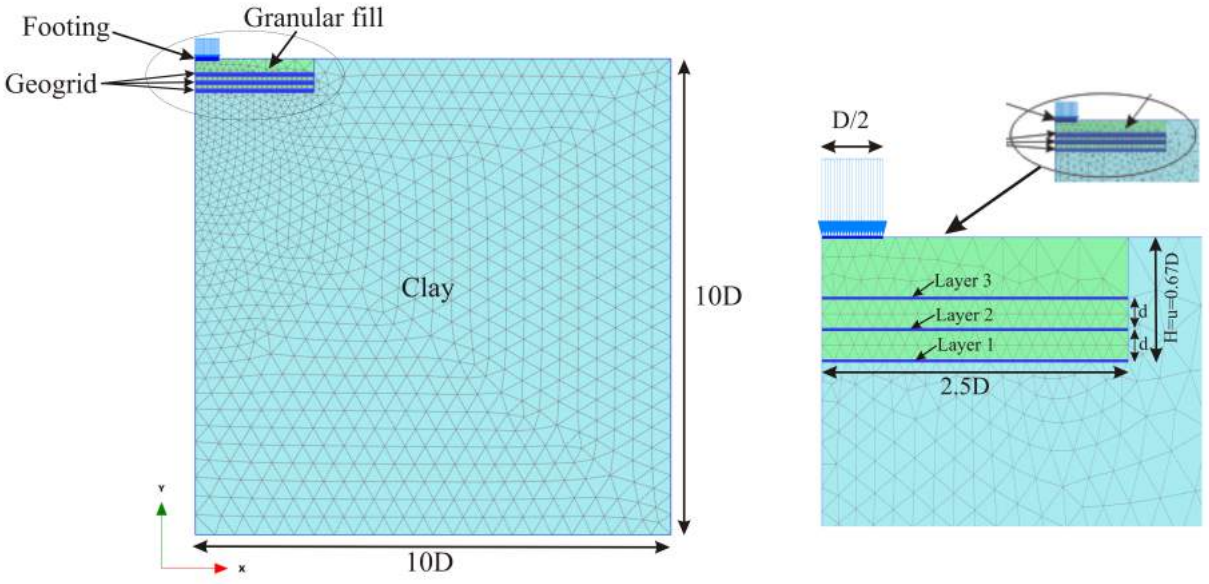

Figure 6.3: Two layer soil system reinforced with three layers of geogrid

6.1.4 *Stiffness of geogrid*

Two layer reinforced soil system with three layers of reinforcement is analysed for different stiffnesses of geogrid layers (E=533000 kN/m^2, E=633000 kN/m^2, E=733000 kN/m^2,

E=833000 kN/m^2, E=933000 kN/m^2, E=1033000 kN/m^2) to see the effect of stiffness of geogrid on the settlement and load bearing behavior of soil. Effect of geogrid stiffness on the axial forces in geogrids is also studied. HS small model is used for this analysis.

6.2 Soil parameters used in dynamic analysis

For dynamic analysis using Mohr Coulomb model, soil parameters given in table 5.1 with 20% soil damping in both clay and granular fill are used. For dynamic analysis using Hardening soil model, soil parameters given in table 6.1 with 20% soil damping in both clay and granular fill are used. For dynamic analysis using HS small model, soil parameters given in table 6.2 with 20% soil damping in both clay and granular fill are used. Properties of footing and geogrid are used as per given in table 5.2 and table 5.3 respectively.

Table 6.1: Hardening soil model parameters used in numerical analysis

Parameter	**Clay**	**Granular-fill material**
Unit weight, γ (kN/m^3)	18	21
E_{50}^{ref} (kN/m^2)	8500	42500
E_{oed}^{ref} (kN/m^2)	8500	30000
E_{ur}^{ref} (kN/m^2)	25500	1275000
power (m)	0.5	0.5
Cohesion (kN/m^2)	80	0.5
Poisson's ratio, ν	0.35	0.2
Friction angle, ϕ (degrees)	0	43
Dilatancy angle, ψ (degrees)	0	13
Permeability, $k_x = k_y$ (m/day)	8.64*10$^-$5	432
Drainage condition	Undrained(B)	Drained
Rayleigh α	2.285	2.285
Rayleigh β	$5.787 * 10^{-3}$	$5.787 * 10^{-3}$

Table 6.2: HS small model parameters used in numerical analysis

Parameter	Clay	Granular-fill material
Unit weight, γ (kN/m^3)	18	21
E_{50}^{ref} (kN/m^2)	8500	42500
E_{oed}^{ref} (kN/m^2)	8500	30000
E_{ur}^{ref} (kN/m^2)	25500	1275000
power (m)	0.5	0.5
Cohesion (kN/m^2)	80	0.5
Poisson's ratio, ν	0.35	0.2
Friction angle, ϕ (degrees)	0	43
Dilatancy angle, ψ (degrees)	0	13
$\gamma_{0.7}$	0.12*10$^-$3	0.15*10$^-$3
G_0^{ref}	11000	60000
Permeability, $k_x = k_y$ (m/day)	8.64*10$^-$5	432
Drainage condition	Undrained(B)	Drained
Rayleigh α	2.285	2.285
Rayleigh β	$5.787 * 10^{-3}$	$5.787 * 10^{-3}$

6.3 Results

All results are presented in the form of graphs. These curves are plotted as dynamic time vs settlement to see the variation of settlement with time, number of cycles vs settlement to see the permanent settlement after 14 cycles and length of geogrid vs axial forces to see the variation of geogrid forces along the length of geogrid.

6.3.1 *Effect of depth of reinforcement layer below the base of footing*

In case of two layer soil system reinforced with single layer of reinforcement for all three soil models used in dynamic analysis, it can be observed from Figures 6.4, 6.7 and 6.10 that with decrease in depth of geogrid below the base of the footing (u) initially maximum settlement at peak loads increases but later as time increase this settlement decreses with decrease in depth of reinforcement upto a value of u=0.33D. With further decrease in value of u (upto u=0.17d) maximum settlement at peak load increases.

It can be observed from Figures 6.5, 6.8 and 6.11 that with decrease in depth of geogrid

below the base of the footing (u), after 14 cycles permanent settlement decreases upto a value of u=0.33D. With further decrease in value of u (upto u=0.17d) permanent settlement after 14 cycles increases.

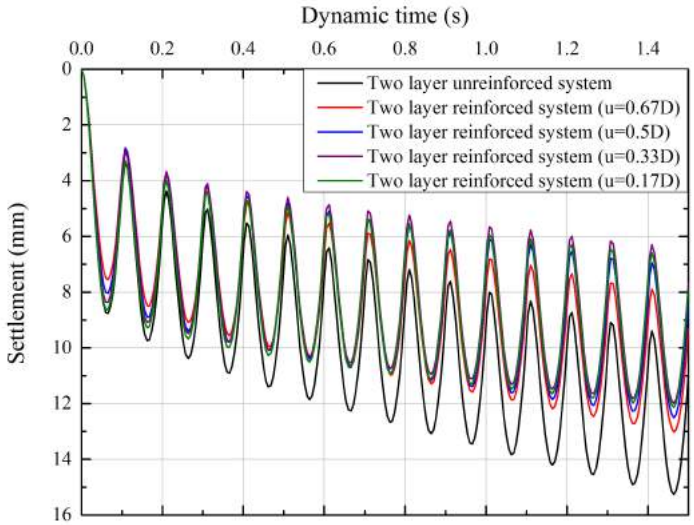

Figure 6.4: Effect of depth of reinforcement from the base of footing(N=1) (Dynamic time vs. Settlement curve, using Mohr Coulomb model)

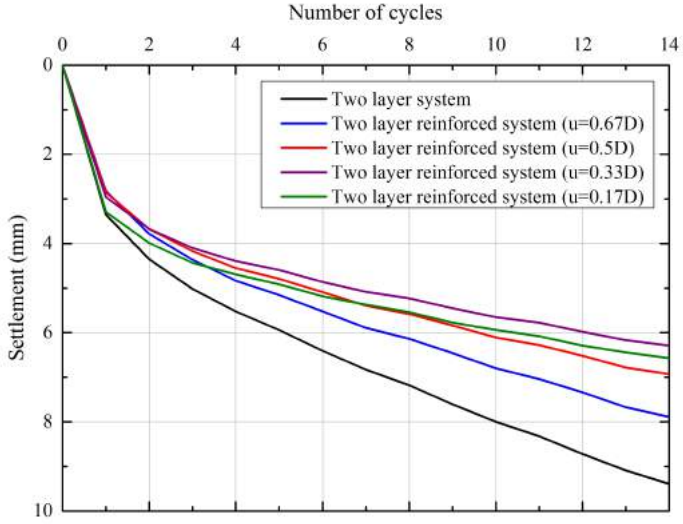

Figure 6.5: Effect of depth of reinforcement from the base of footing(N=1) (No. of cycles vs. Settlement curve, using Mohr Coulomb model)

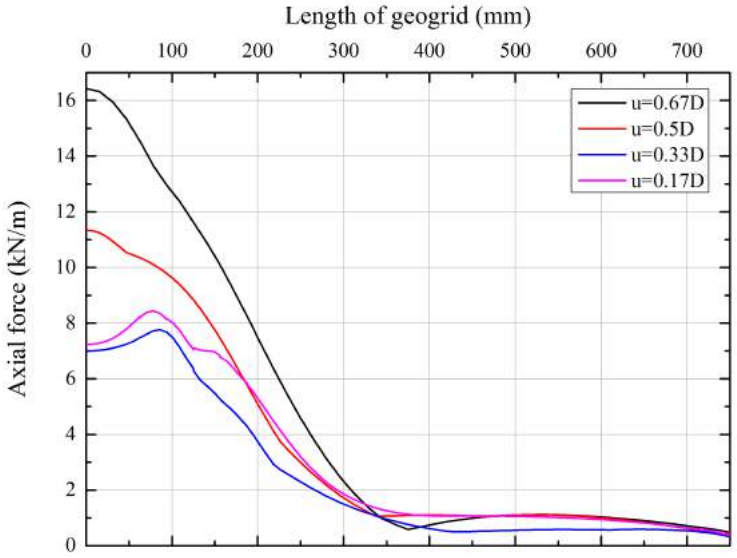

Figure 6.6: Effect of depth of reinforcement below the base of the footing on geogrid forces (using Mohr Coulomb model)

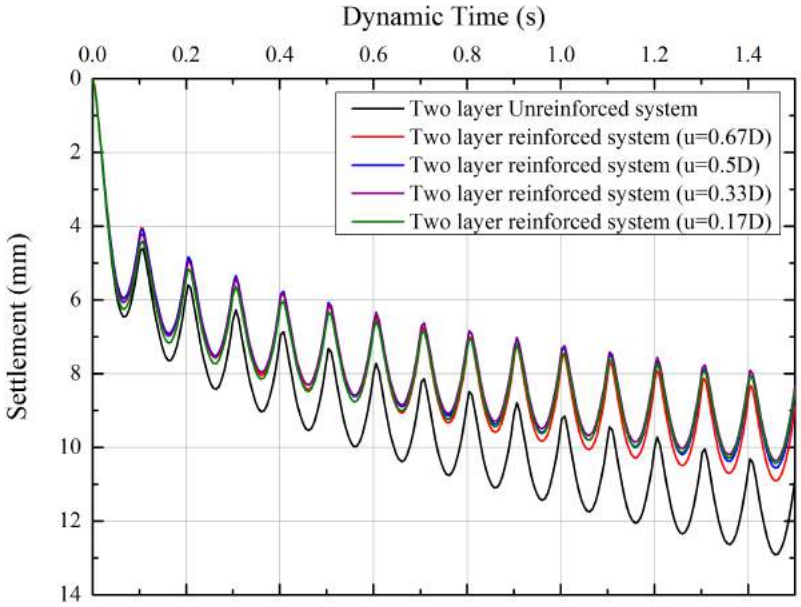

Figure 6.7: Effect of depth of reinforcement from the base of footing(N=1) (Dynamic time vs. Settlement curve, using Hardening soil model)

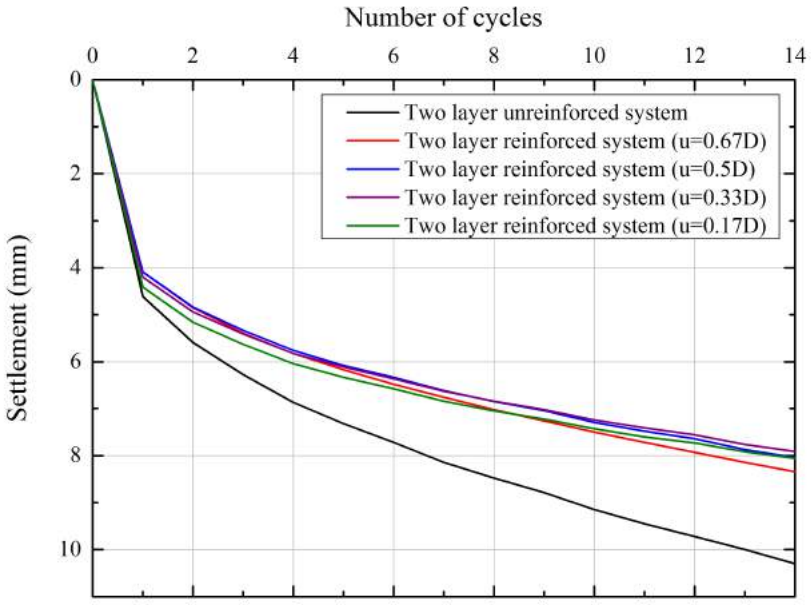

Figure 6.8: Effect of depth of reinforcement from the base of footing(N=1) (No. of cycles vs. Settlement curve, using Hardening soil model)

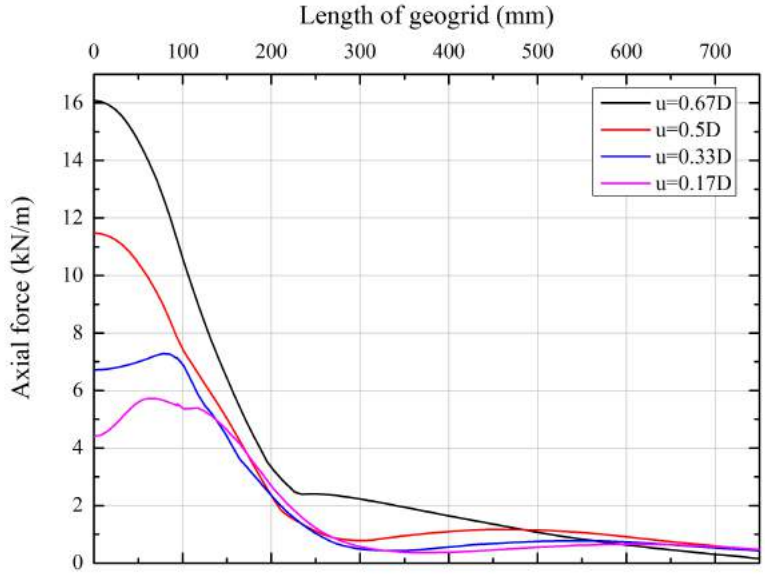

Figure 6.9: Effect of depth of reinforcement below the base of the footing on geogrid forces (using Hardening soil model)

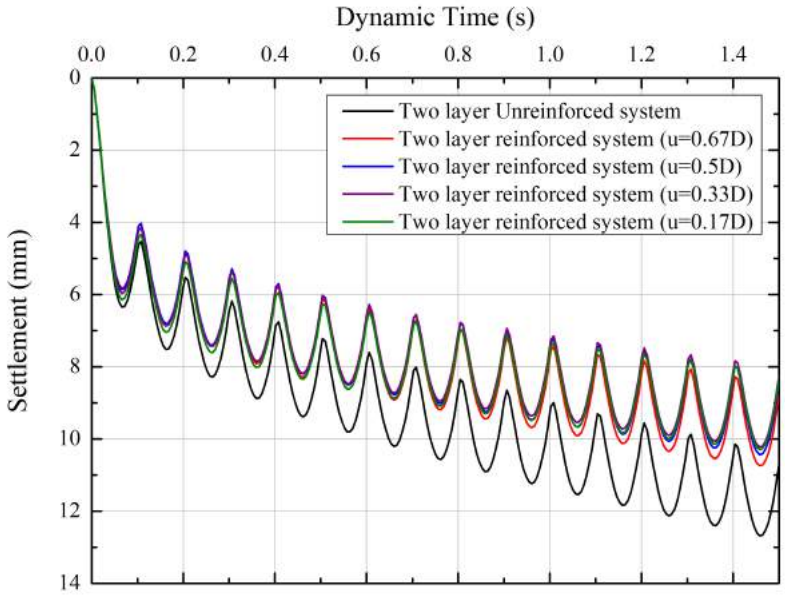

Figure 6.10: Effect of depth of reinforcement from the base of footing(N=1) (Dynamic time vs. Settlement curve, using HS small model)

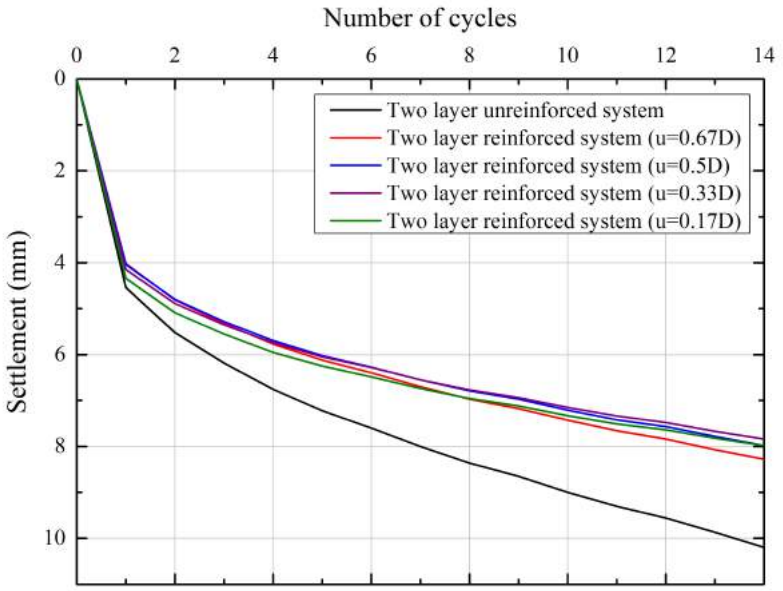

Figure 6.11: Effect of depth of reinforcement from the base of footing(N=1) (No. of cycles vs. Settlement curve, using HS small model)

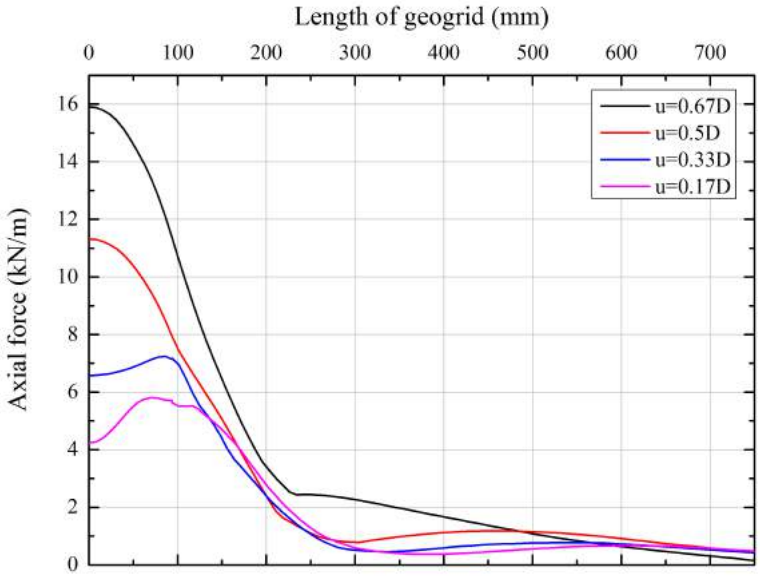

Figure 6.12: Effect of depth of reinforcement below the base of the footing on geogrid forces (using HS small model)

From Figure 6.6 it can be observed that when Mohr coulomb soil model is used, decrease in depth of geogrid layer below the base of footing causes a decrease in the axial force in geogrid upto a value of u=0.33D. With further decrease in value of u (upto u=0.17d) axial force in geogrid increases. It can also be observed that maximum axial force in geogrid is at the center of footing (below the load) and decrease as the distance from center increases, and become very small after a georid length of 1.33D.

From Figures 6.9 and 6.12 it can be observed that when Hardening soil model and HS small model is used respectively, decrease in depth of geogrid layer below the base of footing causes a decrease in the axial force in geogrid. It can also be observed that maximum axial force in geogrid is at the center of footing (below the load) and decrease as the distance from center increases, and become very small after a georid length of 1.33D.

6.3.2 *Effect of distance between layers of geogrids in case of two layers of reinforcement*

In case of two layer soil system reinforced with two layers of geogrid as reinforcement, from Figure 6.13 it can be observed that when Mohr Coulomb model is used initially the maximum settlement at peak load remains same as in single layer of reinforcement case but as time increases maximum settlement at peak loads decreases with increase in the

distance between the two layers of geogrids upto a value d=0.34D, after it shows very less decrease in maximum settlement at peak loads.

From Figures 6.16 and 6.19 it is observed that when Hardening soil model and HS small is used initially the maximum settlement at peak load increases when two layers of reinforcement are used as compare to single layer of reinforcement but as time increases maximum settlement at peak loads decreases with increase in the distance between the two layers of geogrids upto a value d=0.34D, after it shows very less decrease in maximum settlement at peak loads.

From Figures 6.14, 6.17 and 6.20 it is observed that with the used of all three soil models permanent settlement after 14 cycles decreases as distance between the two layers of geogrids increases upto a value d=0.34D, after that when value of d increase further (d=0.5D) permanent settlement after 14 cycles increases.

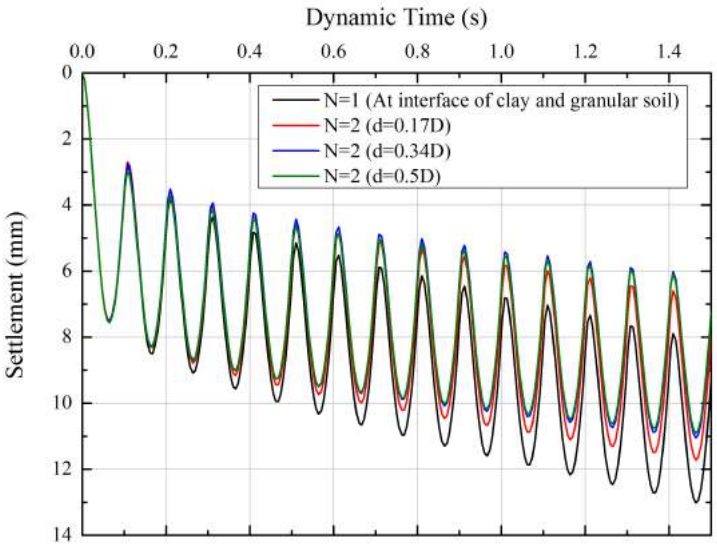

Figure 6.13: Effect of distance between layers of geogrids(N=2) (Dynamic time vs. Settlement curve, using Mohr Coulomb model)

From Figure 6.15 it is observed that when Mohr Coulomb model is used, in case of two layers of reinforcement, axial forces in first layer of geogrid (which is at the interface of clay and granular soil) increases as the distance between two layers of geogrid increases. Axial forces in the second layer also increases as the distance between two layers increases and peak of axial forces shifts to left as the distance between two layers of geogrid increases. It can also be observed that in first layer maximum axial force in geogrid is at the center of footing (below the load), while in second layer maximum

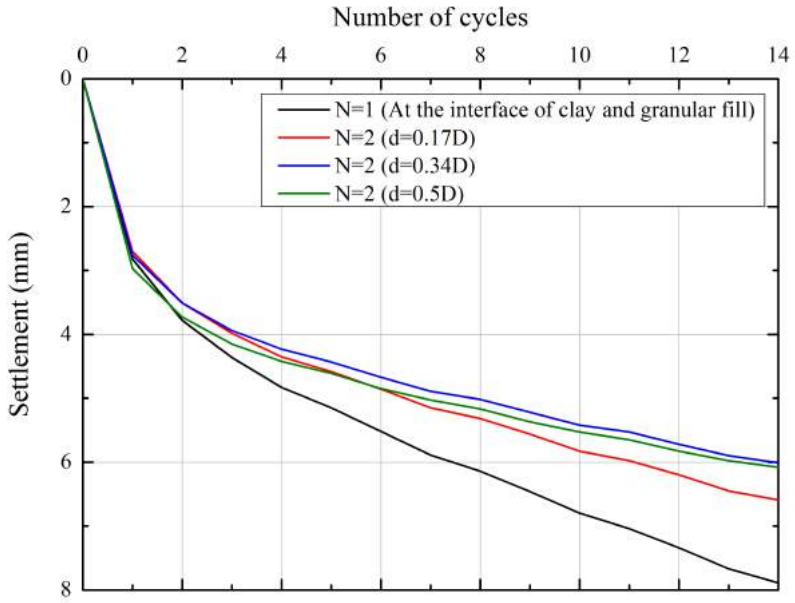

Figure 6.14: Effect of distance between layers of geogrids(N=2) (No. of cycles vs. Settlement curveusing Mohr Coulomb model)

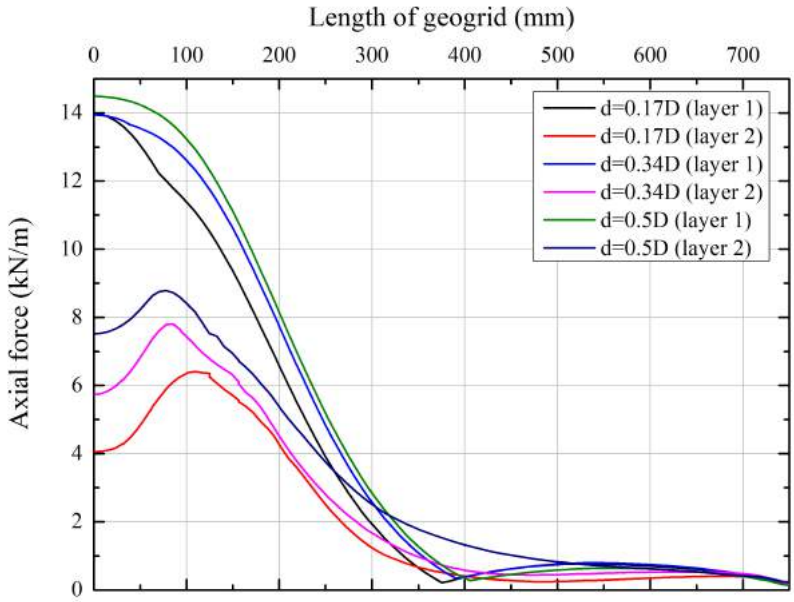

Figure 6.15: Effect of distance between layers of geogrids(N=2) on geogrid forces (using Mohr Coulomb model)

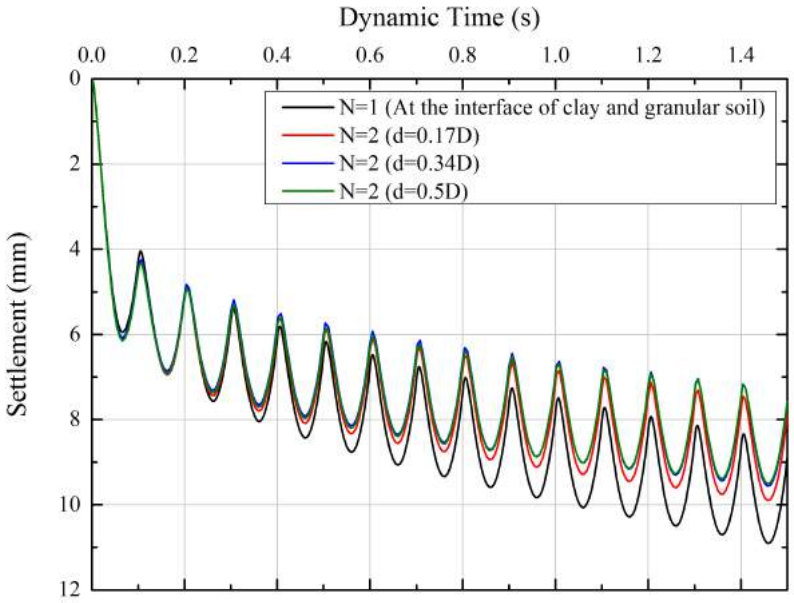

Figure 6.16: Effect of distance between layers of geogrids(N=2) (Dynamic time vs. Settlement curve, using Hardening soil model)

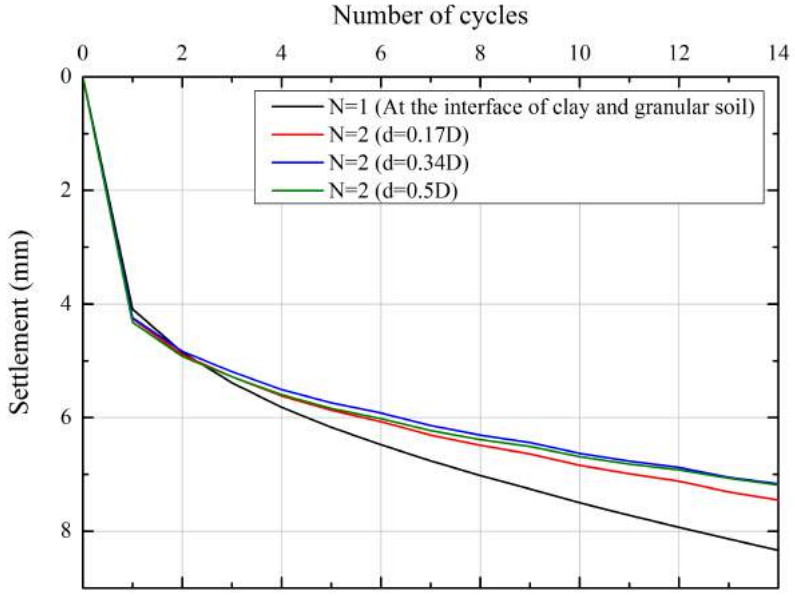

Figure 6.17: Effect of distance between layers of geogrids(N=2) (No. of cycles vs. Settlement curve, using Hardening soil model)

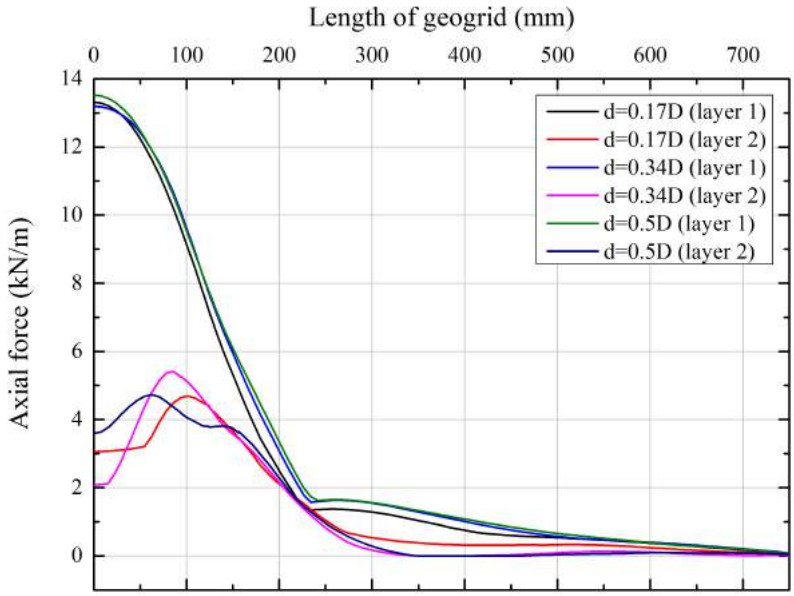

Figure 6.18: Effect of distance between layers of geogrids(N=2) on geogrid forces (using Hardening soil model)

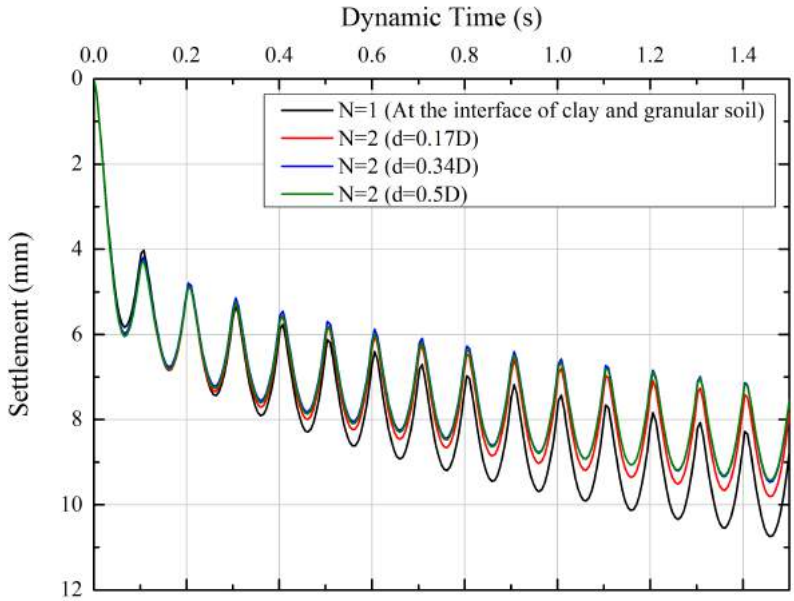

Figure 6.19: Effect of distance between two layers of geogrids(N=2) (Dynamic time vs. Settlement curve, using HS small model)

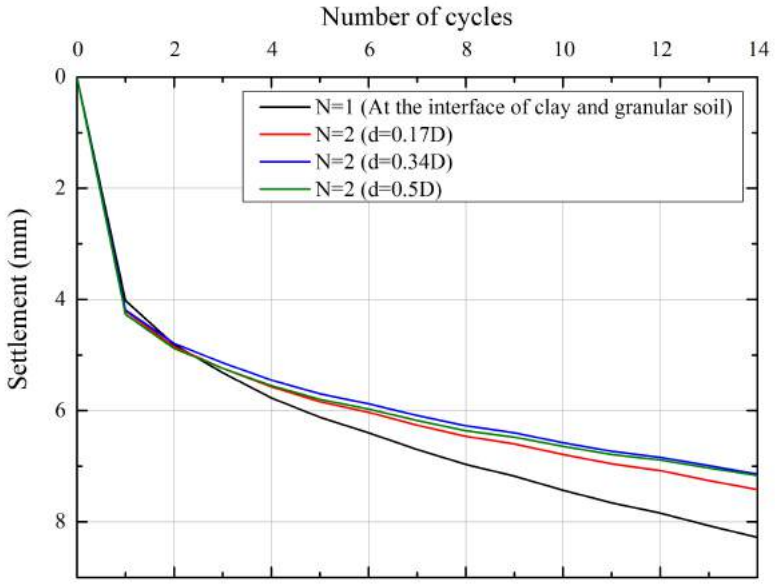

Figure 6.20: Effect of distance between two layers of geogrids(N=2) (No. of cycles vs. Settlement curve, using HS small model)

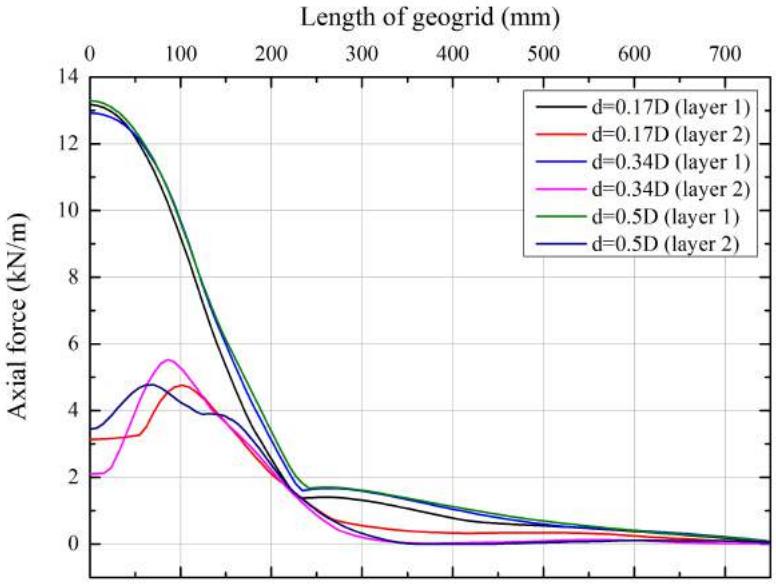

Figure 6.21: Effect of distance between layers of geogrids(N=2) on geogrid forces (using HS small model)

axial force occur at some distance from the center of footing, while in both the layers axial forces decrease as the distance from center increases, and become very small after a georid length of 1.33D.

From Figures 6.18 and 6.21 it is observed that when Hardening soil model and HS small model is used, in case of two layers of reinforcement, axial forces in first layer of geogrid (which is at the interface of clay and granular soil) does not change greatly as the distance between two layers of geogrid increases. In the second layer peak of axial forces shifts to left as the distance between two layers of geogrid increases. It can also be observed that in first layer maximum axial force in geogrid is at the center of footing (below the load), while in second layer maximum axial force occur at some distance from the center of footing, while in both the layers axial forces decrease as the distance from center increases, and become very small after a georid length of 1.33D.

6.3.3 *Effect of number of layers of reinforcement*

From Figures 6.22, 6.25 and 6.28 it is observed that for all three soil models maximum settlement at peak loads decreases as the number of geogrid layers increases from N=0 to N=3, when the lowest settlement cases for N=1 and N=2 are considered for comparison.

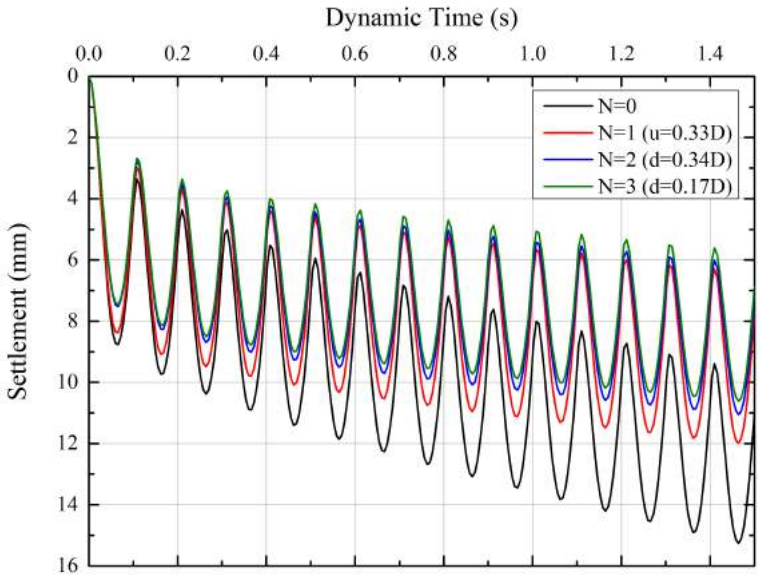

Figure 6.22: Effect of number of layers of reinforcement (Dynamic time vs. Settlement curve, using Mohr Coulomb model)

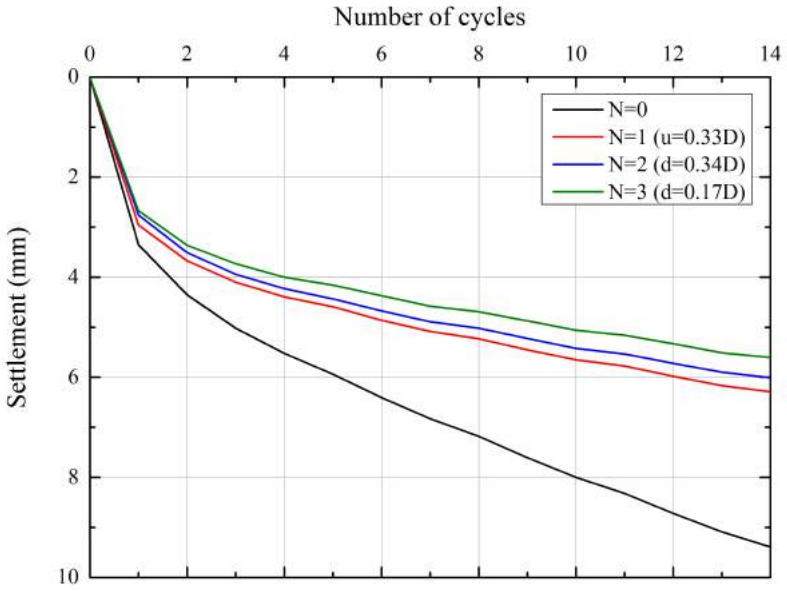

Figure 6.23: Effect of number of layers of reinforcement (No. of cycles vs. Settlement curve, using Mohr Coulomb model)

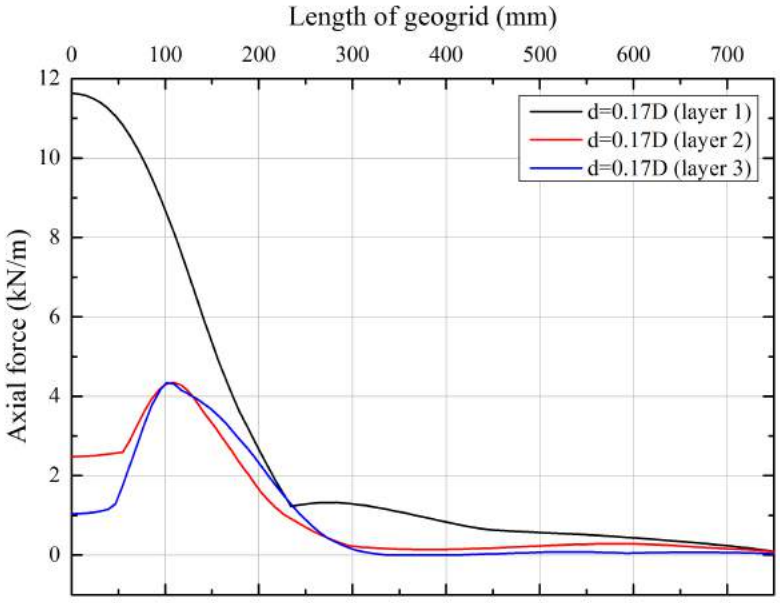

Figure 6.24: Geogrid forces in case of three layers of reinforcement (using Mohr Coulomb model)

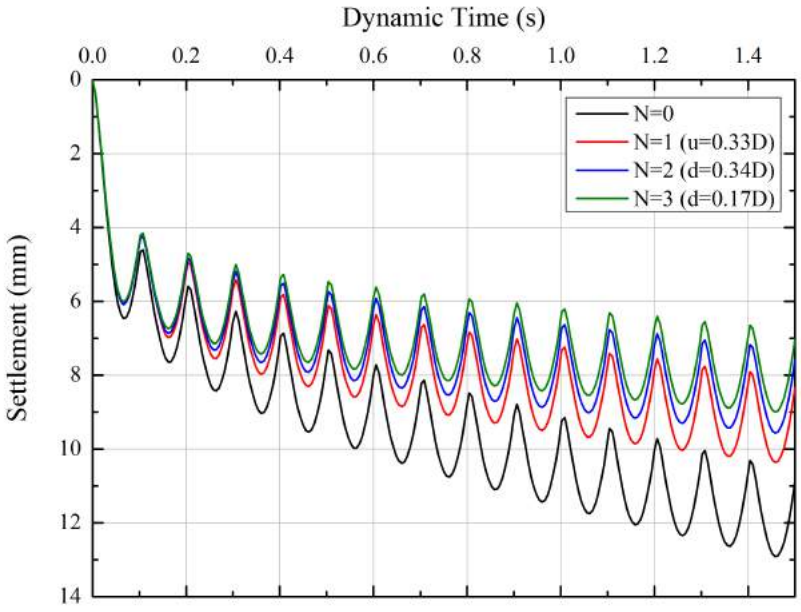

Figure 6.25: Effect of number of layers of reinforcement (Dynamic time vs. Settlement curve, using Hardening soil model)

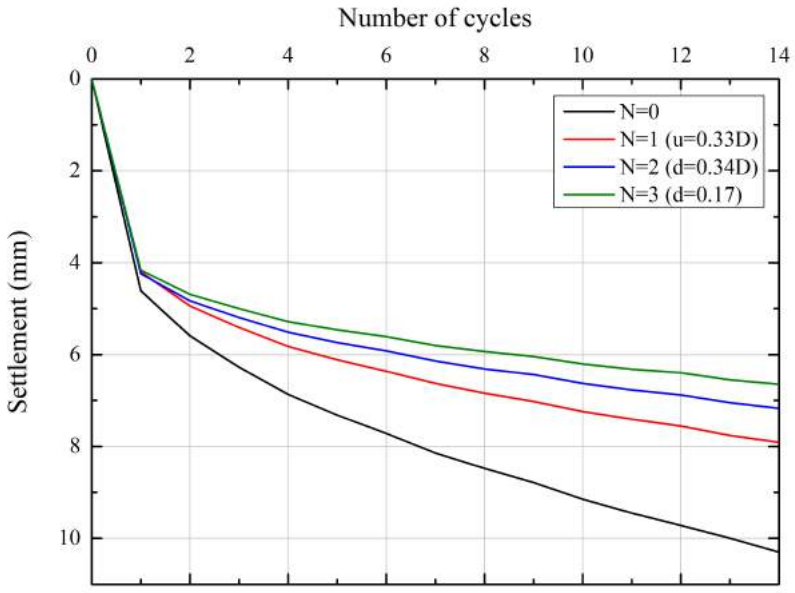

Figure 6.26: Effect of number of layers of reinforcement (No. of cycles vs. Settlement curve, using Hardening soil model)

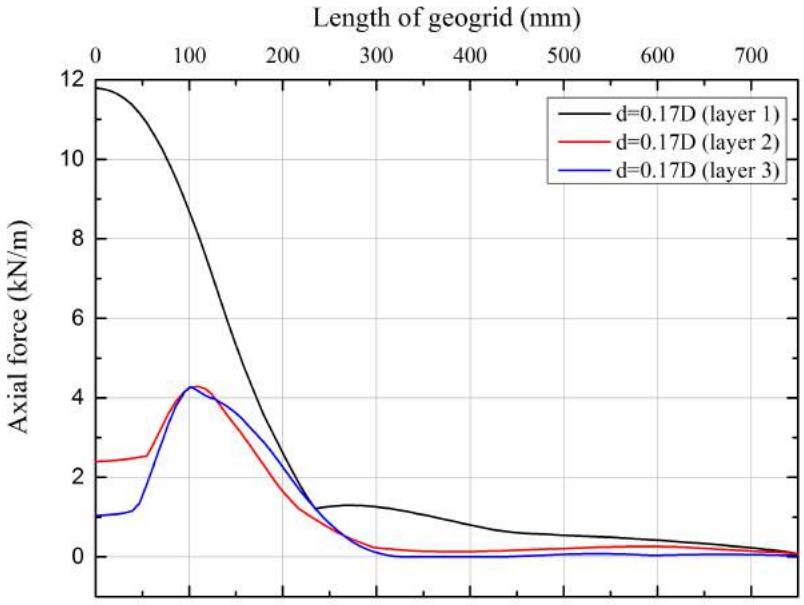

Figure 6.27: Geogrid forces in case of three layers of reinforcement (using Hardening soil model)

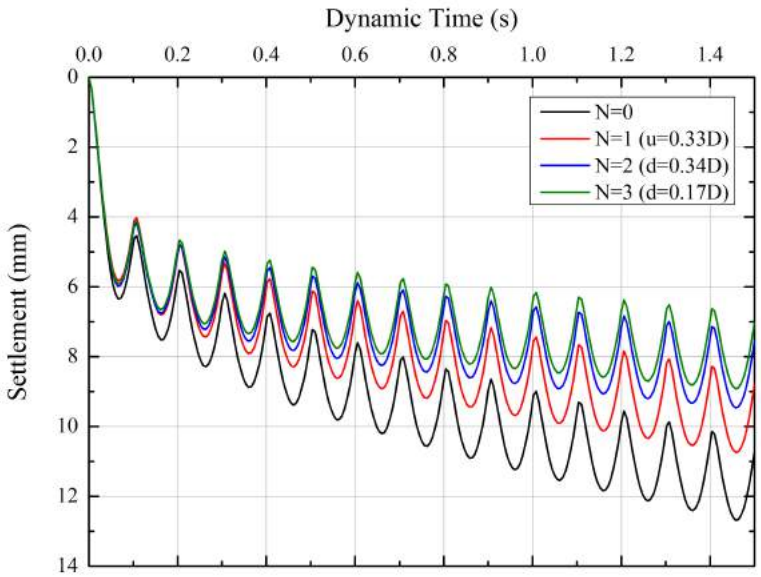

Figure 6.28: Effect of number of layers of reinforcement (Dynamic time vs. Settlement curve, using HS small model)

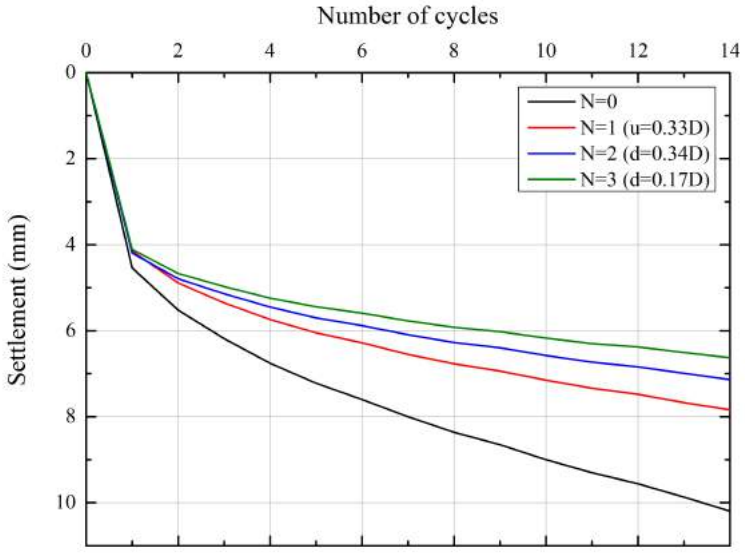

Figure 6.29: Effect of number of layers of reinforcement (No. of cycles vs. Settlement curve, using HS small model)

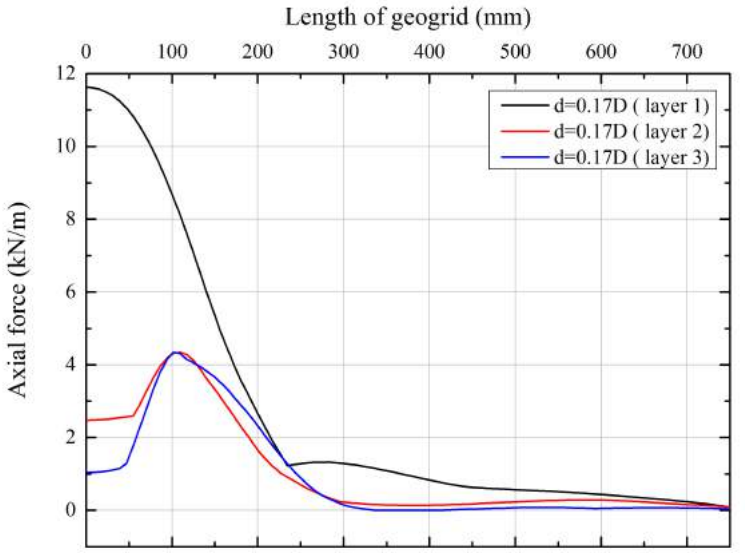

Figure 6.30: Geogrid forces in case of three layers of reinforcement (using HS small model)

From Figures 6.23, 6.26 and 6.29 it is observed that for all three soil models permanent settlement after 14 number of cycles decreases as the number of geogrid layers increases

from N=0 to N=3, when the lowest settlement cases for N=1 and N=2 are considered for comparison.

From Figures 6.24, 6.27 and 6.30 it is observed that in case of three layers of reinforcement, in first layer maximum axial force in geogrid is at the center of footing (below the load), while in second and third layer maximum axial force occur at some distance from the center of footing, while in both the layers axial forces decrease as the distance from center increases, and become very small after a georid length of 1.33D.

6.3.4 *Effect of stiffness of geogrid*

From Figure 6.31 it can be observed that with increase in the stiffness of geogrid layers placed in top granular fill maximum settlements at peak loads decrease. Figure 6.32 shows that permanent settlement after 14 cycles also decreases with increase in the geogrid stiffness.

Figure 6.33 shows that with increase in the stiffness of geogrid layers axial forces in the first layer of geogrid, which is at the interface of clay and granular fill, increase. Maximum axial force in geogrid is at the center of footing (below the load) and become very small after a georid length of 1.33D.

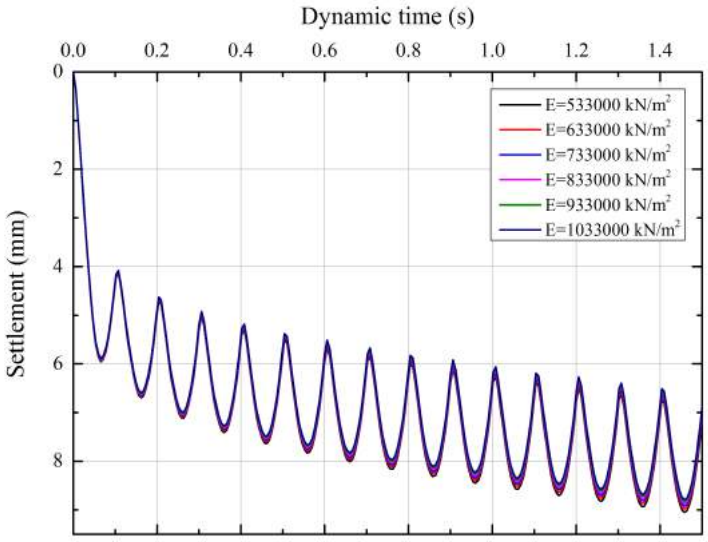

Figure 6.31: Effect of stiffness of geogrid on the settlement behavior of two layer reinforced soil system with three layers of geogrids (Dynamic time vs. Settlement curve, using HS small model)

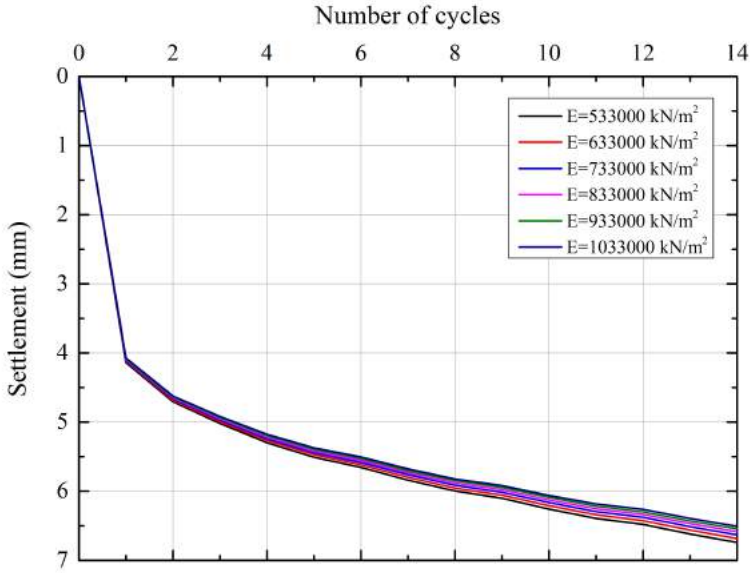

Figure 6.32: Effect of stiffness of geogrid on the settlement behavior of two layer reinforced soil system with three layers of geogrids (No. of cycles vs. Settlement curve, using HS small model)

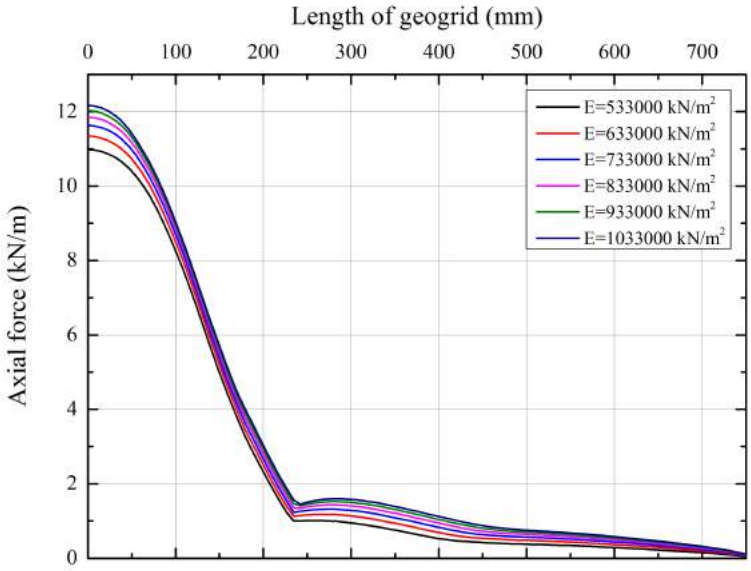

Figure 6.33: Effect of stiffness of geogrid on axial forces in first geogrid layer (using HS small model)

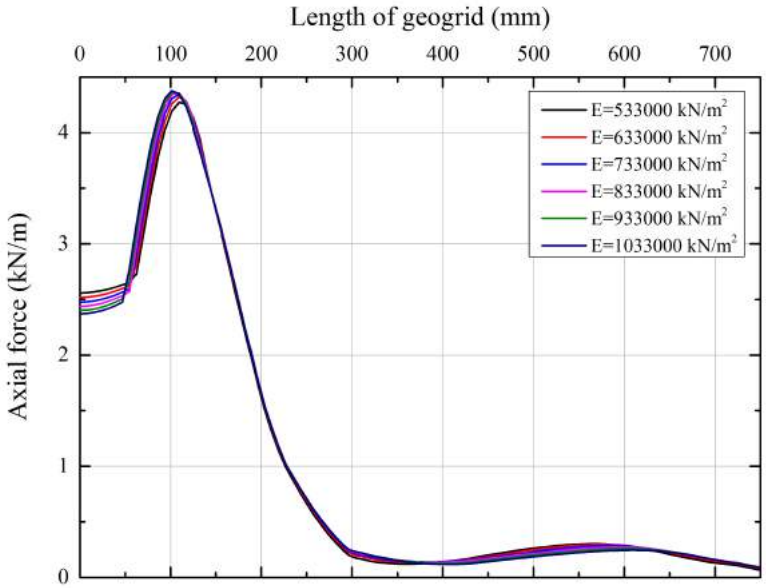

Figure 6.34: Effect of stiffness of geogrid on axial forces in second geogrid layer (using HS small model)

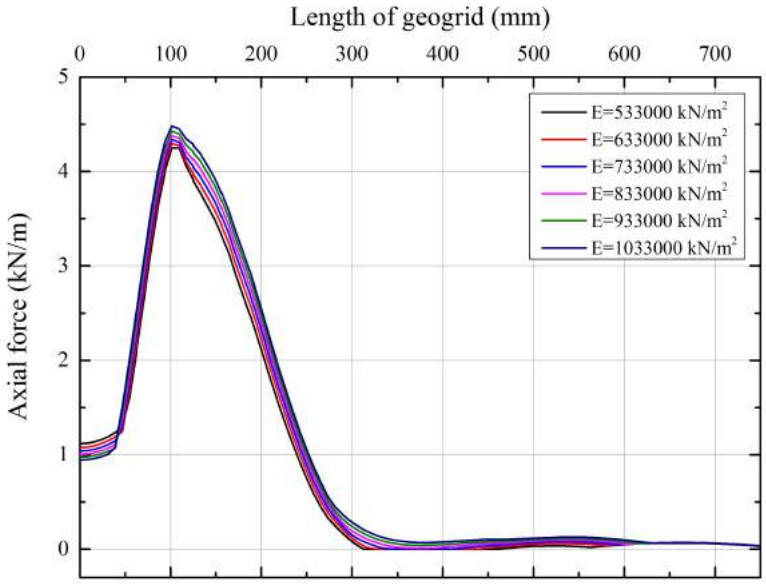

Figure 6.35: Effect of stiffness of geogrid on axial forces in third geogrid layer (using HS small model)

From Figures 6.34 and 6.35 it can be observed that near the center of footing, axial forces in second and third layers of geogrid decrease as stffness of geogrids increase, but away from center axial forces in second and third layers of geogrid increase stffness of geogrids increase.

6.4 Conclusions of Dynamic Analysis

- It can be observed from dynamic analysis that when Mohr Coulomb model is used for analysis in all cases maximum settlement at peak load are much higher than, when Hardening soil model and HS small model are used. But permanent settlements after 14 cycles are less than, when Hardening soil model and HS small model are used.

- It can also be observed that from dynamic analysis that in case of Hardening soil model maximum settlement at peak load and permanent settlement after 14 cycles are slightly more than, when HS small model is used.

- It can also be observed that with increase in number of geogrid layers (from N=0 to N=3), settlement decreases and at N=3, it is lowest and with increase in the distance between two layers of reinforcement settlement decreases upto a limited value after that it increases.

- It can also be observed that as number of geogrid layers increases above the first layer, which is at the interface of clay and granular fill, axial forces in the first geogrid layer decreases.

- It can be observed from dynamic analysis that results using Hardening soil model and HS small model are relatively same and realistic, but form Mohr Coulomb model are unsatisfactory.

- It is observed that increase in the stiffness of geogrid causes an improvement in the load bearing and settlement behavior of two layer reinforced soil system.

Chapter 7

Summary and Conclusions

7.1 Summary

In this thesis static and dynamic analysis are carried out using PLAXIS 2D on the two layer unreinforced and reinforced soil systems to see the effect of providing reinforcement in the two layer soil sytem and other parameters, on the bearing capacity and settlemet behavior of two layer system. For dynamic analysis, it is required to provide viscous boundaries in PLAXIS to reduce the boundary effects and to prevent the reflection of waves from boundaries. A study has also been carried out to compare the various methods of providing silent boundaries and to see the effectiveness of viscous boundary. Static analysis is carried out to simulate a field test numerically and results from the numerical analysis are compared with the results of field test. Dynamic analysis is carried out on the previously validated model and parametric study is performed.

7.2 Conclusions

- It is found that for dynamic analysis in PLAXIS 2D, providing viscous boundaries is very effective method to reduce boundary effects.
- Results of static analysis, obtained from finite element analysis using PLAXIS 2D are in good agreement with the results obtained from experimental analysis.
- Bearing capacity and settlement behavior of two layer soil system improves when reinforcement is provided in the top layer. Bearing capacity of two layer reinforced system further improves with decrease in the depth of reinforcement below the base of footing but up to a limit.
- In dynamic analysis, with increase in number of geogrid layers bearing capacity and settlement behavior of two layer soil system improves.

- When there is only two layers of geogrid are present in two layer soil system with first layer at the interface of two soils and second above this, then with increase in the distance of second layer from first layer (up to a limit) causes an improvement in the settlement behavior of two layer reinforced soil system.

- Geogrid stiffness also affect the bearing capacity and settlement behavior of two layer soil system. Increment in geogrid stiffness causes an improvement in bearing capacity and settlement behavior of two layer soil system.

- Results from Hardening soil model and HS small model are in good agreement and realistic while results from Mohr Coulomb model are not much satisfactory. This is because, for dynamic analysis Hardening soil model and HS small model are more suitable as they include hardening effects of soil due to cyclic loads, which Mohr Coulomb model does not include.

7.3 Further scope of research

- Here width of the granular fill is kept as 2.5D, as used in field test. This width can be varied to see the effect of width of granular fill on the load bearing and settlement behavior of two layer soil system.

- Width of geogrid layer can be varied to determine its effect on the load bearing and settlement behavior of two layer soil systems.

- A study can be carry out with different frequencies and magnitudes of dynamic load to determine the effect of these parameters on the load bearing and settlement behavior.

- Geogrid layers can be simulated with positive and negative interfaces using PLAXIS 2D.

- Value of soil damping can be varied to see the effect of soil damping on the behavior of two layer reinforced soil systems.

Bibliography

Al-Kafaji, I.K.J. (2013), "Formulation of a dynamic material point method (MPM) for geomechanical problems", PhD thesis, Institute of Geotechnical Engineering, University of Stuttgart.

Al-Shenawy, A.O. and Al-Karni, A.A. (2005), "Derivation of bearing capacity equation for a two layered system of weak clay layer overlaid by dense sand layer", Pertanika J. Sci. & Technol. 13(2), 213-235.

Batali, L., Butnarciuc, N. and Klompmaker, J. (2014), "Geocomposite reinforced crane working platform- experimental study and numerical model", DGGT German geotechnical society.

Brinkgreve, R. and Vermeer, P.A. (2013), "PLAXIS material models manual", PLAXIS.

Brinkgreve, R. and Vermeer, P.A. (2013), "PLAXIS scientific manual", PLAXIS.

Burd, H.J. and Frydman, S. (1997), "Bearing capacity of plain-strain footings on layered soils", Canadian Geotechnical Journal 34, 241-253.

Cicek, E. and Guler, E. (2015), "Bearing capacity of strip footing on reinforced layered granular soils", Journal of Civil Engineering and Management 21(5), 605-614.

Dash, S.K., Sireesh, S. and Sitharam, T. (2003), "Model studies on circular footing supported on geocell reinforced sand underlain by soft clay", Geotextiles and Geomembranes 21, 197-219.

Demir, A., Yildiz, A., Laman, M. and Ornek, M. (2014), "Experimental and numerical analyses of circular footing on geogrid-reinforced granular fill underlain by soft clay", Acta Geotechnica 9, 711-723.

Dutta, M. and Gulhati, S. (2005), "Geotechnical engineering", Chapter Reinforced soils, Geosynthetics, Tata Mac-Graw Hill, Delhi pp. 565–576, 585–595.

Dutta, S. and Mandal, J. (2016), "Model studies on geocell-reinforced fly ash overlying soft clay", Journal of Materials in Civil Engineering 28(2).

Floss, R., Laier, H. and Braeu, G. (1990), "Dynamic loading of geotextiles soil-systems", Geotextiles, Geomembranes and Related Products, Vol.1, pp. 183–188.

Ghazavi, M. and Eghbali, A.H. (2008), "A simple limit equilibrium approach for calculation of ultimate bearing capacity of shallow foundations on two-layered granular soils", Geotechnical and Geological Engineering 26, 535-542.

Hanna, A.M. (1981), "Foundations on strong sand overlying weak sand", Journal of the Geotechnical Engineering Division 107(7), 915-927.

Hanna, A.M. and Mayerhof, G.G. (1980), "Design charts for ultimate bearing capacity of foundations on sand overlying soft clay", Canadian Geotechnical Journal 17(2), 300-303.

Ibrahim, K.M.H.I. (2014), "Bearing capacity of circular footing resting on granular soil overlying soft clay", Housing and Building National Research Center.

Joshi, V.C., Dutta, R.K. and Shrivastava, R. (2015), "Ultimate bearing capacity of circular footing on layered soil", Journal of Geoengineering 10(1), 25–34.

Kellezi, L. (2000), "Local transmitting boundaries for transient elastic analysis", Journal of Soil Dynamics and Earthquake Engineering 19(7), 533–547.

Khing, K.H., Das, B.M., Puri, V.K., Yen, S.C. and Cook, E.E. (1994), "Foundation on strong sand underlain by weak clay with geogrid at the interface", Geotextiles and Geomembranes 13(3), 199-206.

Kim, H.S. (2012), "Finite element analysis with paraxial & viscous boundary conditions for elastic wave propagation", Journal of Scientific Research, Engineering 4(12), 843-849.

Kim, H.S. (2014), "A study on the performance of absorbing boundaries using dashpots", Journal of Scientific Research, Engineering 6(10), 593-600.

Kramer, S.L. (1996), "Geotechnical Earthquake Engineering", Prentice-Hall International Series in Civil Engineering and Engineering Mechanics.

Kumar, A. and Walia, B. (2006) "Bearing capacity of square footings on reinforced layered soil", Geotechnical and Geological Engineering 24, 1001-1008.

Laman, M., Yildiz, A., Ornek, M. and Demir, A. (2012), "Field test of circular footings on reinforced granular fill layer overlying a clay bed", Geotechnical Testing Journal 35(4).

Li, P. and Song, E.X. (2015), "A general viscous-spring transmitting boundary for dynamic analysis of saturated poroelastic media", International Journal for Numerical and Analytical methods in Geomechanics.

Liu, G. and Jerry, S.Q. (2003), "A non-reflecting boundary for analyzing wave propagation using finite element method", Finite Elements in Analysis and Design 39, 403-417.

Lysmer, J. and Kuhlemeyer, R.L. (1969), "Finite dynamic model for infinite media", Journal of Engineering Mechanics Division 95, 859-876.

Merifield, R.S. and Nguyen, V.Q. (2006), "Two and three-dimensional bearing-capacity solutions for footings on two layered clays", Geomechanics and Geoengineering 1(2), 151-162.

Meyerhof, G.G. (1951), "The ultimate bearing capacity of foundations", 2(4), 301-332.

Meyerhof, G.G. (1963), "Some recent research on the bearing capacity of foundations", Canadian Geotechnical Journal 1(1), 16-26.

Meyerhof, G.G. (1974), "Ultimate bearing capacity of footing on sand layer overlying clay", Canadian Geotechnical Journal 11(2), 223-229.

Michalowski, R.L. and Shi, L. (1995), "Bearing capacity of footings over two-layer foundation soils", Journal of Geotechnical Engineering 121(5), 421-428.

Mosadegh, A. and Nikraz, H. (2015), "Bearing capacity evaluation of footing on a layered soil using abaqus", J. Earth Sci.Clim. Change 6(3).

Nujid, M.M. and Taha, M.R. (2014), "A review of bearing capacity of shallow foundation on clay layered soils using numerical method", Electronic Journal of Geotechnical Engineering 19D, 811-825.

Oda, M. and Win, S. (1990), "Ultimate bearing capacity tests on sand with clay layer", Journal of Geotechnical Engineering 116(12), 1902-1906.

Okamurai, M., Takemura, J. and Kimura, T. (1998), "Bearing capacity predictions for sand overlying clay based on limit equilibrium methods", Japanese Geotechnical Society 38(1), 181-194.

Palmeira, E.M. and Antunes, L.G. (2010), "Large scale tests on geosynthetic reinforced unpaved roads subjected to surface maintenance", Geotextiles and Geomembranes 28, 547-558.

Ross, M. (2004), "Modeling methods for silent boundaries in infinite media", International Journal of Engineering and Technology (IJET) 2(2).

Sawwaf, M.E. and Nazir, A. (2012), "Behavior of eccentrically loaded small-scale ring footings resting on reinforced layered soil", Journal of Geotechnical and Geoenvironmental Engineering 138(3), 376-384.

Shen, L. and Chen, Z. (2005), "A silent boundary scheme with the material point method for dynamic analyses", Journal of Computer Modeling in Engineering & Sciences 7(3), 305-320.

Shukla, S.K. and Yin, J.H. (2006), "Fundamentals of Geosynthetic Engineering", Taylor and Francis Group, London, UK.

Subaida, E.A., Chandrakaran, S. and Sankar, N. (2009), "Laboratory performance of unpaved roads reinforced with woven coir geotextiles", Geotextiles and Geomembranes 27, 204-210.

Schanz, T., Vermeer, P.A. and Bonnier, P.G. (1999), "The hardening soil model: Formulation and verification", Computational Geotechnics.

Tafreshi, S.M. and Dawson, A. (2010), "Behavior of footings on reinforced sand subjected to repeated loading – comparing use of 3D and planar geotextile", Geotextiles and Geomembranes 28, 434-447.

Ti, K.S., Bujang, B.K.H., Noorzaei, J., Jaafar, M.S. and Sew, G.S. (2009), "A review of basic soil constitutive models for geotechnical application", Electronic Journal of Geotechnical Engineering 14, 1-18.

Yadu, L. and Tripathi, D.R. (2013), "Effect of length of geogrid layers in the bearing capacity ratio geogrid reinforced granular fill-soft subgrade soil system", Procedia - Social and Behavioral Sciences 104, 225-234.

Zhou, H. and Wen, X. (2008), "Model studies on geogrid- or geocell-reinforced sand cusion on soft soil", Geotextiles and Geomembranes 26(3), 231-238.

Zhu, M. (2004), "Bearing capacity of strip footings on two-layer clay soil by finite element method", ABAQUS Users' Conference, pp. 777-787.

Zhu, M. and Michalowski, R.L. (2005), "Bearing capacity of rectangular footings on two-layer clay", Geotechnology Harmony with the Global Environment, University of Michigan, Ann Arbor, United States, Vol. 2, pp. 997–1000.

Zienkiewicz, O. (1967), "The finite element method", McGraw-Hill, London.